2013

Solid Phase Extraction Room Temperature Fluorescence Spectroscopy For The Direct Quantification Of Monohydroxy Metabolites Of Polycyclic Aromatic Hydrocarbons In Urine Samples

Korina Jesusa Calimag
University of Central Florida

SOLID PHASE EXTRACTION ROOM TEMPERATURE FLUORESCENCE SPECTROSCOPY FOR THE DIRECT QUANTIFICATION OF MONOHYDROXY METABOLITES OF POLYCYCLIC AROMATIC HYDROCARBONS IN URINE SAMPLES

by

KORINA JESUSA CALIMAG - WILLIAMS
B.S. University of the Philippines Los Baños, 2001

A dissertation submitted in partial fulfillment of the requirements
for the degree of Doctor of Philosophy
in the Department of Chemistry
in the College of Sciences
at the University of Central Florida
Orlando, Florida

Summer Term
2013

Major Professor: Andres D. Campiglia

ABSTRACT

Polycyclic aromatic hydrocarbons (PAH) are important environmental pollutants generally formed during incomplete combustion of organic matter containing carbon and hydrogen. Introduced into the human body by adsorption through the skin, ingestion or inhalation, the biotransformation processes of PAH lead to the formation of multiple metabolites. Due to the short elimination lifetime from the body, the quantitative determination of monohydroxy-PAH (OH-PAH) in urine samples provides accurate information on recent exposure to environmental PAH. Urine analysis of OH-PAH with established methodology relies on sample clean-up and pre-concentration followed by chromatographic separation and quantification. Although chromatographic techniques provide reliable results in the analysis of OH-PAH, their experimental procedures are time consuming and expensive. Additional problems arise when laboratory procedures are scaled up to handle thousands of samples under mass screening conditions. Under the prospective of a sustainable environment, the large usage of organic solvents is one of the main limitations of current chromatographic methodology. It is within this context that new analytical approaches based on easy-to-use and cost-effective methodology become extremely relevant. This dissertation focuses on the development of screening methodology for the routine analysis of PAH metabolites in numerous samples. It explores the room-temperature fluorescence properties of six metabolites originating from parent PAH included in the Environmental Protection Agency priority pollutants list. 1-hydroxyfluorene, 1-hydroxypyrene, 6-hydroxychrysene, 9-hydroxyphenanthrene, 3-hydroxybenzo[*a*]pyrene and 4-hydroxybenzo[a]pyrene are used as model biomarkers to investigate the analytical potential of new methods based on solid-phase extraction (SPE) and

room-temperature fluorescence (RTF) spectroscopy. Quantitative determination of metabolites is carried out either in the eluent extract[1, 2] or on the surface of extraction membranes[3, 4]. The direct determination – i.e., no chromatographic separation - of the six metabolites is based on the collection of excitation-emission matrices and synchronous fluorescence spectra.

ACKNOWLEDGMENTS

I would like to express my sincerest gratitude to my advisor Prof. Andres D. Campiglia for his enormous help and support towards the fulfillment of my Ph.D. degree. For imparting his knowledge, time, patience, and enthusiasm towards our research work.

To my dissertation committee: Dr. Kevin D. Belfield, Dr. Cherie Yestrebsky, Dr. Alfons Schulte and Dr. Karin Chumbimuni-Torres – Thank You. It was such a privilege to have you on my dissertation committee.

I like to thank the friends that I gained during my PhD days. You are too many to mention but you always touched my heart and you made my PhD days more colorful. I would also like to thank for the valuable help from my lab mates, Keerthika Vatsavai, Dr. Matthew Rex, Dr. Huiyong Wang, Dr. Gaston Knobel, Dr. Emily Heider, Krishnaveni Appalaneni – Immani, Anthony Moore, Walter Wilson, Nirvani Mujumdar, Josh Knorr, Victor Diaz, Khang Trieu, and Bassam Alfarhani.

My deepest gratitude goes to my husband, Henry E. Williams Jr. and my daughter, Khloe E. Williams for inspiring me to not give up and finish the raise. To my parents and parents-in-law I thank them for their undying support and love. To my siblings for their love thank you.

Lastly I thank my God, Who made this all possible. I lift up to you all the glory and honor.

TABLE OF CONTENTS

LIST OF FIGURES

LIST OF TABLES

CHAPTER 1: GENERAL INTRODUCTION

1.1 Polycyclic Aromatic Hydrocarbons

Polycyclic aromatic hydrocarbons (PAH) are important environmental pollutants originating from a wide variety of natural and anthropogenic sources. PAH are generally formed during incomplete combustion of organic matter containing carbon and hydrogen.[5-15] Due to the carcinogenic nature of some PAH, their chemical analysis is of great environmental and toxicological importance. Among the hundreds of PAH present in the environment, the EPA lists the following sixteen as "Consent Decree" priority pollutants: benz[*a*]anthracene, benzo[*b*]fluoranthene, benzo[*k*]fluoranthene, benzo[*a*]pyrene, dibenzo[*a,h*]anthracene, indeno[*1,2,3-cd*]pyrene, naphthalene, acenaphthylene, acenaphthene, fluorene, phenanthrene, anthracene, fluoranthene, pyrene, chrysene, and benzo[*g,h,i*]perylene. Their molecular structures are shown in Figure 1.1. According to the EPA, these PAH should be routinely monitored to avoid human exposure to contaminated sites.

Human exposure to PAH derives from a variety of sources such as air pollution from automobile, diesel and industrial or incinerator emissions, which may modulate a spectrum of their other combustion, dietary and occupational sources. The primary source of PAH exposure in humans is through food consumption.[16, 17] Cereal and vegetables are the major dietary sources of PAH, except when there is a high consumption of meat cooked over an open flame.[18] More than 150 PAH have been found in tobacco smoke,[19] which also contributes significantly to exposure to PAH[20] and to adverse health effects.[21]

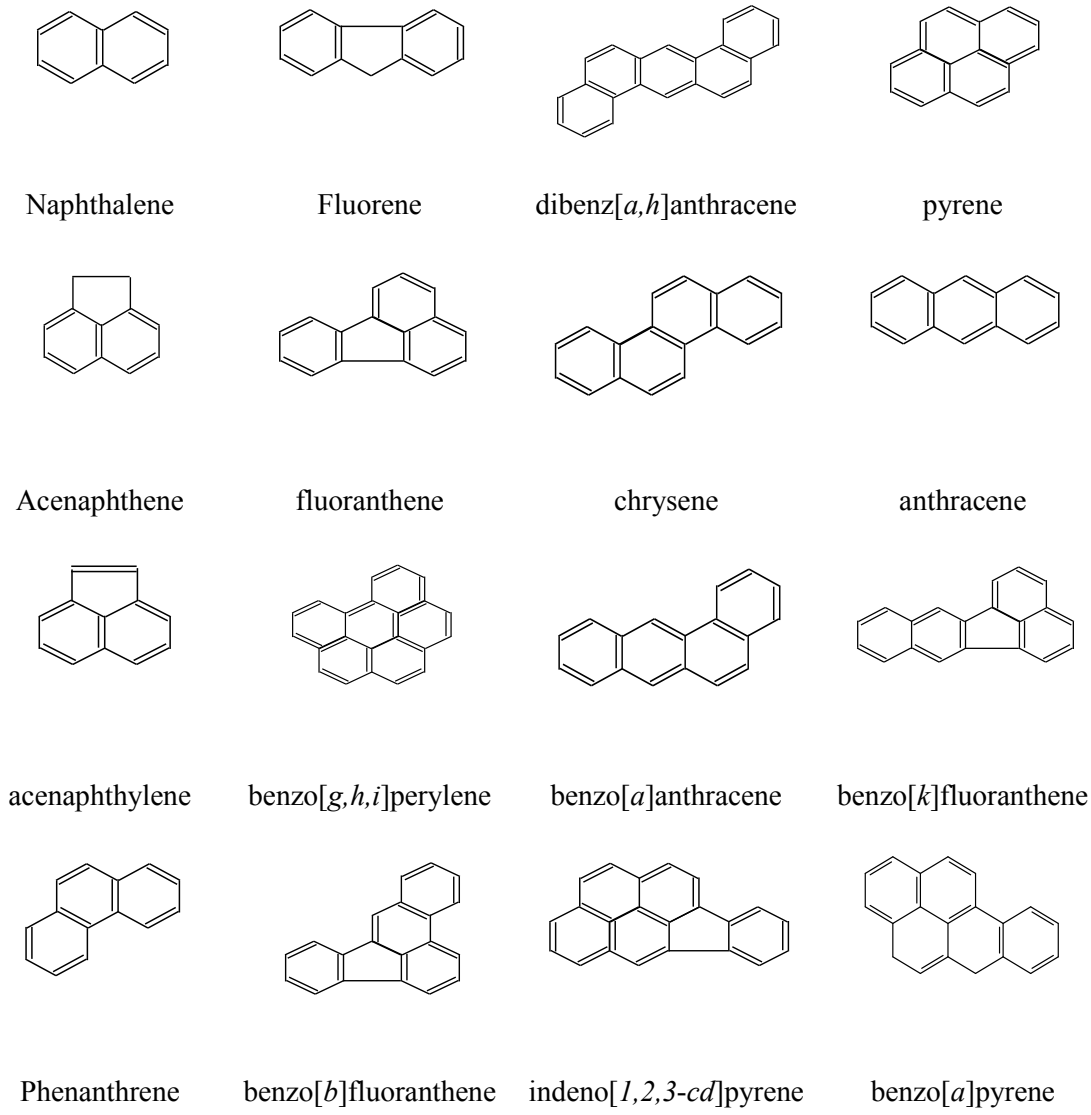

Figure 1.1 Molecular structures of 16 EPA PAH.

A less pervasive source of air pollution leading to PAH exposure involves biomass burning from forest fires and peat bogs resulting from incidental incineration, or from deliberate forest cleaning strategies that expend beyond planned boundaries.[18] Wood combustion as an energy source for heating and/or cooking also generates a source of indoor PAH pollution

leading to health problems.[22, 23] Occupational exposures may result from daily contact with intensive combustion processes such as iron and steel production,[24] coke production,[25] waste incinerators,[26] transportation maintenance,[27] mining exhaust exposure[28] and aluminum smelters,[29] or from tobacco smoke in commercial venues[21] such as bars, restaurants and nightclubs. More intensive PAH exposures in occupational environments – relative to the general population – have resulted in reports of lung, genitourinary and skin cancers.[30]

1.2 Metabolites of Polycyclic Aromatic Hydrocarbons

Although environmental monitoring of PAH is an important step to prevent exposure to contaminated sites, it provides little information on the actual uptake and subsequent risks. PAH are introduced in the body by adsorption through the skin, ingestion or inhalation and can be subsequently metabolized to their more polar metabolites. The biotransformation process consists of two phases. In phase I metabolism, PAH are oxidized by the cytochrome P450 enzymes to form reactive epoxide intermediates, followed by reduction or hydrolysis to hydroxylated derivatives. In phase II metabolism, hydroxyl-PAH form glucoronate and sulfate conjugates to facilitate their excretion through urine, bile and feces.[31] These biological processes lead to the formation of multiple metabolites including epoxide, dihydrodiols, monohydroxylated-PAH (OH-PAH) and polyhydroxy-PAH. Covalent binding to DNA is believed to be the first critical step in the initiation of the tumor formation process. [32, 33] This is depicted in Figure 1.2 which shows the metabolic pathways of benzo[a]pyrene (B[a]P), which is the most carcinogenic compound in the EPA priority pollutants list. [34] The metabolic pathways of B[a]P include the formation of diol epoxides and their subsequent binding to DNA to form the PAH-DNA adducts. These adducts can then be repaired, restoring the original healthy DNA, or

they can originate mutant DNA leading to the formation and proliferation of tumors.

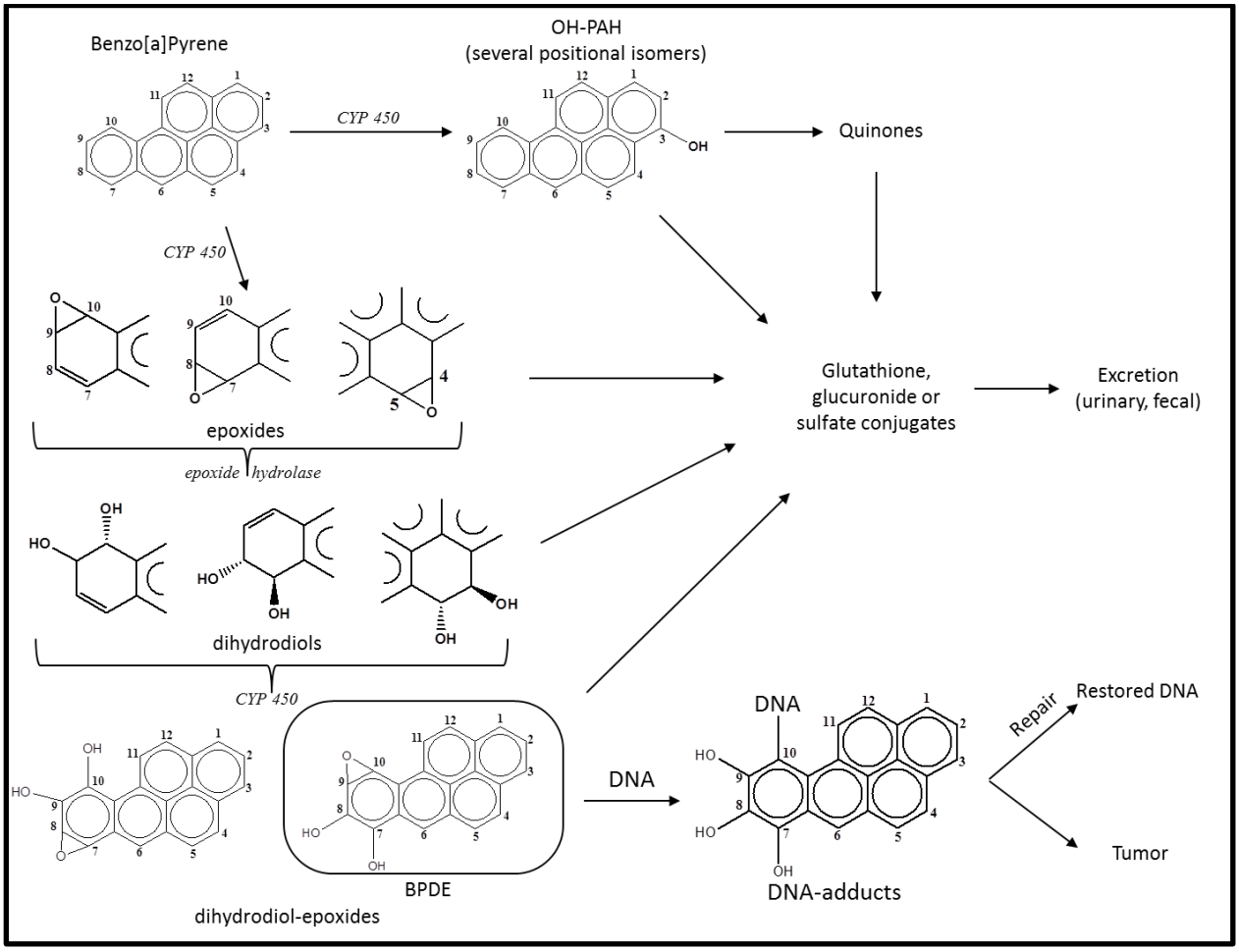

Figure 1.2 Overview of B[a]P metabolism. CYP: Cytochrome P450. Adapted from [31].

Due to the short average lifetime of OH-PAH elimination from the body, their quantitative determination in biological fluids such as urine and blood samples provides accurate information on recent exposure to environmental PAH.[35] Early methods[35-37] for the analysis of urine samples focused on a few OH-PAH, with particular emphasis on 1-hydroxypyrene.[36] Considering that human exposure often occurs to complex mixtures with numerous PAH, recent

methods have expanded their scope to a larger number of metabolites. [1, 38] Particular attention has been paid to metabolites resulting from exposure to EPA-PAH, i.e. PAH included in the EPA priority pollutants list.

1.3 Urine analysis of OH-PAH

The general trend for the analysis of OH-PAH in urine samples follows the pattern of sample collection and hydrolysis, sample clean-up and pre-concentration, and chromatographic separation and quantification. The hydrolysis step – which can be either enzymatic or acidic – dissociates OH-PAH from their glucuronide and/or sulfate conjugates.[1] Popular approaches for sample clean-up and pre-concentration include liquid-liquid extraction (LLE)[39] and SPE[40]. Both methodologies are well suited to automation, which increases sample throughput and reduces variability due to manual sample handling. Chromatographic separation and quantification has been based on high-performance liquid chromatography-room temperature fluorescence detection (HPLC)[41-43] and gas chromatography-mass spectrometry (GC-MS). [44-47] Table 1.1 summarizes several features of previously reported methods for the chromatographic analysis of OH-PAH in urine samples. The tabulated information only includes five of the six the metabolites investigated in this dissertation, namely 2-hydroxyfluorene (2OH-Flu), 1-hydroxypyrene (1OH-Pyr), 9-hydroxyphenanthrene (9OH-Phen), 6-hydroxyxhrysene (6OH-Chry), 3-hydroxybenzo[a]pyrene (3OH-B[a]P). No reports were found on the analysis of 4-hydroxybenzo[a]pyrene (4OH-B[a]P) in urine samples.

Numerous HPLC and GC-MS methods have been published for the analysis of OH-PAH metabolites in urine samples. Interesting to note is the wide range of recoveries reported for the metabolites under investigation. Unfortunately, the standard deviations of the analytical

recoveries were not reported, which make difficult the statistical comparison of the observed differences in their average values. Comparison of the analytical recoveries for those metabolites with reported values via the two methods reveals better recoveries via GC-MS for 2OH-Flu. 9OH-Phen and 1OH-Pyr presented approximately the same recovery via HPLC and GC analysis. The best limits of detection (LOD) were clearly obtained via GCMS. Unfortunately GC-MS procedures are more complicated than HPLC methodology.[38, 45] GC-MS requires a chemical derivatization step prior to metabolite separation to avoid peak tailing in the chromatographic column.

1.4 Overall goal of this dissertation

Although chromatographic techniques provide reliable results in the analysis of OH-PAH, their experimental procedures are time consuming and expensive. Elution times of 30-60 minutes are typical and standards must be run periodically to verify retention times. If the concentrations of target species are found to lie outside the detector's response range, the sample must be diluted and the process repeated. On the other end of the concentration range, many samples are "zeroes," i.e. the concentrations are below detection limits. Additional problems arise when laboratory procedures are scaled up to handle thousands of samples under mass screening conditions. Under the prospective of a sustainable environment, the large usage of organic solvents is one of the main limitations of the current chromatographic methodology.

It is within this context that new analytical approaches based on easy-to-use and cost-effective methodology that provide large sample throughput become extremely relevant. The research presented here focuses on the development of screening methodology for the routine analysis of PAH metabolites in numerous samples. It explores the room-temperature

fluorescence properties of 2OH-Flu, 1OH-Pyr, 9OH-Phen, 6OH-Chry, 3OH-B[a]P and 4OH-B[a]P. These metabolites are used as model biomarkers to investigate the analytical potential of simple methods based on SPE and Room-Temperature Fluorescence spectroscopy (SPE-RTF). The remaining of this chapter is then devoted to cover basic principles of SPE, fluorescence spectroscopy, excitation-emission matrices (EEMs), synchronous fluorescence spectroscopy (SFS) and data analysis techniques.

SPE of OH-PAH is usually carried out with the aid of non-polar sorbents such as octadecyl-silica particles. The effectiveness of octadecyl-silica sorbents is based on the same sorption-desorption phenomena as in reversed-phase liquid chromatography. The main mechanism of OH-PAH isolation is a non-polar interaction, i.e. Van der Waals forces. OH-PAH will pass into the solid surface, and given time, the equilibrium will be established between the two phases. The equilibrium for each OH-PAH is described by its partition coefficient, which is simply the ratio of OH-PAH concentrations in the two phases. The driving force for the partition mechanism results from the difference in the chemical potential of the metabolite in the solid (sorbent) and the liquid phase (aqueous sample). The chemical potential equation of any given metabolite ($OH\text{-}PAH_i$) in any given phase (p) is given by:

$$\mu_i^p = (\mu^0)_i^p + RTInC_i \qquad (1.1)$$

Table 1.1 Analytical figures of merit reported for OH-PAH analysis in urine samples by HPLC and GC-MS

Metabolite	LOD (ng/mL)	Recovery (%)	Sample Preparation	Instrumental method	Analysis time (min)[a]	Reference
2-hydroxyfluorene	727	62	SPE, evap.	HPLC	40	[43]
2-hydroxyfluorene	3.6	82	SPE, evap., derivatization	GC-MS	27	[45]
9-hydroxyphenanthrene	165	57	SPE, evap.	HPLC	40	[43]
9-hydroxyphenanthrene	200	50	SPE, evap., derivatization	GC-MS	40	[46]
1-hydroxypyrene	40	83	SPE, evap.	HPLC	40	[43]
1-hydroxypyrene	44	68	SPE, evap.	HPLC	40	[43]
1-hydroxypyrene	1.6	99	SPE, evap., derivatization	GC-MS	24	[34]
1-hydroxypyrene	3.3	80	SPE, evap., derivatization	GC-MS	27	[45]
3-hydroxybenzo[*a*]pyrene	1615	40	SPE, evap.	HPLC	40	[43]
3-hydroxybenzo[*a*]pyrene	40	48	SPE, evap.	HPLC	45	[48]
3-hydroxybenzo[*a*]pyrene	10.0	NA	SPE, evap., derivatization	GC-MS	27	[42]
6-hydroxychrysene	1.7	68	SPE,evap.	HPLC	23	[49]

[a]Instrumental analysis only; does not include sample preparation procedures

where μ_i^p is the chemical potential of OH-PAH_i in phase "p", $(\mu^0)_i^p$ is the standard chemical potential of OH-PAH_i in phase "p", and C_i is the OH-PAH_i concentration in phase "p". When equilibrium is established, the chemical potential of OH-PAH_i in the sorbent (s) and aqueous (a) phases reaches the same value, i.e.:

$$\mu_i^s = \mu_i^a \qquad (1.2)$$

The concentration of OH-PAH_i in each phase depends on its partition coefficient. The larger the partition coefficient the better the retention of OH-PAH_i will be in the solid phase. The partition coefficient or capacity factor (K) can be represented by

$$C_i^s/C_i^a = \exp[-\Delta\mu^0_i / RT] \qquad (1.3)$$

$$K = C_i^s/C_i^a \qquad (1.4)$$

SPE materials are packed in two formats, discs and cartridges. A SPE cartridge consists of a small column (generally an open syringe barrel) containing a sorbent with an average particle size of about 40 packed between plastic frits. The sorbent bed occupies about one-third of the syringe barrel volume. The remaining volume is used as sample reservoir. SPE discs are particle-loaded membranes in the form of flexible discs of various diameters and 0.5-1.0 mm of thickness. They are packed in a way that the sorbent is enmeshed into a web of some other inert polymer, e.g., Teflon, or is trapped in a glass fiber or paper filter. SPE discs are preferred over cartridges because their larger cross-sectional area and shorter bed depth allow higher flow rates and shorter analysis time.

The experimental procedure for SPE consists of four steps: conditioning, retention, rinsing and drying. The solid sorbent must undergo proper conditioning to wet the packing

material before the sample passes through the SPE device. In its dry form, the octadecyl (C_{18}) bonded-phase material is randomly oriented on the surface. If the sorbent is placed in contact with an aqueous sample, the environment surrounding the bonded organic moiety would be highly polar and entirely incompatible with a C_{18} bonded-phase. The bonded groups try to minimize the exposure to the high polarity medium by forming clusters among them that are close to each other. In such a configuration, the organic surface that is exposed to the solute is very small. This arrangement of the bonded organic groups diminishes the extraction efficiency of SPE. The conditioning step "activates" the sorbent by treatment with an organic solvent, typically methanol. Under these conditions, the bonded-organic moiety is more open and available for interaction with the solute. This process can be determined as one of the most important steps for a successful SPE.

After conditioning, the sample is loaded to the SPE device by gravity feed, pumping, or vacuum. Depending on the type of sample, micro-liters to liters of liquid sample can be applied through the sorbent phase. During this step, OH-PAH are extracted and pre-concentrated in the solid sorbent. Some of the matrix concomitants may also be retained along with OH-PAH, making matrix composition more challenging for further OH-PAH analysis.

A rinsing step is then used to remove potential interferences from the SPE material. For aqueous samples, a water-organic-solvent mixture is usually used as the rinsing solvent. The final step is the elution of OH-PAH from the sorbent with an appropriate solvent specifically chosen to disrupt the metabolite-sorbent interaction. The elution solvent should remove as little as possible of the other substances sorbed on the column.

Tables 1.2 and Table 1.3 summarize the typical composition of human urine samples. The molecular structures of the major components are shown in Appendix A in this dissertation. Urea, sodium and potassium salts are very soluble in water and should not be retained by C18 silica sorbents. The same is not true for creatinine and ammonium salts – such as ammonium hippurate – which could be retained by the sorbent and co-eluted with OH-PAH. In addition to the potential interference of common urine components, the analyst should keep in mind the chemical variations that occur due to internal and external factors [50]. Internal factors include body temperature, pressure and mental state of the individual that can lead to the production or breakdown of different metabolites in any given period. The same is true for external factors such as food, drug intake, and environmental contamination due to inhalation or skin contact. These include compounds with low solubility in water such as vitamins, phenolic compounds, and anti-inflammatory, antibiotic and antipyretic drugs [51-55].

Table 1.2 Composition of typical human urine

Item	Formula
Inorganic Salts	
Sodium Chloride	NaCl
Potassium Chloride	KCl
Potassium Sulfate	K_2SO_4
Magnesium Sulfate	$MgSO_4$
Magnesium Carbonate	$MgCO_3$
Potassium Bicarbonate	$KHCO_3$
Potassium Phosphate	K_3PO_4
Calcium Phosphate	$Ca_3(PO4)_2$
UREA	H_2NCONH_2
Organic Compounds	
Creatinine	$C_4H_7N_3O$
Uropepsin (as Tyrosine)	$HO.C_6H_4.C_2H_3(NH_2).CO_2H$
Creatine	$HN:C(NH_2)N(CH_3).CH_2.CO_2H.H_2O$
Glycine	$NH_2.CH_2.CO_2H$
Phenol	$C_6H_5.OH$
Histidine	$C_3H_3N_2.CH_2.CH.(NH_2).CO_2H$
Androsterone	$C_{19}H_{30}O_2$
Glucose	$C_6H_7O_6(COCH_3)_5$
Taurine	$NH_2.CH_2.CH_2.SO_3H$
Organic Ammonium salts	
Hippurate	$NH_4C_6H_5CO.NHCH_2.CO_2$
Citrate	$(NH_4)_2HC_6H_5O_7$
Glucuronate	$NH_4C_6H_9O_7$
Urate	$(NH_4)_2C_5H_3O_3N_4$
Lactate	$(NH_4)_2C_3H_5O_3$
Asparate	$NH_4C_4H_6O_4N$
Formate	$(NH_4)_2.HCO_2$

Adapted from **[56]**

Table 1.3 Major Constituents of Human Urine

Item	Range	
	Min (mg/L)	Max (mg/L)
Total Solutes	36,700	46,700
Urea	9,300	23,300
Chloride	1,870	8,400
Sodium	1,170	4.390
Potassium	750	2,610
Creatinine	670	2.150
Sulfur, Inorganic	163	1,800
Hippuric Acid	50	1,67.0
Phosphorus, Total	410	1,070
Citric Acid	90	930
Glucuronic Acid	70	880
Ammonia	200	730
Uric Acid	40	670
Uropepsin(as Tyrosine)	70	560
Bicarbonate	20	560
Creatine	0	530
Sulfur, Organic	77	470
Glycine	90	450
Phenol	130	420
Lactic Acid	30	400
Calcium	30	390
Histidine	40	330
Glutamic Acid	<7	320
Androsterone	2	280
Magnedum	30	260
Glucose	90	200

Adapted from **[56]**

For efficient retention on the SPE substrate, one would desire the capacity factor of the metabolite to be very large in aqueous urine solutions. Similarly, the capacity factor should approach zero in 100% organic eluting solvent unless non-reversed-phase interactions were taking place. Unfortunately, non-reversed-phase interactions in C_{18} sorbent materials result from the existence of residual silanol groups on the surface of silica particles. These groups, which interact with OH-PAH through both hydrogen bonding and dipole-dipole interactions, make difficult OH-PAH desorption for subsequent chromatographic analysis. The large variations observed for the recoveries of individual OH-PAH in Table 1.1 can be partially attributed to the difficulty of metabolite desorption from C_{18} sorbents. Although previously reported data on the standard deviations of average recoveries of individual OH-PAH is scarce and incomplete, the reported values show relatively high standard deviations that affect both the precision and the accuracy of analysis. It is within this context that development of new SPE approaches and instrumental methods become relevant to the analysis of OH-PAH in urine samples.

1.5 Fluorescence Spectroscopy

Photoluminescence spectroscopy is based on the detection of radiation of 200-700 nm emitted during the deactivation of electronically excited molecules.[57-59] Under normal conditions, the orbital of lowest energy of an organic molecule are occupied by pairs of electrons with spin in opposite directions.[60] Since most of the organic molecules have an even number of valence electrons, the resulting electron spin is zero. Such a state, with no net spin, is called a singlet state. The singlet state of lowest energy is known as the ground state, and it is represented in the Jablonski diagram[61] of Figure 1.3 by S_0.

Through the absorption of electromagnetic radiation (A), a molecule can pass from the ground state to an excited state of higher energy. This transition occurs in approximately 10^{-15} s and entails the promotion of an electron from the highest occupied orbital to a previously unoccupied one. If the transition occurs with no change in the spin of the promoted electron, the excited state will have two unpaired electrons with anti-parallel spins and, therefore, net spin equal to zero. An electronic state with these characteristics is known as a singlet excited state. In Figure 1.3, the first and second singlet-excited states are represented by S_1 and S_2, respectively. If the transition involves a change in the electronic spin, the excited state will be characterized by two unpaired electrons with parallel spins. In this case, the resultant spin is one, and the excited state receives the name of triplet state. In Figure 1.3, the triplet state of the lowest energy is symbolized by T_1 while any other triplet state of higher energy is represented by T_n.

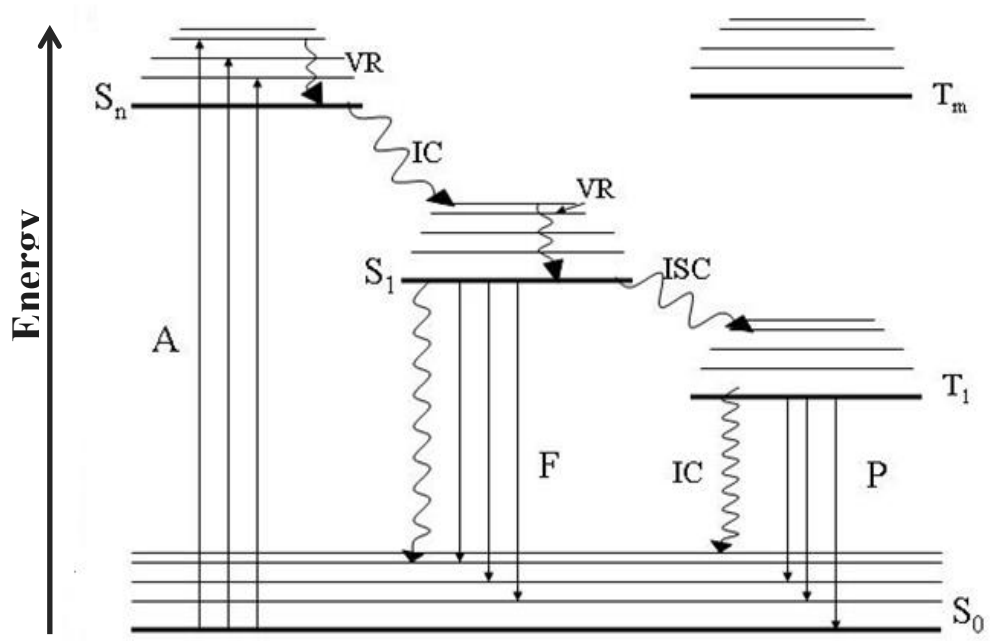

Figure 1.3 Jablonski diagram. A is the absorption, F is the fluorescence, P is the phosphorescence, VR is the vibrational relaxation, IC is the internal conversion, and ISC is the intersystem crossing.

From the S_1 state, deactivation of the molecule may happen through various processes. External conversion (EC) is a non-radiative deactivation process in which the excited molecule transfers its excess electronic energy to surrounding molecules or solvent molecules through collisions. From the lowest vibrational level of S_1, the molecule may also release the excess of electronic energy in the form of a photon. This process is known as fluorescence (F) and it occurs on the order of 10^{-10} to 10^{-6}s. Since IC and VR are comparatively rapid process, fluorescence most often occurs from the ground vibrational lever of the first excited single state and is of a longer wavelength than absorption. Fluorescence from the S_2 state is rare and will only occur if the energy gap between the S_1 and S_2 states is large enough that IC is not favored.

The S_1 state may also be deactivated by a non-radiative process called inter-system crossing (ISC). This process involves a crossover of electronic states similar to IC but it occurs between states of different spin multiplicity. Population of the upper vibrational levels of the triplet state manifold is followed by VR and IC into the ground vibrational level of the first triplet excited state (T_1). Deactivation of T_1 via the emission of a photon is called phosphorescence (P) and it occurs on the order of 10^{-3} to 10^{3} s. Since phosphorescence occurs on a relatively long time scale, T_1 is particularly susceptible to collisional deactivations. [62] Non-radiative deactivation of T_1, or quenching, can be a particular problem in the presence of oxygen. Molecular oxygen resides naturally in a ground triplet configuration possessing two low-lying singlet states with excitation energies of approximately 23 and 38 kcal/mol. Any species having excitation energy as low as 23 kcal/mol may be quenched by oxygen via energy transfer. Excited singlet states may also be affected by oxygen, but since oxygen quenching is diffusion controlled, a high oxygen concentration is necessary to quench the relatively short-lived excited singlet state. The removal of oxygen is often accomplished through de-oxygenation of sample solution or purging the sample compartment with inert gasses. Similar to phosphorescence, fluorescence is always in competition with the various non-radiative deactivation processes of the excited state. As a result, fluorescence and phosphorescence intensities intrinsically depend on the relative efficiencies of all competing processes affecting their respective excited states. The efficiencies of fluorescence and phosphorescence are often expressed in terms of quantum yield (ϕ).

The quantum yield for fluorescence, ϕ_F, is the ratio of the rate of fluorescence with the

rate of absorption, Φ_F/Φ_A, where $\Phi_F = k_F n_{S1} V$ and $\Phi_A = k_A n_{S0} V$. V is the volume of sample illuminated; n_{Sx}.is the number of molecules occupying the given electronic state x; and k_F and k_A are the rate of fluorescence and absorption, respectively. Under steady state conditions, we can assume that $n_{S1} = n_{S0} k_A / (k_F + k_{nr})$, where k_{nr} is the sum of rates for the non-radiative processes (external conversion, k_{ec}; internal conversion, k_{ic}; and inter-system crossing, k_{isc}). Using these relationships, the fluorescence quantum yield in terms of the rates of the various activation and deactivation processes is given by equation (1.5):

$$\phi_F = \frac{k_F}{k_F + k_{nr}} \qquad \textbf{(1.5)}$$

which shows that, in order to improve the fluorescence quantum yield, and hence the fluorescence intensity, one needs to minimize the rate contributions from non-radiative processes .A similar situation arises for phosphorescence. The phosphorescence quantum yield (ϕ_P) can be expressed as:

$$\phi_P = \frac{k_{isc}}{k_{isc} + k_F + k_{nr}} \times \frac{k_P}{k_P + k_{nr}} \qquad \textbf{(1.6)}$$

Note that the first term in equation (1.6) takes into account the efficiency of Inter-system crossing. Therefore, to maximize the phosphorescence efficiency, hence the phosphorescence intensity, minimization of both non-radiative processes and fluorescence relative to inter-system crossing becomes evident.

The detection of luminescence (fluorescence and/or phosphorescence) is the basis of several photoluminescence techniques. Fluorescent and/or phosphorescent compounds usually

consist of molecules with extensive π electron systems. These include a large variety of aromatic molecules either with or without hetero-atoms in the conjugated system. [58-60, 63] The free movement of π electrons throughout the delocalized molecular orbitals facilitates the electronic transitions responsible for fluorescence and phosphorescence. For molecules with no hetero-atoms in the aromatic system, transitions frequently involve the promotion of an electron from a bonding π orbital to an anti-bonding π* orbital (π – π* transition). Aliphatic molecules, on the other end, rarely exhibit luminescence since the high energy required for σ – σ* transitions usually causes decomposition prior to excitation. [58-60, 63]

Among the numerous photoluminescence techniques known in the analytical field, RTF spectroscopy is the most popular. RTF offer the advantages of relatively inexpensive instrumentation, calibration curves with excellent linear dynamic ranges and appropriate limits of detection. In most cases, de-oxygenation of the sample is not critical and fluorescence measurements are rapidly performed by placing a quartz cell in the sample compartment of a spectrofluorimeter. Conventional fluorometric methods - in which either the excitation or the emission wavelength is set at its maximum position while the other is scanned – present limited selectivity. The similarity and/or overlapping of broad fluorescence bands at room-temperature usually interfere in the characterization of targeted compounds without previous separation. Several strategies exist to improve the selectivity of RTF measurements. These include EEMs data formats[64, 65] and SFS[66-68].

1.6 Excitation-Emission Matrices (EEMs)

The most popular data format in fluorescence spectroscopy is a two-dimensional (2D) plot correlating fluorescence intensities to emission wavelengths. The usual procedure for recording 2D fluorescence spectra consists of measuring the emission spectrum at a fixed excitation wavelength. Similarly, 2D excitation spectra are recorded by monitoring the excitation wavelength at a fixed fluorescence wavelength. In most cases, the fluorescence spectral profile of a pure compound is independent of the excitation wavelength. The same is true for its excitation spectral profile, which remains the same independent of the monitored emission wavelength. Maximum fluorescence intensity is always obtained at the maximum excitation wavelength of the fluorophor.

Recording a 2D fluorescence spectrum from a mixture with numerous fluorescence components only provides partial information on the total fluorescence of the mixture. The emission profile of a mixture with numerous fluorescence components varies with the relative positions of the excitation wavelength and the excitation maxima of the fluorophors in the mixture. Individual fluorophor contributions to the total fluorescence spectrum of the sample also depend on the fluorescence quantum yields of the fluorophors and possible quenching due to synergistic effects. For a sample of unknown composition, therefore, variations in the fluorescence profile with variations in the excitation wavelength suggest that more than fluorescence compound is present in the sample. A similar statement could be made from variations in its excitation profile with the monitored emission wavelengths.

The total fluorescence of the sample, which includes possible quenching and synergistic effects, can be gathered in a single data format known as excitation-emission matrix (EEM)[69, 70].

The experimental procedure for collecting EEMs is rather simple. It consists of recording fluorescence spectra at various excitation wavelengths. The resulting I by J data matrix (EEM) is compiled from an array of 2D fluorescence spectra while the excitation wavelength is increased incrementally between each scan[71, 72]. Each I row in the EEM corresponds to the emission spectrum at the *ith* excitation wavelength. Each J column in the EEM corresponds to the excitation spectrum at the *jth* emission wavelength. For a single emitting species in a sample, the elements of the EEM are given by:

$$\mathbf{M_{ij} = 2.303\Phi_F I_0(\lambda_i)\varepsilon(\lambda_i)bc\gamma(\lambda_j)\kappa(\lambda_j)} \qquad \mathbf{(1.7)}$$

where $\boldsymbol{I}_0(\lambda_i)$ is the intensity of the incident light exciting the sample in units of quanta/s; $2.303\boldsymbol{\varepsilon}(\lambda_i)bc$ represents the optical density of the sample, which results from the product of the analyte's molar absorptivity $\boldsymbol{\varepsilon}(\lambda_i)$, the optical path-length b, and the concentration of the emitting species c; Φ_F is the quantum yield of fluorescence; $\boldsymbol{\gamma}(\lambda_j)$ is the fraction of fluorescence photons emitted at wavelength λ_j and $\boldsymbol{\kappa}(\lambda_j)$ is an instrumental factor that represents the wavelength dependence of the spectrofluorimeter's sensitivity[71]. The condensed version of equation (1.7) may be expressed as:

$$\mathbf{M_{ij} = \alpha x_i y_j} \qquad \mathbf{(1.8)}$$

where $\boldsymbol{\alpha} = 2.303\Phi_F bc$ is a wavelength independent factor containing all of the concentration dependence, $x_i = \boldsymbol{I}_0(\lambda_i)\boldsymbol{\varepsilon}(\lambda_i)$ and $yi = \boldsymbol{\gamma}(\lambda_j)\boldsymbol{\kappa}(\lambda_j)$. The observed relative fluorescence excitation spectrum may be represented by x_i, the wavelength sequenced set, and thought of as a column vector, x in λ_i space. The wavelength sequenced set, y_i, may be thought of as a row vector y in λ_i space, representing the observed fluorescence emission spectrum. Therefore, for a single component, **M** is simply represented as:

$$\mathbf{M = \alpha xy} \qquad \textbf{(1.9)}$$

Where **M** is the product of the vectors x and y multiplied by the compound specific parameter **α**. When data is taken from a sample containing multiple, r, different species, M is given by the following expression:

$$\boldsymbol{M = \sum_{k=1}^{r} \alpha_k x^k y^k} \qquad \textbf{(1.10)}$$

where k is used to detail the species. For a recorded M, the spectral characterization of single components then relies on finding r, $\boldsymbol{\alpha}_k$, x^k, and y^k.

Figure 1.4 and Figure 1.5 provides a schematic representation of an EEM of a compound obeying Kasha's rule[73]. The 2D excitation and fluorescence spectra are depicted along the sides of the EEM plot. Within the defined contour levels, this pure compound adheres to the two properties of excitation and emission previously discussed, i.e. its fluorescence profile does not change with the excitation wavelength and vice-versa. As always observed from an EEM of a pure compound, the center of the contour plot corresponds to the maximum excitation and emission wavelengths of the fluorophor.

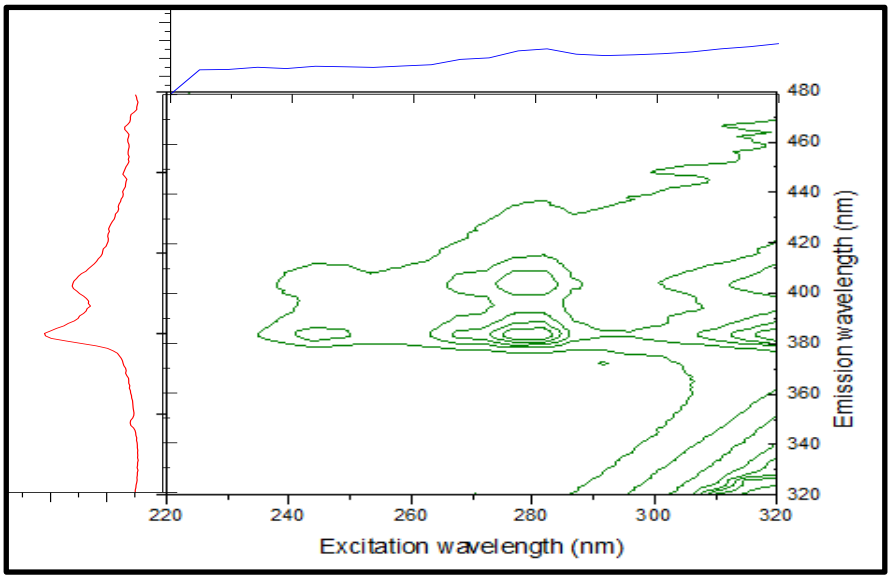

Figure 1.4 Contour map of EEM of 3.5ppb 1OH-Pyr on C_{18} membrane adpated from Chapter 3 of this dissertation.

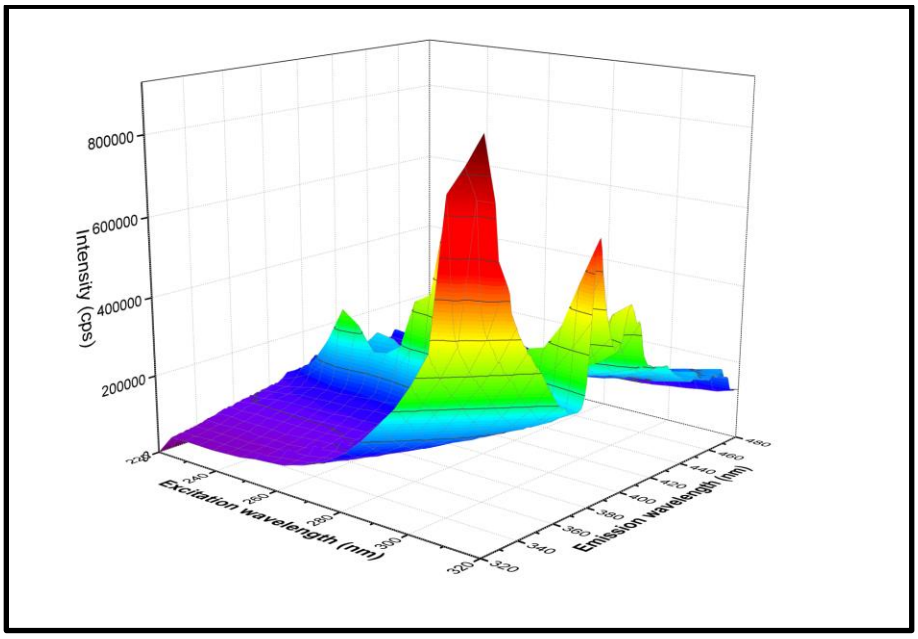

Figure 1.5 Color map surface of EEM of 3.5ppb 1OH-Pyr on C_{18} membrane adpated from Chapter 3 of this dissertation.

Figure 1.6 provides an example of a more complex EEM recorded from a multicomponent fluorescence mixture. Evidence of the multicomponent nature of the EEM becomes clear with the multiple changes of the emission profile due to variations in the excitation wavelength. The same is true for the variations in excitation spectra with emission wavelengths. The number of changes noted in the emission or excitation profiles provides visual indication of the number of fluorescence components in the mixture.

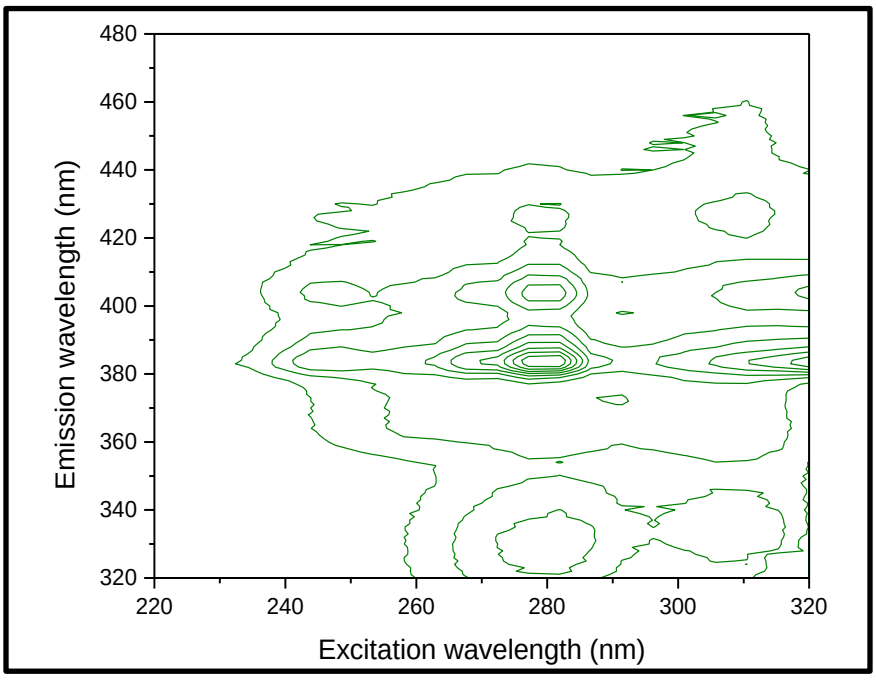

Figure 1.6 Contour plot of an EEM of a four - component mixture of polycyclic aromatic compounds namely 2OH-Flu, 1OH-Pyr, 9OH-Phen, and 3OH-B[a]P on C_{18} membrane adpav ted from Chapter 3 of this dissertation.

1.7 Synchronous Fluorescence Spectroscopy

Conventional fluorescence spectra - in which either the excitation or the emission wavelength is set at its maximum position while the other is scanned – present limited selectivity. The similarity and/or overlapping of broad fluorescence bands at room temperature usually interfere in the characterization of targeted compounds without previous separation. Several strategies exist to improve the selectivity of room temperature fluorescence measurements. The one employed here is known as synchronous fluorescence spectroscopy (SFS). The synchronous excitation approach consists of varying simultaneously both the excitation (λ_0) and emission (λ) wavelengths while keeping constant a wavelength interval ($\Delta\lambda = \lambda - \lambda_0$) between them. The judicious choice of the $\Delta\lambda$ parameter often leads to spectral simplification and resolution of spectral overlapping. An example of spectral simplification due to the judicious choise of wavelength interval is shown in Figure 1.7, which compares the exitation and flurescence spectra of perylene (top) to synchronous fluorescence spectra recorded at two $\Delta\lambda$ values (bottom). The synchronous fluorescence spectrum obtained with a $\Delta\lambda$ = 10nm consists of a single emission peak. The 30nm wavelength difference results in two emission peaks. In the analysis of a complex mixture without previous chromatographic separation, the direct determination of perylene with a $\Delta\lambda$ = 10nm should be less prone to spectral overlapping than its determination with a $\Delta\lambda$ = 30nm. This spectral simplification usually improves the selectivity of the technique for multicomponent analysis.[68, 74]

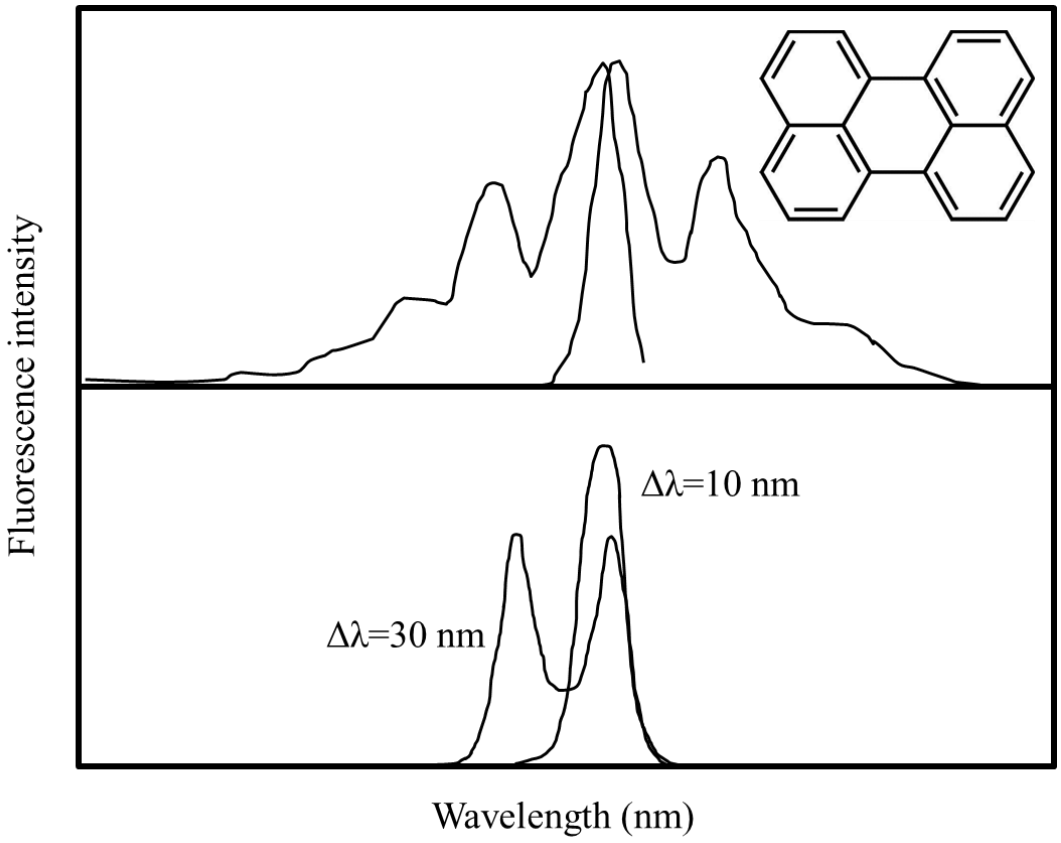

Figure 1.7 Excitation and fluorescence spectra (top) and SFS (bottom) of perylene. Adapted from [74]

1.8 Chemometric Algorithms for Background Correction

Baseline reduction/correction is the process of eliminating "background noise" and/or background signal. The effect of baseline differs from spectrum to spectrum. In spectroscopic techniques, it is not unusual to encounter a non-smooth or non-zero baseline. The simplest kind of baseline correction is where the spectrum to be corrected must lay or start on the line where there is a zero signal. This can be done by calculating the average signal over the spectral region for each spectrum and subtract it from each wavelength in the respective spectrum. Alternatively, background correction procedures can be applied for more complicated spectrum. If the

background signal is curved and multiple peaks are available in the spectrum, it may be possible to fit a polynomial equation through all the peaks. The spectrum is then corrected by subtracting the resulting curved polynomial line from the corresponding spectrum. Among the more sophisticated schemes already published for background correction [75-81], the one we chose is known as the asymmetric least square (ALS) algorithm. ALS uses a Whittaker smoother series for background correction and it is further described in chapter 2 of this dissertation.

1.9 Multivariate Calibration Algorithms

The relevance of using multivariate calibration algorithms in analytical chemistry results from their ability to extract information from complex samples without the need of previous separation procedures. Depending on the complexity of the sample, chemometric algorithms used for analytical purposes can be classified into zero-, first-, second- and higher-order methods. The progression of orders reflects the power of the algorithm to handle and obtain reliable data from matrixes of increasing complexity. Calibration methods that process first order data – first order algorithms – carry with them the first-order advantage, i.e. the ability to identify targeted species in the presence of sample concomitants with potential interference. In order to provide accurate quantitative information, first-order calibration methods require the laborious preparation of extensive calibration data sets containing all sample components with potential spectral overlapping.

A more attractive approach is to handle spectral overlapping with algorithms of second- or higher order. Calibration methods capable to provide accurate quantitation of numerous targeted species in the presence of un-calibrated interference carry with them the second-order

advantage. The application of second-order calibration methods requires second-order or tri-linear data, i.e. data describing each targeted species with a triad of invariant pure profiles. EEMs and total synchronous fluorescence spectroscopy data (TSFS) – i.e. synchronous spectra recorded from a multi-component fluorescence mixture at various $\Delta\lambda$ values - fit into the latter category. Spectral overlapping in EEM data of OH-PAH was here resolved with N-PLS/RBL, an algorithm for processing second order data that combines multi-way partial least-squares (N-PLS) to the residual bi-linearization procedure (RBL).[1, 82] The performance of N-PLS/RBL was then compared to the well-established multivariate curve resolution-alternating least-squares (MCR-ALS) algorithm. The elimination of matrix interference in TSFS data was achieved with N-PLS/RBL and with unfolded partial least squares (U-PLS) followed by RBL. A full description of N-PLS/RBL, MCR-ALS and UPL/RBL are provided in chapters 3 and 4 of this dissertation.

CHAPTER 2: ROOM TEMPERATURE FLUORESCENCE SPECTROSCOPY OF MONOHYDROXY METABOLITES OF POLYCYCLIC AROMATIC HYDROCARBON ON OCTADECYL EXTRACTION MEMBRANES

Calimag-Williams K, Goicoechea HC, and Campiglia AD.
Analytica Chimica Acta 717 (2012) 100– 109

2.1 Introduction

Considerable efforts have been made to improve analytical measurements of the fluorescence and phosphorescence of compounds on solid materials.[59, 83] As a result, solid surface luminescence analysis is a widely accepted tool in environmental, pharmaceutical, food and agricultural science.[84] A variety of solid substrates has been used in solid-surface luminescence such as filter paper, silica gel, sodium acetate and polymers. Particularly attractive is the use of SPE membranes for the analysis of polycyclic aromatic compounds in water samples. [85-89] The analytical merits include simple experimental procedures for routine screening of numerous samples and compatibility with portable instrumentation for field analysis. Because of the non-destructive nature of luminescence measurements, can be brought to the lab for subsequent elution and confirmation of compounds via high-resolution techniques.[90-93]

The concept was first applied to the analysis of PAH in water samples.[86, 94] Octadecyl extraction membranes were cut in tabs and suspended into aqueous solutions for PAH extraction. Depending on the PAH, extraction times varied between one and two hours. After drying for 5min the tabs were examined via front-surface RTF. LOD were estimated at the parts-per-billion

(ng.mL^{-1}) level.[86, 94] Campiglia's group extended the concept to room-temperature phosphorescence (RTP) analysis. SPE-RTP was applied to the analysis of PAH[87, 95-97], polychlorinated biphenyls[97, 98] and polychlorinated dibenzofurans[96, 98]. Bulky glassware and vacuum pumps, common to classic SPE lab procedures, were replaced with a syringe kit well-suited for manual extraction under field conditions. 47mm octadecyl membranes were cut into 13mm diameter extraction disks to fit into the substrate holder of the spectrofluorimeter. A rapid air-drying step, which was accomplished by applying positive pressure to the syringe, removed the excess of water from the extraction membrane prior to spectroscopic measurements. The same extraction procedure was later applied to the water analysis of PAH via SPE-RTF[99]. Total analysis time took less than 10min per sample and provided LOD at the parts-per-billion (pg.mL^{-1}) level.

The main disadvantages of SPE-RTP and SPE-RTF for the quantitative analysis of polycyclic aromatic compounds in water samples are relatively poor precision of measurements and background interference from extraction membranes. The presence of broad, featureless excitation and emission bands deteriorates LOD and often interferes with the determination of weak emitters at the ng.mL^{-1} concentration level.[87, 95, 100] This chapter presents advances in both fronts. Signal reproducibility is improved with the aid of a sample holder specifically designed for the manual optimization of luminescence signals. Background correction of solid substrates is carried out with the aid of ALS, a smoothing algorithm originally devised for baseline correction of chromatographic data[101] and often applied to matrix interference in chromatographic analysis[102, 103]. To the extent of our literature search, the application of ALS to

background reduction from extraction membranes and improvement of SPE-RTF precision of measurements has not been reported yet.

The successful application of our proposition is demonstrated here with the analysis of 2OH-Flu, 1OH-Pyr, 3OH-B[a]P and 9OH-Phen in synthetic urine samples. Extraction membranes serve the dual purpose of sample pre-concentration and solid substrate for RTF measurements. This approach – which eliminates elution steps and solvent evaporation prior to metabolite determination – provides excellent recoveries via a two-step procedure extremely appealing for routine analysis of numerous samples. Recovery values for the studied OH-PAH varied from 99.0 ± 1.2% (3OH-B[a]P) to 99.9 ± 0.05% (1OH-Pyr). The new sample holder improved the precision of measurements for analytical use. Relative standard deviations (RSD) of the studied metabolites varied from 3.5% (2OH-Flu) to 9.5% (9OH-Phe). The application of ALS to SPE-RTF improved the LOD by approximately two orders of magnitude. With only 10mL of urine sample, the LOD of OH-PAH varied from 57pg.mL^{-1} (2OH-Flu) to 2pg.mL^{-1} (1OH-Pyr).

2.2 Experimental

2.2.1 Chemicals and Ma*terials*

All solvents were Aldrich HPLC grade. All chemicals were analytical-reagent grade and utilized without further purification. Unless otherwise noted, Nanopure water was used throughout. 2OH-Flu, 1OH-Pyr and 9OH-Phen were purchased from Sigma–Aldrich. 3OH-B[a]P was from Midwest Research Institute. All other chemicals were purchased from Fisher

Chemical. The Sep-Pak C-18 membranes were purchased from Varian/Agilent. The synthetic urine solution was manufactured by RICCA Chemical Company (Arlington, TX) and purchased from Fischer Scientific. Its chemical composition mimicked main components of human urine at the concentrations found in healthy urine samples.

Note: Use extreme caution when handling OH-PAH known to be extremely toxic.

2.2.2 Preparation of stock solution of PAH metabolites

Stock solutions of PAH metabolites (100 μg/mL) were prepared by dissolving 1.0 mg of standard in 10 mL of methanol. All stock solutions were kept in the dark at 4 ^{o}C. Prior to use, stock solutions were monitored via RTF spectroscopy for possible photo-degradation of metabolites. Spectral profiles and fluorescence intensities of stock solutions remained the same for a period of six months. Working solutions of OH-PAH were prepared daily by serial dilution with the appropriate solvent.

2.2.3 Hydrolysis of urine samples

Synthetic urine samples (8 mL) were spiked with 1 mL of metabolite stock solution of appropriate concentration and equilibrated for 30 min to allow for the interaction of OH-PAH with urine components such as urea and various salts. Then 500 μL of 0.1 M HCl was added to the sample and the mixture was buffered with 500 μL of 0.05 M potassium biphthalate sodium hydroxide buffer (pH 5.0). The buffered sample was shaken for 30 min at 1400 rpm to allow for urine hydrolysis.

2.2.4 SPE with octadecyl membranes

A cork borer with an inside diameter of 10 mm was used to dissect a 47 mm C18 membrane into 10 mm extraction disks. A 10 mm disk was loaded into a stainless steel filter syringe kit (Alltech) and connected to a 10 mL Hamilton syringe (see Figure 2.1). Positive pressure was used to force all liquid solutions through the disk. Prior to sample application, the extraction membrane was conditioned with 5 mL of methanol and 5 mL of water. Optimization of experimental parameters concerning the retention of PAH metabolites led to the following procedure: aqueous metabolite solutions or synthetic urine samples were processed through extraction membranes previously conditioned with 5 mL methanol and 5 mL water. Following sample extraction, each membrane was sequentially rinsed with 10 mL water and 10 mL of 20% methanol/water. Void water was mechanically removed with a 100 mL syringe forcing three 100 mL volumes of air through the disk.

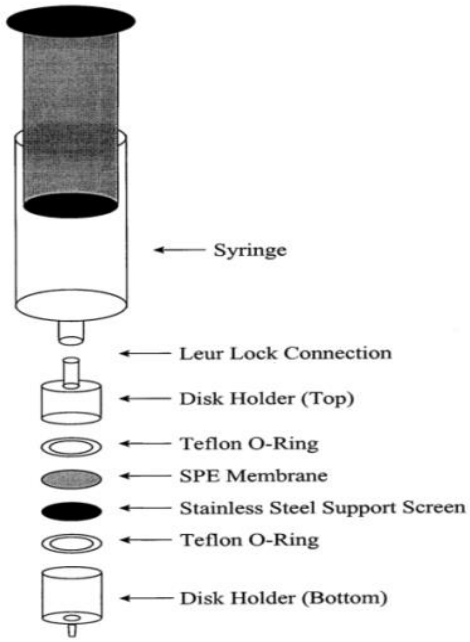

Figure 2.1 Syringe kit for SPE with C-18 membranes.

2.2.5 Sample holder for SPE-RTF measurements

The sample holder used for surface substrate measurements is shown in Figure 2.2. Its design allows for the optimization of the fluorescence signal via manual rotation of its cover. The diameter of the cover indention fits into the opening of the sample compartment's lid of the spectrofluorimeter. The extraction disk is mounted on a rectangular platform and held in place by a plate with a circular window for sample excitation. The substrate platform is connected to the cover with the aid of a cylindrical rod made hollow for gas purging and sample degassing. The height of the platform inside the sample compartment is adjustable by means of a knob placed on the rectangular rod of the cover. The cover rod allows for x–y adjustment of the substrate position with respect to the excitation beam. Once the excitation beam had been aligned with the circular window of the platform, no further optimization was needed. Maximum fluorescence

intensities were observed rotating the platform to around 45^{o} in relation to the excitation beam.

2.2.6 RTF measurements

Steady state excitation and fluorescence spectra and signal intensities were recorded with a commercial spectrofluorimeter (Photon Technology international). The excitation source was a continuous-wave 75 W pulsed xenon lamp with broadband illumination from 200 to 2000 nm. The excitation and emission monochromators had the same reciprocal linear dispersion (4 nm mm^{-1}) and accuracy ($\pm$1 nm with 0.25 nm resolution). The gratings were blazed at 300 and 400 nm, respectively. Detection was made with a photomultiplier tube with spectral response from 185 to 650 nm. The instrument was computer controlled using commercial software (Felix32) specifically designed for the system. Appropriate cut off filters were used to reject straight-light radiation and second-order emission. All the spectra are uncorrected for instrumental response.

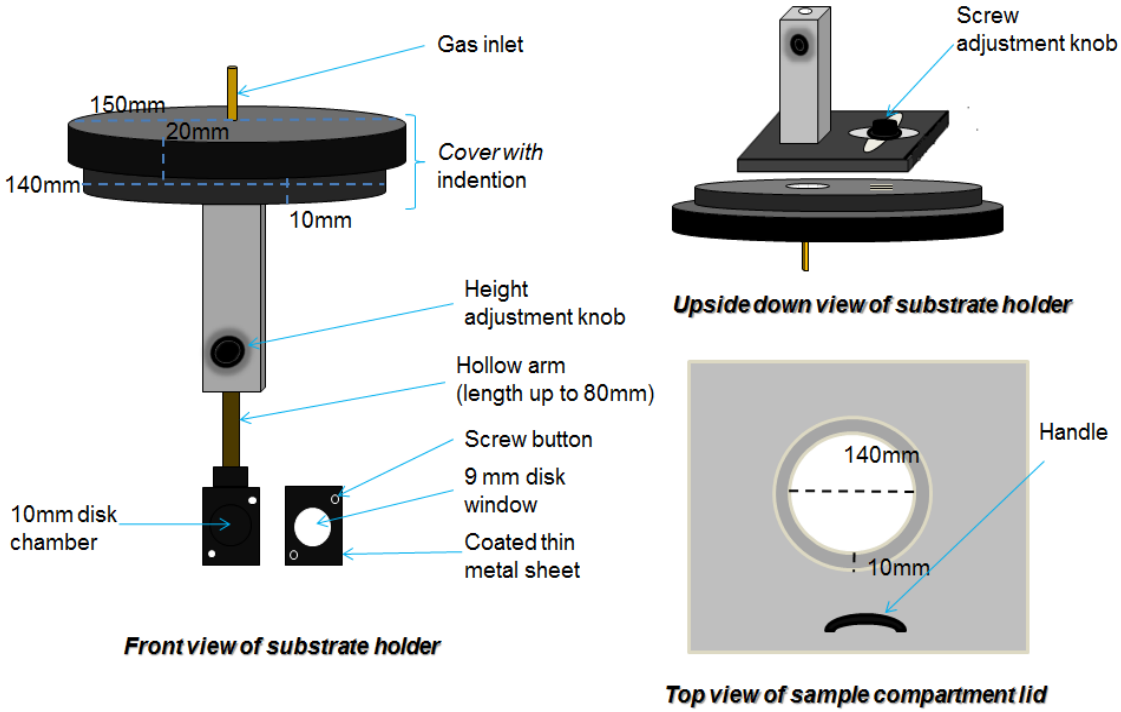

Figure 2.2 Solid-substrate holder for solid-surface room-temperature fluorescence measurements.

2.2.7 Software

Routines for data pre-treatment and processing were written in MATLAB[104]. Baseline routines for emission background correction were adapted from routines previously described in the literature for baseline correction of chromatographic data.[105] Implementation of the ALS algorithm included a smoothing parameter equal to 1×10^7, an asymmetry parameter equal to 0.001, an order of differences in penalty equal to 3 and a single regularization parameter, whose value was 1.

2.3 Results and Discussion

The four metabolites chosen for this study were selected as a tentative means of comparing our analytical figures of merit (AFOM) of SPE-RTF with previously reported data by chromatographic methods. Reported methods usually elute OH-PAH from SPE cartridges with milliliter volumes of methanol. Pre-concentration is made via methanol evaporation. Recoveries as low as 45–48% have been reported for 3OH-B[a]P[45, 106] one of the metabolites studied here. Reported recoveries for the other three metabolites have varied from 62 to 82% (2OH-Flu)[43, 106] 80 to 99% (1OH-Pyr) [45, 106] and 93 to 96% (9OH-Phen) [45, 106].

2.3.1 RTF analytical figures of merit (AFOM) of OH-PAH in aqueous solutions and urine samples

Figure 2.3 shows the initial survey of room-temperature excitation and fluorescence spectra of OH-PAH in methanol/water (1% v/v) solutions. All measurements were made from standard (1 × 1 cm) quartz cuvettes filled with undegassed solutions. All spectra were collected at 90◦ from the excitation beam using 2 nm excitation and emission band-pass. No attempts were made to adjust slit widths for optimum spectral resolution, nor were the spectra corrected for instrumental response. The 2 nm band-pass provided signal-to-blank ratios higher than 3 for all the studied metabolites at the trace concentration level. No significant changes were observed from spectra of OH-PAH in hydrolyzed urine samples or adsorbed on extraction membranes.

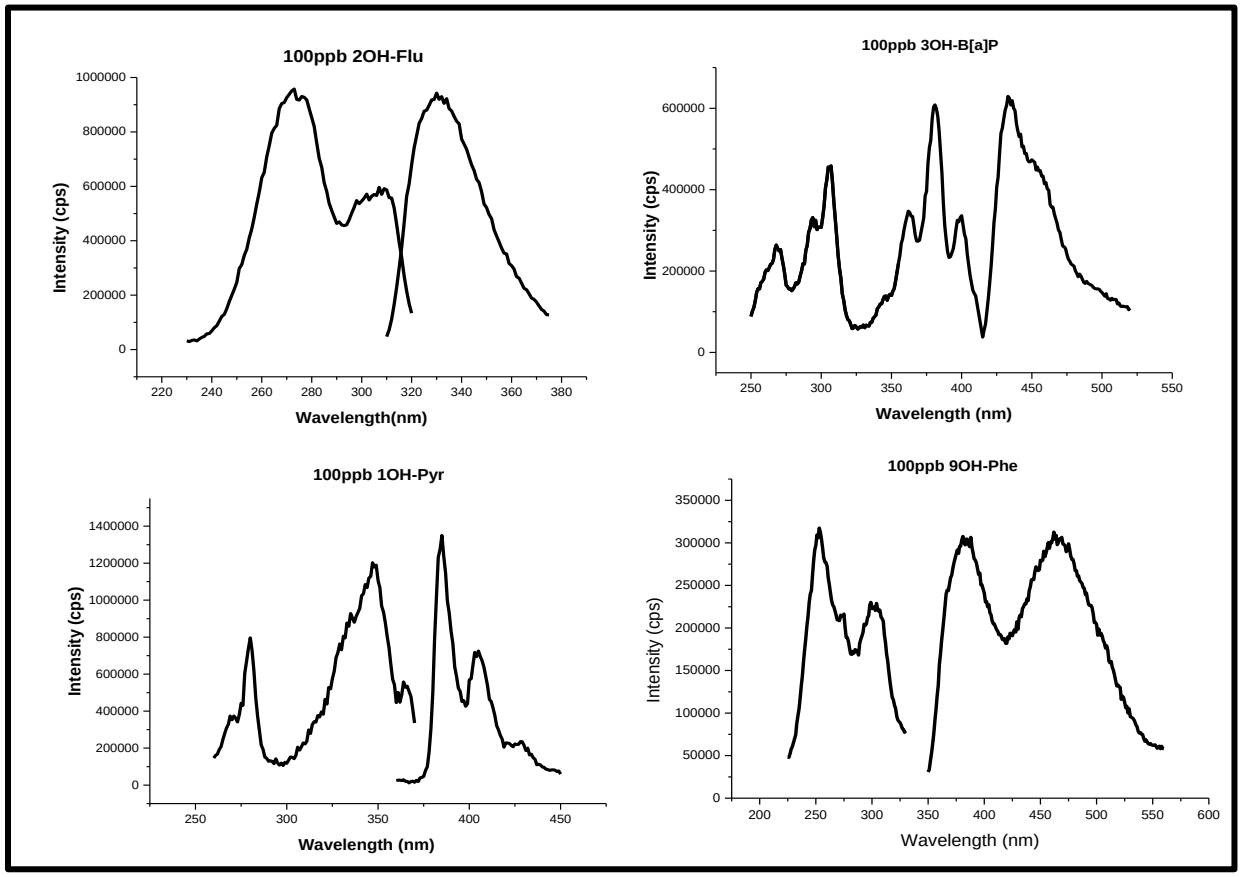

Figure 2.3 Excitation and fluorescence spectra of OH-PAH metabolites in methanol/water (1% v/v)

Table 2.1 summarizes the AFOM of the studied metabolites. All measurements were made at the maximum excitation and fluorescence wavelengths of each compound. Each calibration curve was built with a minimum of five OH-PAH concentrations. For each concentration plotted in the calibration graph, the RTF intensity was the average of three determinations taken from three sample aliquots (N = 3). No efforts were made to experimentally obtain the upper concentration limit of the calibration curve. The correlation coefficients of the

calibration curves were close to unity, indicating a linear relationship between metabolite concentration and signal intensity. The linearity was also evaluated by an ANOVA test as suggested by IUPAC[107] with satisfactory results. The LOD were calculated using the equation LOD = 3 ×SB/m, were S_B is the standard deviation of 16 blank determinations and m is the slope of the calibration curve. The limits of quantitation (LOQ) were calculated with the formula LOQ = 10 × SB/m. The slopes of the calibration curves were obtained with the least squares method [108]. The strong fluorescence intensity resulting from the rigid and delocalized π-electron system of OH-PAH provides LOD and LOQ values at the ng mL^{-1} concentration level.

2.3.2 Extraction efficiency of SPE membranes

The percentages of extraction (%E) were calculated with the formula %E = (I_{BE} – I_{AE} / I_{BE}) x 100, where I_{BE} and I_{AE} refer to the fluorescence signals before and after extraction, respectively. In all cases, the volume of extracted sample was 10mL. The mass of extracted metabolite did not surpass the nominal breakthrough mass (30mg) of extraction membranes [109]. Table 2.2 compares %E values obtained from standard solutions to those from hydrolyzed urine samples. All values are the averages of three aliquots submitted to the entire extraction procedure. Within a confidence interval of 95%, all %E are equivalent to 100% [110]. This fact excludes the possibility of matrix interference on the retention of OH-PAH. Similar results were obtained with other OH-PAH concentrations within the LDR of Table 2.1. Keeping in mind that metabolite elution is not required for the determination of OH-PAH via SPE-RTF, the %E values in Table 2.2 correspond to the analytical recovery of the method.

Table 2.1 Analytical Figures of Merit of OH-PAH in aqueous and synthetic urine solution

PAH Metabolite	1% Methanol – Water					Hydrolysed synthetic urine				
	$\lambda_{exc}/\lambda_{ems}$ (nm)[a]	LDR[b] (ng/mL)	R^2[c]	LOD[d] (ng/mL)	LOQ[e] (ng/mL)	$\lambda_{exc}/\lambda_{ems}$ (nm)[a]	LDR[b] (ng/mL)	R^2[c]	LOD[d] (ng/mL)	LOQ[e] (ng/mL)
2OH-Flu	273/330	1.20 – 100	0.9999	0.36	1.20	275/328	1.05 – 100	0.9992	0.32	1.05
1OH-Pyr	344/386	0.30 – 100	0.9999	0.09	0.30	346/385	0.32 – 100	0.9972	0.10	0.32
3OH-B[a]P	382/434	0.63– 100	0.9947	0.19	0.63	384/430	0.81– 100	0.9940	0.24	0.81
9OH-Phen	303/384	3.00– 100	0.9984	0.90	3.0	307/384	3.82– 100	0.9946	1.14	3.82

[a] *Excitation and emission wavelengths.*

[b] *LDR = linear dynamic range in ng.mL^{-1} extending from the limit of quantification (LOQ) to an arbitrarily chosen upper linear concentration.*

[c] *Correlation coefficient of calibration curve. .*

[d] *Limit of detection calculated as $3xS_B$ / m; where S_B is the standard deviation of 6 blank measurements and m is the slope of the calibration curve*

.[e] *LOQ defined as 3.3 x LOD.*

Table 2.2 Percent (%) Retention of OH-PAH in C_{18} membrane from aqueous and synthetic urine solutions.

PAH Metabolite [a]	%Retention[b]	
	1% methanol- water	Hydrolysed synthetic urine
2OH-Flu	99.5± 0.93	99.2 ± 0.24
1OH-Pyr	99.9± 0.05	99.4 ± 1.32
3OH-B[a]P	99.0 ± 1.19	99.7 ± 0.49
9OH-Phen	99.4 ± 0.99	96.2 ± 1.35

[a] *Concentration are all 50ppb.*
[b] *%Retention = $(I_{before} - I_{after})/ I_{before}$ * 100*

2.3.3 Reproducibility of RTF measurements on extraction membranes

Previous work in our lab studied the deposition pattern of OH-PAHs on extraction membrane surfaces [111]. We monitored the fluorescence images of membranes used to extract trace concentration levels ($ng.mL^{-1}$) of OH-PAHs dissolved in 1% methanol/water (v/v) solutions. Random deposition patterns of OH-PAHs were observed at all concentration levels. The heterogeneous deposition of OH-PAHs on the surfaces of extraction membranes leads to poor reproducibility of measurements. One way to improve precision of measurements is to irradiate the entire area of the solid substrate via laser excitation with a fiber optic probe [111]. With commercial spectrofluorimeters equipped with broad band irradiation sources and excitation monochromators, one possibility is to opening the excitation slits for complete PAH excitation on the extraction membrane. Unfortunately, opening excitation slits compromises

spectral resolution and deteriorates the selectivity of the technique. A practical way to overcome this limitation is to using the sample holder in Figure 2.2. This device optimizes the position of the extraction membrane for maximum fluorescence signal. Maximum intensity results from the irradiation of the membrane area with the highest mass of deposited PAH.

Table 2.3 summarizes the precision of SPE-RTF measurements made with the sample holder in Figure 2.2. All extraction membranes were dissected from 47-mm-diameter disks belonging to the same commercial lot. Three extraction membranes per metabolite (M_1, M_2 and M_3) were used to calculate the average background signals. The same is true for the average intensities of extracted metabolites. Standard deviations from single membrane measurements were based on signal intensities recorded after three repetitive optimizations of the substrate holder position. The relative standard deviations of single membrane measurements were equal or lower than 2%, which demonstrates the reproducibility of the signal optimization procedure. Fluorescence background was observed from all the examined membranes. It consisted of a broad, featureless emission band between 350 and 500nm. Comparison of average background values shows considerable intensity variations with excitation and emission wavelengths. The same is true with their respective standard deviations. As expected, relatively large background variations deteriorate the reproducibility of measurements from extracted metabolites.

Table 2.3 Reproducibility study of OH-PAH on C_{18} membrane

PAH Metabolite	$\lambda_{exc}/\lambda_{ems}$ (nm)[a]	$I_{Background} \pm S_{background}$[c] ($x10^4$)			$I_{OH\text{-}PAH} \pm S_{OH\text{-}PAH}$[c] ($x10^4$)			Average±standard deviation[d] ($x10^5$)	
		M_1	M_2	M_3	M_1	M_2	M_3	$I_{Background}$	$I_{OH\text{-}PAH}$
2OH-Flu	282/330	3.37±0.07 (2.0)[b]	3.27±0.07 (2.1)[b]	3.49±0.05 (1.4)[b]	7.38±0.03 (0.4)[b]	7.15±0.02 (0.3)[b]	7.63±0.02 (0.3)[b]	0.34±0.01 (2.9)[b]	7.39±0.24 (3.2)[b]
1OH-Pyr	348/384	4.82±0.02 (0.4)[b]	5.08±0.05 (1.0)[b]	5.28±0.04 (0.8)[b]	21.2±0.21 (1.0)[b]	22.0±0.20 (0.9)[b]	23.40±0.27 (1.2)[b]	0.51±0.02 (3.9)[b]	22.0±1.10 (5.0)[b]
3OH-B[a]P	383/430	2.95±0.02 (0.7)[b]	3.10±0.04 (1.3)[b]	3.34±0.04 (1.2)[b]	13.9±0.31 (2.2)[b]	12.6±0.31 (2.5)[b]	12.34±0.27 (2.7)[b]	0.31±0.02 (6.4)[b]	12.9±0.83 (6.4)[b]
9OH-Phen	307/382	2.63±0.04 (1.5)[b]	2.85±0.06 (2.1)[b]	2.35±0.01 (0.l)[b]	2.91±0.03 (1.0)[b]	2.39±0.03 (1.2)[b]	2.67±0.04 (1.5)[b]	0.26±0.02 (7.7)[b]	2.60±0.26 (10.0)[b]

[a] *Excitation and emission wavelengths*

[b] *Percent Relative Standard Deviation(% RSD) = (std dev)/(I_{ave}) x 100*

[c] *Average values based on three dependent easurements*

[d] *Average values calculated as $[M_1 + M_2 + M_3]x\ 1/3$; standard deviation $[s_1^2 + s_2^2 + s_3^2]^{1/2}$, where s_1, s_2, and s_3 corresponds to their standard deviations of M_1, M_2 and M_3, respectively*

2.3.4 Fluorescence background treatment of extraction membranes

Several attempts were made to decrease the fluorescence background of commercial membranes. All attempts assumed the presence of at least one inherent impurity as the source of fluorescence background. These included: (a) "pre-flushing" individual membrane disks with the syringe kit using increasing volumes (10, 20 and 30mL) of high purity methanol; (b) ultraviolet irradiation of membrane disks for eight hours in a photochemical reactor equipped with a total of twelve lamps irradiating at 254nm, 300nm and 320nm, and thin-layer chromatography (TLC) of membrane strips using high purity methanol as the mobile phase. All these attempts were chosen based on their previous success for background reduction of paper substrates [59, 83, 89, 112-114].

The best background reductions with extraction membranes were obtained via TLC. Each chromatographic run was carried out with 34mm x 40mm membrane strips immersed 5mm deep in methanol. Visual inspection of membrane strips under an ULTRA-LUM UV-VIS irradiation box equipped with 254 and 365nm revealed the maximum migration distance of the fluorescence background towards the top of the strip after 10-15min of chromatographic run. The membrane disks used for further measurements were cut from the strip area with low fluorescence background. Figure 2.4 correlates the background intensity to the number of TLC runs. Intensities plotted in the graph correspond to average values calculated from 3 individual measurements of 6 membrane disks. The fluorescence background reaches a minimum after 3 chromatographic runs. Based on this fact, all further experiments were than carried out with

extraction disks previously treated with 3 TLC runs.

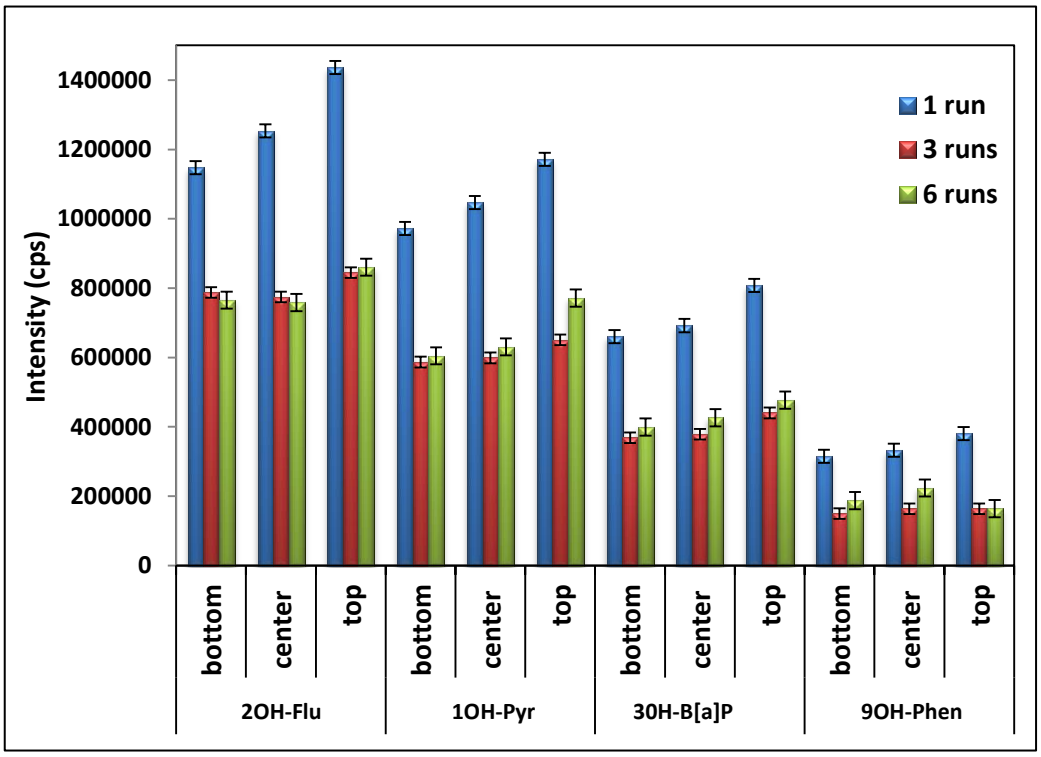

Figure 2.4 Fluorescence background of extraction membranes as a function of chromatographic runs with methanol as the carrier solvent. Wavelength measurements were the following: $\lambda_{exc}/\lambda_{em}$ = 282/330nm 2OH-Flu, $\lambda_{exc}/\lambda_{em}$ = 348/384nm 1OH-Pyr, $\lambda_{exc}/\lambda_{em}$ = 383/430nm 3OH-B[a]P, and $\lambda_{exc}/\lambda l_{em}$ = 307/382nm 9OH-Phen.

2.3.5 AFOM of OH-PAH via SPE-RTF

The SPE-RTF AFOM of the four studied metabolites are summarized in Table 4.4. SPE was carried out with 10mL of standards prepared in 1% methanol/water (v/v). For each concentration plotted in the calibration graph, the RTF intensity was the average of at least three

determinations taken from three extraction disks. The LDR were obtained with a minimum of five OH-PAH concentrations. No efforts were made to experimentally obtain the upper concentration limits of the calibration curve. It is important to note, however, that the highest concentration plotted in each calibration curve did not surpass the breakdown volume of the SPE device [99]. The correlation coefficients of the calibration curves and the slopes of the log-log plots (data not shown) were close to unity, indicating a linear relationship between OH-PAH concentration and fluorescence intensity. Satisfactory results were also obtained by the ANOVA test suggested by IUPAC [107]. The RSD at medium linear concentrations were lower than 10%. The LOD were estimated at the parts-per-billion to sub-parts-per-billion concentration levels. Their comparison to the LOD values in Table 2.1 shows no advantage of pre-concentrating the sample prior to RTF.

Table 2.5 compares the slopes of the calibration curves, blank intensities and their standard deviations from aqueous solutions to those obtained on extraction membranes. The calibration graphs are shown in Figures 2.5 and Figure 2.6. As expected, sample pre-concentration provides 10-fold improvements on the slopes of the calibration curves. The main reason for the lack of LOD improvements is the higher intensities of blank signals and their respective standard deviations on extraction membranes. Better SPE-RTF LOD could have been obtained by extracting 100mL volumes of standard solutions, i.e. an alternative with little appealing in the screening context of human urine samples.

Table 2.4 RTF Analytical Figures of Merit of OH-PAH on C-18 membrane

PAH Metabolite	λ_{exc} / λ_{em} (nm) [a]	LDR [b]	R^2 [c]	LOD [d]
2OH-Flu	282/330	4.33 – 100	0.9987	1.30
1OH-Pyr	348/384	0.85 – 100	0.9944	0.26
3OH-B[a]P	383/430	2.35 – 100	0.9984	0.71
9OH-Phen	307/382	12.83 – 100	0.9969	3.85

[a] *Excitation and emission wavelengths.*

[b] *LDR = linear dynamic range in ng.mL^{-1} extending from the limit of quantification (LOQ) to an arbitrarily chosen upper linear concentration. LOQ defined as 3.3 x LOD.*

[c] *Correlation coefficient of calibration curve.*

[d] *Limit of detection calculated as $3xS_B$ / m; where S_B is the standard deviation of 6 blank measurements and m is the slope of the calibration curve.*

Table 2.5 Slope and Blank Signals of PAH Metabolites in Aqueous Solution and Extraction Membranes

PAH Metabolite	Slope[a]		Ave Blank Intensity $\pm$ Std. Dev[b]	
	H_2O	Membrane	H_2O ($x10^3$)	Membrane ($x10^4$)
2OH-Flu	8.6×10^2	7.2×10^3	1.90 ± 0.10	3.5 ± 0.31
1OH-Pyr	2.4×10^3	3.2×10^4	0.62 ± 0.07	3.9 ± 0.29
3OH-B[a]P	1.6×10^2	1.3×10^4	0.70 ± 0.09	3.4 ± 0.31
9OH-Phen	5.8×10^2	2.4×10^3	9.2 ± 0.17	2.5 ± 0.31

[a] *Slope of linear dynamic range obtained via the least squares method.*
[b] *Average values based on three individual measurements recorded from extraction membranes submitted to the entire extraction procedure.*

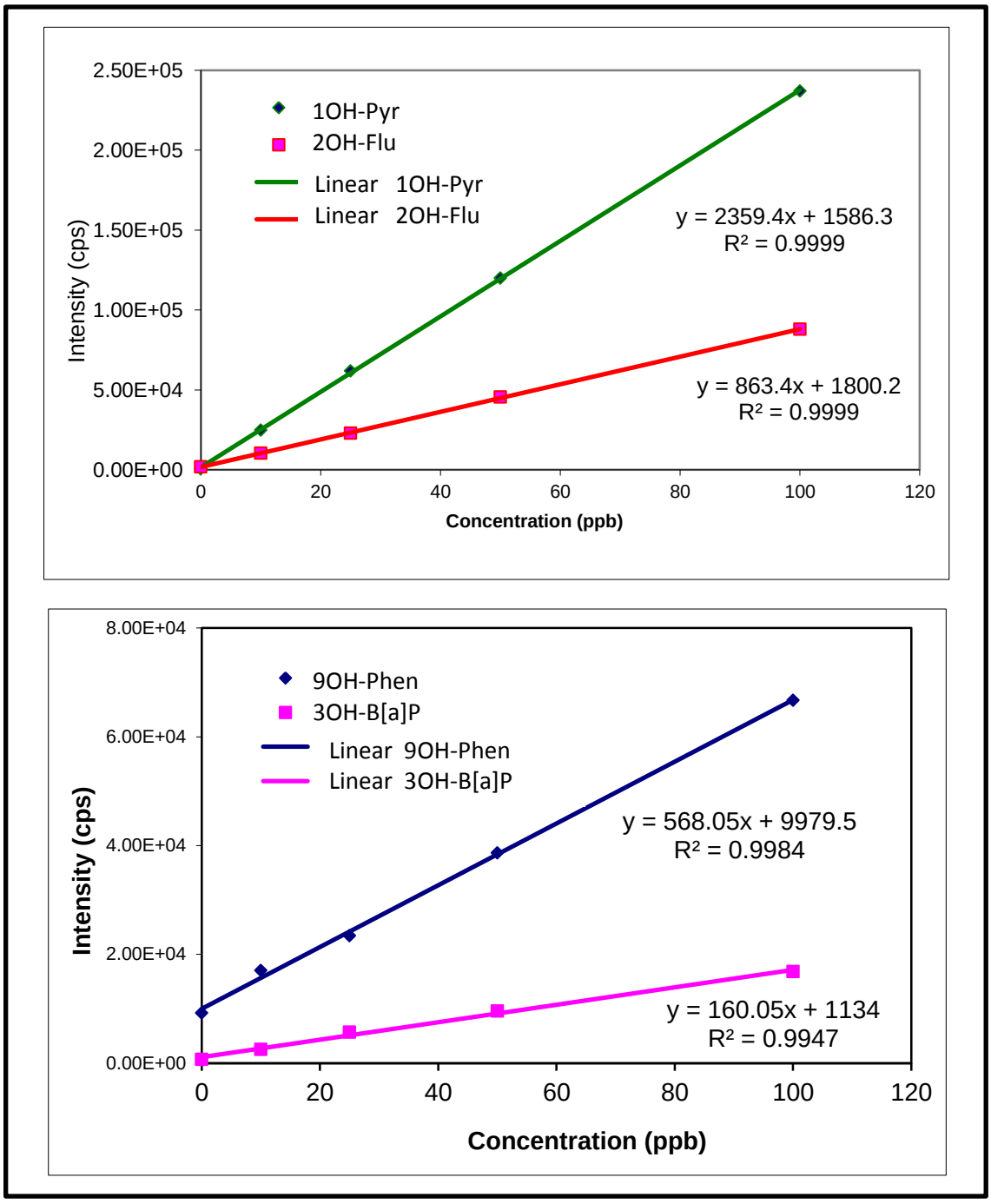

Figure 2.5 Calibration curve of studied metabolites 1% methanol/water (v/v).

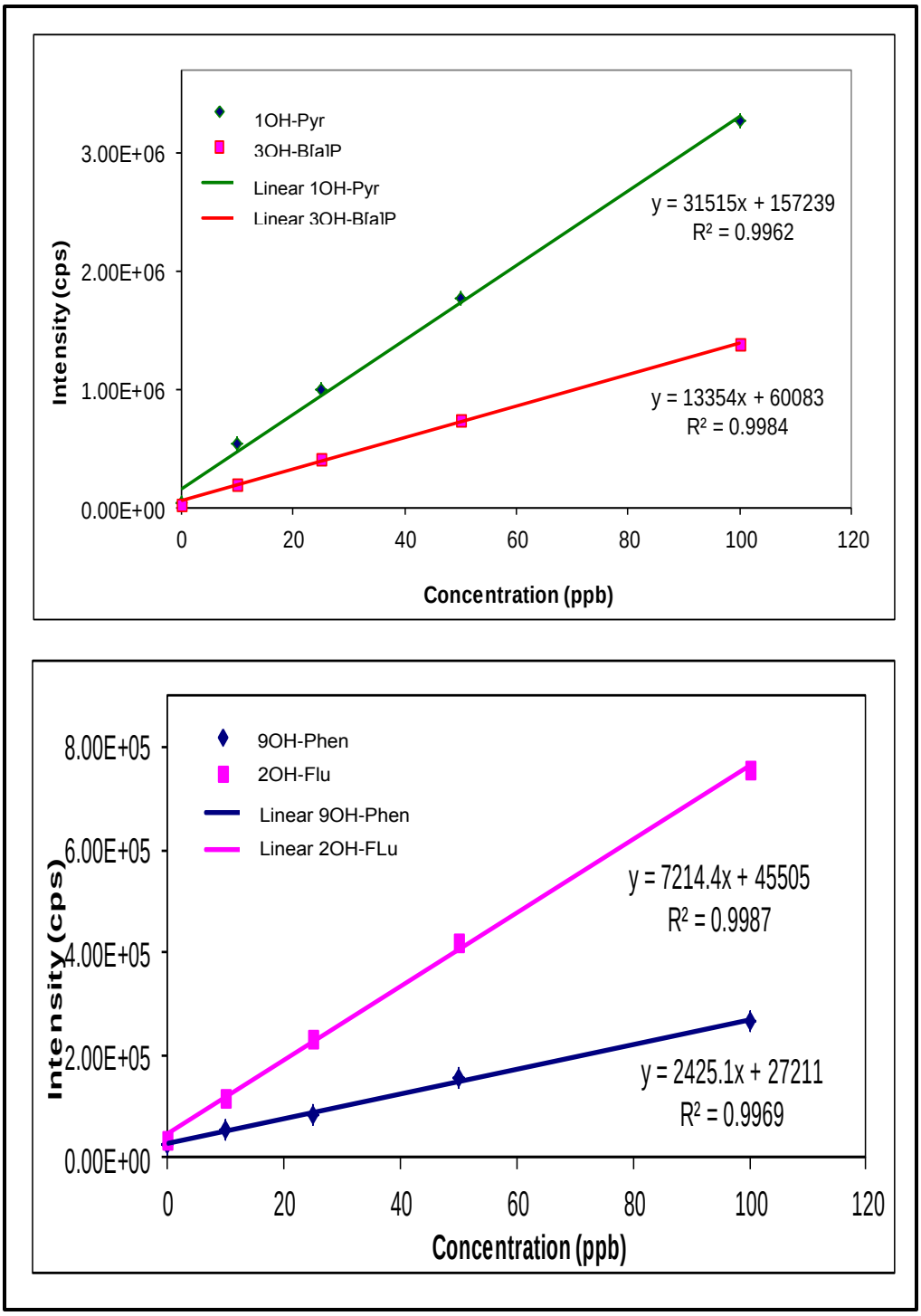

Figure 2.6 Calibration of studied metabolites in C_{18} membrane

2.3.6 Background correction via ALS

The ALS algorithm uses the Whittaker smoother for discrete (time) series, which minimizes the function[101]:

$$Q = \sum_{i} \nu_i (y_i - f_i)^2 + p \qquad \textbf{(2.1)}$$

where y is the data (experimental signal), f a smooth trend (or baseline estimation), ν prior weights, and p the asymmetry parameter. The successful implementation of ALS to the background correction of extraction membranes was achieved with a smoothing parameter equal to 1 x 10^7, an asymmetry parameter equal to 0.001, an order of differences in penalty equal to 3 and a single regularization parameter, whose value was 1. Figure 2.7 provides a visual demonstration of the clear improvement upon ALS implementation. The background intensity(I_B) of extraction membranes (see Figure 2.7)was considerably reduced and so it was the standard deviation (S_B) of the average background signal. At the maximum fluorescence wavelength of 1OH-Pyr (380nm), the I_B and S_B values before and after ALS treatment were 4.11x10^5 ± 0.44x10^5 counts per second (cps) and 5.4 10^2 ± 2.09 x 10^2 cps, respectively. Table 6 summarizes the AFOM obtained via SPE-RTF-ALS. Comparison to Table 5 reveals LOD improvements ranging from 79.8x (2OH-Flu) to 158.8x (1OH-Pyr). The LOD in Table 2.6 meet the expectations for the analysis of OH-PAH in urine samples.

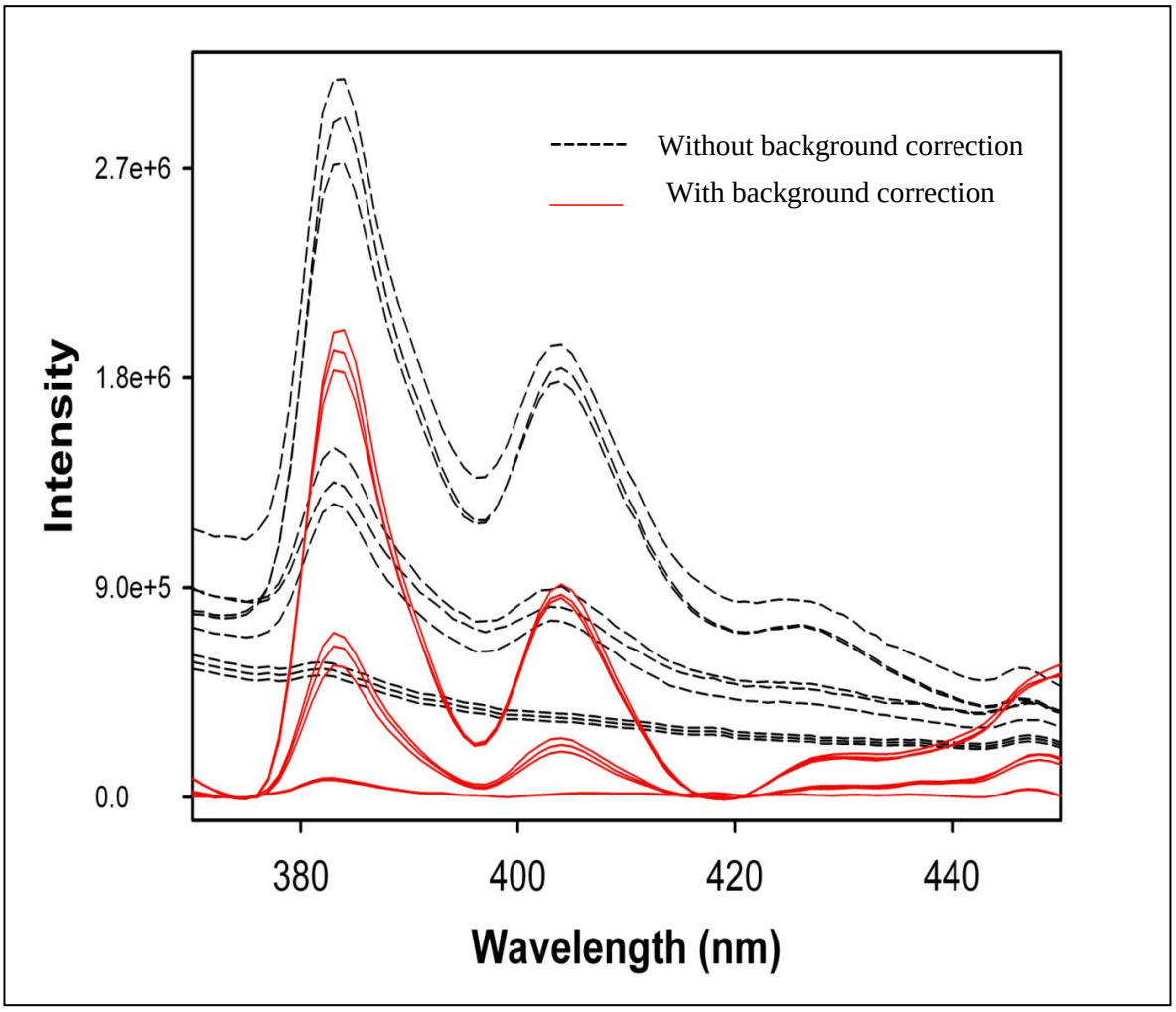

Figure 2.7 Fluorescence spectra of 2.5 and 5 ng mL^{-1} of 1OH-Pyr recorded from extraction membranes with and without background correction.

Table 2.6 RTF Analytical Figures of Merit of OH-PAH on C-18 membrane with background correction

PAH Metabolite	l_{exc} / l_{em} *(nm)* [a]	*LDR* [b]	R^2 [c]	*LOD* [d]
2OH-Flu	282/330	0.17 – 5.0	0.9939	0.057
OH-Pyr	348/384	0.006 – 5.0	0.9944	0.0017
3OH-B[a]P	383/430	0.25 – 5.0	0.9949	0.0075
9OH-Phen	307/382	0.036 – 5.0	0.9951	0.011

[a] *Excitation and emission wavelengths.*

[b] *LDR = linear dynamic range in ng.mL^{-1} extending from the limit of quantification (LOQ) to an arbitrarily chosen upper linear concentration. LOQ defined as 3.3 x LOD.*

[c] *Correlation coefficient of calibration curve.*

[d] *Limit of detection calculated as $3xS_B$ / m; where S_B is the standard deviation of 6 blank measurements and m is the slope of the calibration curve.*

2.4 Conclusion

Several features make SPE-RTF spectroscopy a well-suited approach for screening OH-PAH in urine samples. Its straightforward experimental procedure is attractive for routine analysis of numerous samples. The direct determination of OH-PAH on the surface of the extraction membrane eliminates the need for subsequent elution steps and provides excellent (~ 100%) metabolite recoveries. Acceptable precision for analytical work is possible with the aid of a substrate holder specifically designed for manual optimization of maximum fluorescence signals. Background correction of extraction membranes via ALS provides LOD at the parts-per-trillion concentration level. With 10mL of urine samples, the LOD varied from 60 (2OH-Flu) to 2 $pg.mL^{-1}$ (1OH-Pyr). These values compare favorably to LOD previously reported via other methods of analysis, including HPLC[48, 115-118] and RTF- excitation-emission matrix spectroscopy of SPE extracts[100].

CHAPTER 3: MULTI-WAY PARTIAL LEAST-SQUARES AND RESIDUAL BI-LINEARIZATION FOR THE DIRECT DETERMINATIONN OF MONO-HYDROXY POLYCYCLIC AROMATIC HYDROCARBONS ON OCTADECYL MEMEBRANES VIA ROOM TEMPERATURE FLUORESCENCE EXCITATION EMISSION MATRICES

Goicoechea HC, Calimag-Williams K, and Campiglia AD. Talanta 85(4):1805. 2011

3.1 Introduction

The previous chapter reported the first application of SPE-RTF to the analysis of 2OH-Flu, 9OH-Phen, 1OH-Pyr and 3OH-B[a]P in urine samples .[3] Its successful application was made possible with the aid of a sample holder specifically designed to improve the reproducibility of measurements on solid substrates. Background correction of extraction membranes was carried out with the aid of ALS, a smoothing algorithm originally devised for baseline correction of chromatographic data [101] and often applied to matrix interference in chromatographic analysis [102, 119]. Recovery values varied from 99.0 ± 1.2% (3OH-B[a]P) to 99.9 ± 0.05% (1OH-Pyr). The new sample holder improved the precision of measurements for analytical use. RSD of the studied metabolites varied from 3.5% (2OH-Flu) to 9.5% (9OH-Phen). The application of ALS to SPE-RTF improved the LOD by approximately two orders of magnitude. With only 10mL of urine sample, the LOD of OH-PAH varied from 57pg.mL^{-1} (2OH-Flu) to 2pg.mL^{-1} (1OH-Pyr).[3] The individual determination of any given metabolite in the presence of the other three was not attempted due to the strong overlapping we observed among their excitation and fluorescence spectra.

In this chapter, we investigate the analytical potential of EEM data formats for the direct

determination of 2OH-Flu, 9OH-Phen, 1OH-Pyr and 3OH-B[a]P without previous chromatographic separation. Spectral overlapping of EEMs was resolved via second order chemometric analysis. Coupling multidimensional data formats – such as EEMs - with chemometric algorithms carrying the second order advantage permits the determination of calibrated species in the presence of un-calibrated concomitants, an immensely useful property in the present content. EEMs have been traditionally processed by the application of two well-known algorithms: parallel factor (PARAFAC)[120] or MCR-ALS[121]. Recently attention has been paid to alternative second order multivariate calibration algorithms based on latent-structured methodologies, namely U-PLS/RBL and N-PLS/RBL.[122-125] PLS-based methods appear to be more flexible and provide better figures of merit than their competitors [124, 125]. U-PLS/RBL was recently applied in our lab to the direct analysis of OH-PAH in SPE extracts (methanol solutions).[1] Here, we apply N-PLS/RBL to the analysis of OH-PAH adsorbed on extraction membranes and compare its performance to the well-established MCR-ALS algorithm. Background correction of extraction membranes was carried out with a new ALS procedure adapted to second order data. [101] Potential interference from naproxen, ibuprofen, diclofenac and amoxicillin (see Appendix B for molecular structures) –over-the-counter pharmaceutical drugs - was investigated as well. The AFOM obtained via a two-step experimental procedure make this approach a well-suited tool for the routine analysis of OH-PAH in numerous samples.

3.2 Theory

3.2.1 NPLS/RBL

Different to other second order algorithms, N-PLS/RBL includes concentration information only in the calibration step. The *I* calibration data arrays and the vector of calibration concentrations **y** (size *I*×1) are combined to generate regression coefficients **v** (size *A*×1) and two sets of loadings, namely **W***j* and **W***k* of sizes *J*×*A* and *K*×*A*. *J* and *K* refer to digitized wavelengths in emission and excitation, respectively.[120] *A* is the number of latent factors, which is usually selected by leave-one-out cross-validation. In the absence of unexpected components, the analyte concentration in the test sample can be estimated with equation 3.1:

$$\mathbf{y_u} = \mathbf{t^T_u}\,\mathbf{v} \qquad \textbf{(3.1)}$$

where $\mathbf{t}_u$ is the test sample score vector obtained by appropriate projection of the test data onto the calibration loading matrices.

Equation 1 does not apply in the presence of unexpected components in the test sample. In those cases, the residuals from the N-PLS modeling of the test sample signals should be considered before making predictions. In comparison to typical instrumental noise levels, the residuals contained in the matrix $\mathbf{E}_p$ (see equation 3.2) should be abnormally large:

$$s_p = ||\mathbf{E_p}||/(JKI - A)^{1/2} = ||\mathbf{X_u} - \mathbf{reshape}\{\mathbf{t_u}[(\mathbf{W}_j| \otimes |\mathbf{W}_k)]\}||/(JKI - \mathbf{A})^{1/2} \qquad \textbf{(3.2)}$$

In this equation, "reshape" indicates transforming a *JK*×1 vector into a *J*×*K* matrix and |⊗| is the Kathri-Rao operator. In order to handle the presence of unexpected constituents, residual bi-linearization resorts to the principal component analysis (PCA) of their contribution by minimizing the computed residuals while fitting the sample data to the sum of the relevant

contributions. For N-PLS, the sum of contributions is given by equation 3.3:

$$\mathbf{X}_u = \text{reshape}\{\mathbf{t}_u[(\mathbf{W}_j| \otimes |\mathbf{W}_k)]\} + \mathbf{B}_{unx}\mathbf{G}_{unx}(\mathbf{C}_{unx})^T + \mathbf{E}_u \quad \textbf{(3.3)}$$

where matrices $\mathbf{B}_{unx}$, $\mathbf{G}_{unx}$ and $\mathbf{C}_{unx}$ are obtained by singular value decomposition (SVD) of the error matrix $\mathbf{E}_p$:

$$\mathbf{B}_{unx}\mathbf{G}_{unx}(\mathbf{C}_{unx})^T = \text{SVD}(\mathbf{E}_p) \quad \textbf{(3.4)}$$

During the RBL procedure, the loadings are kept constant at the calibration values, and $\mathbf{t}_u$ is varied until the final RBL residual error s_u is minimized using a Gauss–Newton procedure:

$$s_u = ||\mathbf{E}_u||/(JKI)^{1/2} \quad \textbf{(3.5)}$$

Analyte concentrations are then obtained by introducing the values of $\mathbf{t}_u$ vectors into equation 3.1. Due to the use of PCA, retrieved RBL profiles do not necessarily resemble true spectra. The aim of RBL is to minimize the residual error term s_u to a level compatible with the degree of instrumental noise. With this in mind, one should always explore an increasing number of unexpected components and select the simplest model giving a s_u value statistically similar to the minimum.

3.2.2 MCR-ALS

In this algorithm, each matrix data (EEM) is unfolded in a column-wise augmented matrix **D**, instead of forming a three-dimensional data array. The bilinear decomposition of the augmented matrix **D** is carried out according to the expression:

$$\mathbf{D} = \mathbf{C} \times \mathbf{S}^T + \mathbf{E} \quad \textbf{(3.6)}$$

where **D** rows refer to emission spectra as a function of excitation wavelengths, **C**

columns contain the excitation profiles of the compounds involved in the process and the **S** columns their related emission spectra, and **E** is the matrix of residuals not fitted by the model. The appropriate dimensions of **D**, **C**, **S** and **E** are thus $K\times(1 + I)\times J$, $K\times(1 + I)\times F$, $J\times F$ and $K\times(1 + I)\times J$ respectively (I = number of training samples, J = number of digitized emission wavelengths, F = number of extracted factors and K = number of digitized excitation wavelengths). Decomposition of **D** is achieved by iterative least-squares minimization of $\| \mathbf{E} \|$ under suitable constraining conditions, i.e. non-negativity in spectral profiles. It is important to keep in mind that MCR-ALS requires initialization with system parameters as close as possible to the final results. In the column-wise augmentation mode, the use of spectra is required, which should be preferentially obtained from pure analyte standards.

3.2.3 ALS Background Correction Adapted to Second Order Data

The background matrix **F** ($J\times K$) is estimated from the data matrix **M** ($J\times K$), where J and K are the number of digitized wavelengths in the emission and the excitation ranges, respectively. With this purpose, a $\mathbf{B}_1$ ($L\times J$) spline basis matrix along the rows of the **M** matrix and a $\mathbf{B}_2$ ($M\times K$) spline basis matrix along the columns of the **M** matrix are used along with a compromise of 10 basis function[126], i.e., L = M = 10. **F** can be represented as:

$$f_{\mathrm{j,k}} = \sum_{\mathrm{L,M}} \mathrm{b1_{LJ}\,b2_{MK}}\, a_{\mathrm{LM}} \qquad \textbf{(3.7)}$$

where a_{LM} is the (L,M) element of an **A** matrix containing the regression coefficients, which can be calculated by minimizing the following cost function:

$$Q = \sum_{L,M} \nu_{JK} (y_{JK} - f_{JK})^2 + p \qquad \textbf{(3.8)}$$

In equation 8, y is the experimental signal, f is a smooth trend (the baseline approximation), and ν are the prior weights. The elements of ν should have large values in the parts of the signal where it is allowed to affect the estimation of the baseline. Considering the choice of the following asymmetric weights: $\nu_{JK} = p$ if $\nu_{JK} > f_{JK}$ and $\nu_{JK} = 1 - p$ if $\nu_{JK} \leq f_{JK}$ with $0 < p < 1$, positive deviations from the trend will result in weights different from negative residuals. Experience shows that starting from $\nu \cong 1$, and iterating between the two computations, quickly and reliably leads to a solution in about 10 iterations. The penalty term in equation 8 is defined as follows:

$$p = \left[\sum_{L} (\Delta_1{}^{d} \mathbf{a}_{.L})^2 + \sum_{L} (\Delta_2{}^{d} \mathbf{a}_{.M})^2 \right] \qquad \textbf{(3.9)}$$

where Δ_1 and Δ_2 are differences of order d calculated for each column ($\mathbf{a}_{.L}$) and row ($\mathbf{a}_{.M}$) of **A**, respectively. If different values are used for the regularization parameter Δ, the penalty may have different influence for vertical and horizontal directions.

3.3 Experimental

3.3.1 Instrumentation

Excitation spectra, fluorescence spectra and signal intensities were recorded with a commercial spectrofluorimeter and the aid of an in-house sample holder previously described in previously described in chapter 2.

3.3.2 Reagents

All solvents were Aldrich HPLC grade. All chemicals were analytical-reagent grade and utilized without further purification. Unless otherwise noted, Nanopure water was used throughout. 2OH-Flu, 1OH-Pyr, 9OH-Phen and naproxen were purchased from Sigma-Aldrich. 3OH-B[a]P was from Midwest Research Institute. All other chemicals were purchased from Fisher Chemical. The Sep-Pak C18 membranes were purchased from Varian/Agilent. The synthetic urine solution was manufactured by RICCA Chemical Company (Arlington, TX) and purchased from Fischer Scientific. Its chemical composition mimicked main components of human urine at the concentrations found in healthy urine samples.

Note: Use extreme caution when handling OH-PAH known to be extremely toxic.

3.3.3 Preparation of Stock Solutions

Stock solutions of PAH metabolites were prepared by dissolving pure standards in methanol. Naproxen stock solutions were prepared in methanol. All stock solutions were kept in the dark at 4^{o}C. Prior to use, stock solutions were monitored via RTF spectroscopy for possible photo-degradation of metabolites. Spectral profiles and fluorescence intensities of stock solutions remained the same for a period of six months. Working solutions of OH-PAH and naproxen were prepared daily by serial dilution with methanol.

3.3.4 Hydrolysis of Urine Samples

Urine samples were spiked with micro-litters of stock solutions of appropriate

concentrations and equilibrated for 30 min to allow for the interaction of metabolites and naproxen with urine components such as urea and various salts. Then 500 μL of 0.1 M HCl was added to the sample and the mixture was buffered with 500 μL of 0.05 M potassium biphthalate sodium hydroxide buffer (pH 5.0). The buffered sample was shaken for 30 min at 1400 rpm to allow for urine hydrolysis.

3.3.5 Synthetic mixtures of OH-PAHs and spiked urine samples

All metabolite concentrations were within toxicological relevant levels. Their values were adjusted to record EEM with both their true fluorescence fingerprints and fluorescence profiles with significant spectral contributions from fluorescence background and instrumental noise. Validation set #1 consisted of six synthetic mixtures (S1 – S_6) containing the four OH-PAH at 2 to 4ng.mL^{-1} final concentrations in methanol-water (1% v/v). Validation set #2 consisted of six urine samples (U1 – U6) previously spiked with the four OH-PAHs at 2 to 4ng.mL^{-1} final concentrations. Validation set # 3 consisted of three urine samples (UN1 – UN3) previously spiked with the four OH-PAH at 2 to 4ng.mL^{-1} final concentrations and naproxen at either 0.2 or 0.5μg.mL^{-1} final concentration. Naproxen concentrations include the usual values found in urine samples from patients taking this anti-inflammatory drug.

3.3.6 SPE

SPE was carried out with the syringe kit shown in Figure 2.1 (from Chapter 2 of this dissertation). Positive pressure was used to force all liquid solutions through the disk. Prior to

sample application, the extraction membrane was conditioned with 5mL of methanol and 5mL of water. Optimization of experimental parameters concerning the retention of PAH metabolites led to the following procedure: aqueous metabolite solutions or synthetic urine samples were processed through extraction membranes previously conditioned with 5 mL methanol and 5 mL water. Following sample extraction, each membrane was sequentially rinsed with 10 mL water and 10 mL of 20% methanol/water. Void water was mechanically removed with a 100mL syringe forcing three 100mL volumes of air through the disk.

3.3.7 Software

Routines for data pre-treatment and processing were written in MATLAB[104]. Baseline routines for matrix background correction were adapted from previously reported routines for baseline correction of chromatographic data[101]]. Implementation of the ALS algorithm included a smoothing parameter equal to 1 x 10^7, an asymmetry parameter equal to 0.005, an order of differences in penalty equal to 3 and a single regularization parameter equal to 1. MCR-ALS was applied with a graphical interface available in the literature[127]. N-PLS/RBL was implemented with an integrated chemometric toolbox (MVC2) previously currently available in the literature[128, 129].

3.4 Results and Discussion

The initial survey of room-temperature excitation and fluorescence spectra on C18 membranes was carried out by extracting OH-PAH from methanol/water (1% v/v) solutions and hydrolyzed urine samples. All spectra were collected using 2nm excitation and emission band-

pass. No attempts were made to adjust slit widths for optimum spectral resolution, nor were the spectra corrected for instrumental response. The 2nm band-pass provided signal-to-blank ratios higher than 3 for all the studied metabolites at the parts-per-billion ($ng.mL^{-1}$) concentration level. Figures 3.1A-D compare their spectral features recorded from C18 membranes previously used to extract methanol/water (1% v/v) solutions. The strong overlapping that exists among the spectra of OH-PAH prevents the direct determination of individual metabolites with a single set of excitation and fluorescence wavelengths. No significant changes were observed from spectra on C18 membranes previously used to extract hydrolyzed spiked urine samples.

Naproxen, ibuprofen, diclofenac and amoxicillin were selected to modeling the pharmacological interference that might occur in the simultaneous determination of co-extracted metabolites from urine samples of unhealthy individuals (see Appendix B of this dissertation for their molecular structures). Figure 3.2A-D shows their excitation and fluorescence spectra recorded from C18 membranes previously used to extract a standard solution of the compound in methanol/water (1% v/v). Fluorescence spectra recorded from spiked and hydrolyzed urine samples looked virtually the same. Comparison to Figures 3.1A-D confirms the strong spectral overlapping that exists with the four studied metabolites.

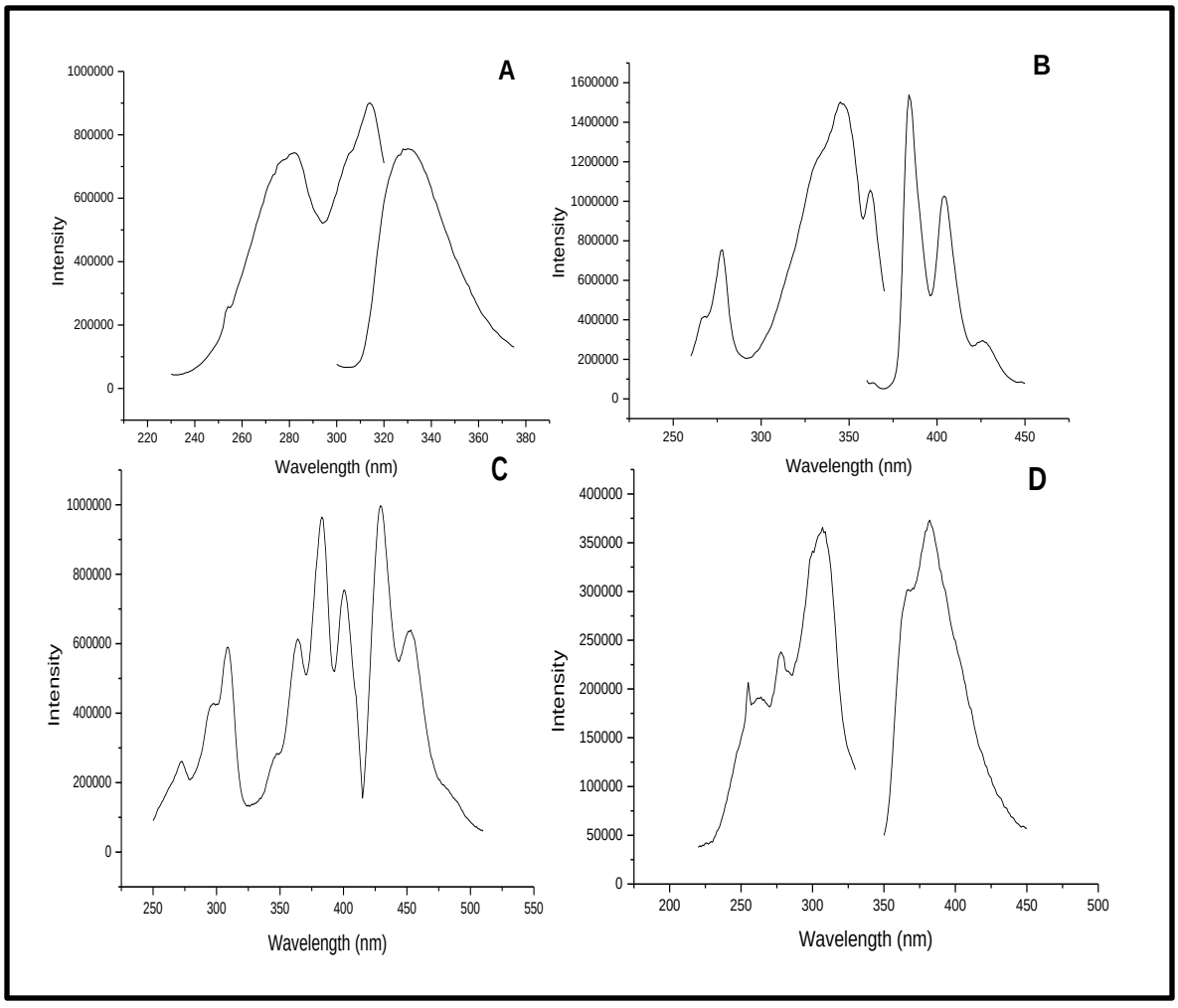

Figure 3.1 Excitation and Emission Fluorescence spectra of (A) 2OH-Flu (100 μg L^{-1}, $\lambda_{exc}/\lambda_{em}$ = *282nm/330nm);* (B) 1OH-Pyr (100 μg L^{-1}, $\lambda_{exc}/\lambda_{em}$ = *348nm/384nm);* (C) 3OH-B[a]P (100 μg L^{-1}, $\lambda_{exc}/\lambda_{em}$ = *383nm/430nm); and* (D) 9OH-Phen (100 μg L^{-1}, $\lambda_{exc}/\lambda_{em}$ = *307nm/382nm)* on extraction membranes.

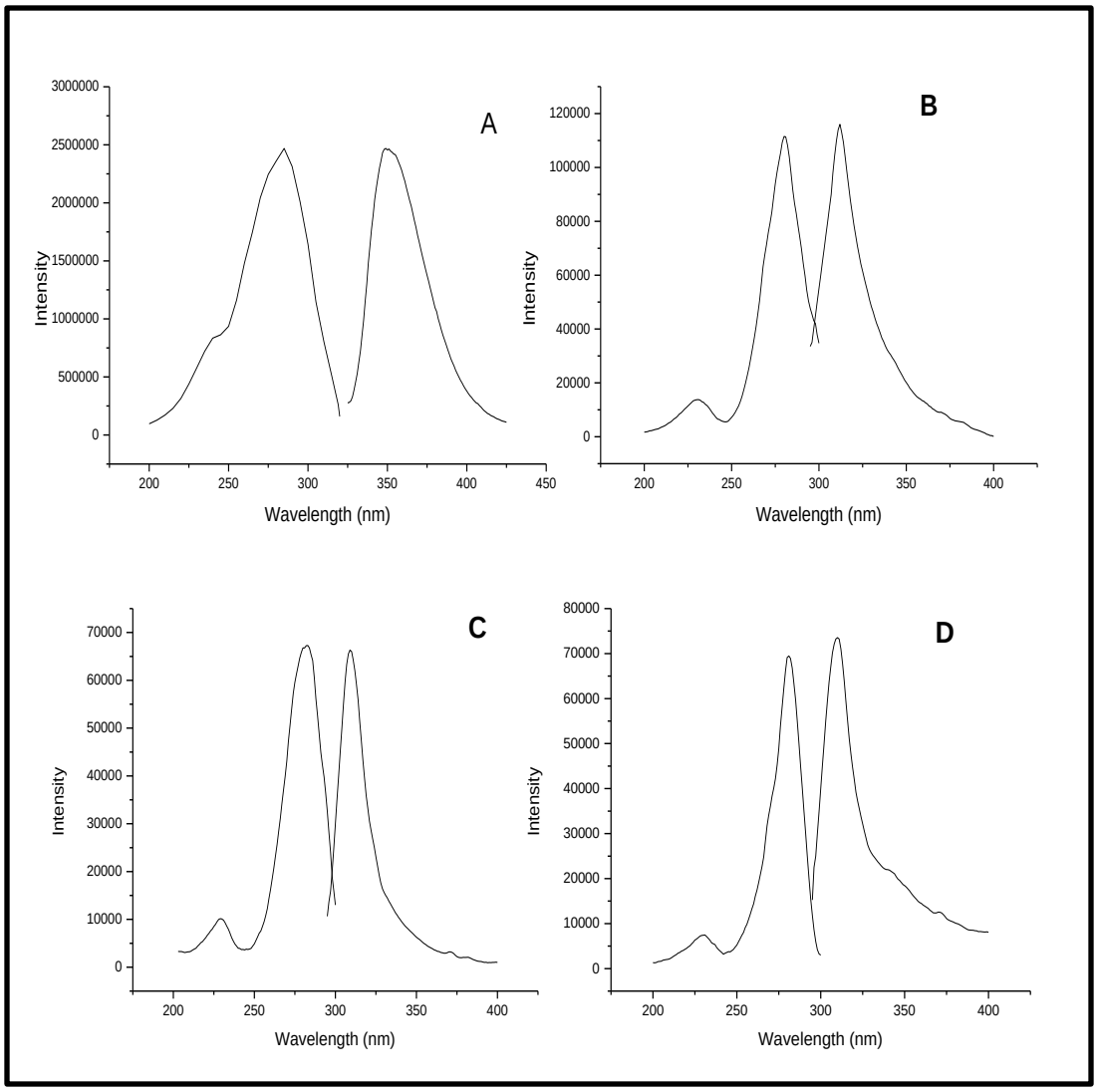

Figure 3.2 Excitation and Emission Fluorescence spectra of (A) Naproxen (10 μg L $^{-1}$, λ_{exc} /λ_{em} = *284nm/350nm) ;* (B) Ibuprofen (100μg L $^{-1}$, λ_{exc} /λ_{em} = *280nm/308nm);* (C) Diclofenac (10 μg L $^{-1}$, λ_{exc} /λ_{em} = *282nm/308nm); and* (D) Amoxicillin (50 mg L $^{-1}$, λ_{exc} /λ_{em} = *280nm/310nm)* on extraction membranes.

3.4.1 EEM background corrections on extraction membranes

As previously mentioned, the main disadvantage of SPE-RTF for quantitative analysis at trace concentration levels is the background interference from extraction membranes. The presence of broad, featureless excitation and emission bands deteriorates the LOD and often interferes with the determination of fluorescence emitters at the $ng.mL^{-1}$ concentration level. Several attempts have been made in our lab to reduce the fluorescence background of extraction membranes[3]. Because the best results were obtained via thin-layer chromatography (TLC), all further experiments in this chapter are carried out with extraction disks previously treated via TLC. The treatment consists of immersing membrane strips (34mm x 40mm) 5mm deep in methanol three consecutive times.

Figure 3.3A depicts a three-dimensional plot of the RTF-EEM recorded from an extraction membrane used to extract 10mL of a hydrolyzed urine sample previously spiked with the four studied metabolites. The landscape corresponds to a data matrix **M** (161x21), which was recorded using 5nm (excitation) and 1nm (emission) steps. The excitation and emission wavelength ranges were selected to provide a visual comparison of the membrane background and the fluorescence signal of the metabolites mixture. The background contribution to the total fluorescence of the sample is significant within the entire wavelength ranges of the EEM. The matrix background estimation **F** (161×21) obtained via ALS is shown in Figure 3.3B. The estimated matrix was obtained by setting L and M to a value of 10 and the asymmetry parameter (p) in equation 8 to 0.005. The subtraction of the **F** matrix to the **M** matrix provides the background corrected matrix shown in Figure 3.3C. All further experimental EEM were

background subtracted generating an ALS matrix within the excitation and emission wavelength ranges of interest.

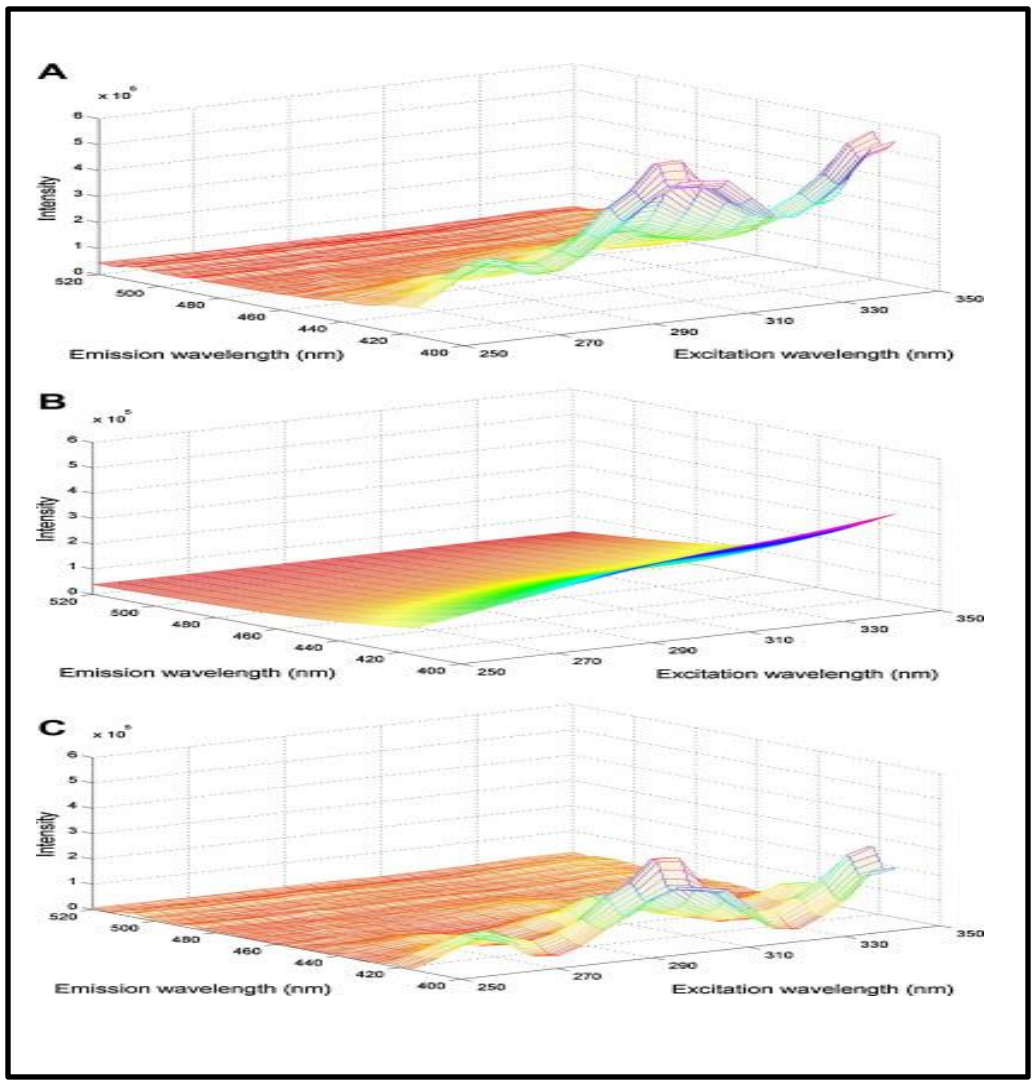

Figure 3.3 (A) RTF-EEM from a C18 membrane used to extract 10 mL of hydrolyzed urine sample previously spiked with the four studied metabolites at the ng mL^{-1}concentration level. Excitation and emission steps = 5 and 1 nm, respectively. (B)Background EEM estimated via ALS.(C) EEM resulting from (A) to (B).

3.4.2 Second order multivariate calibration

3.4.2.1 N-PLS/RBL

The first step in the application of N-PLS/RBL was the assessment of the optimum number of calibration factors (*A*). This was done by resorting to the leave-one-out cross-validation procedure, which computes the ratios $F(A)$ = PRESS(A<A*)/PRESS(A); where PRESS is the predicted error sum of squares, defined as PRESS = $\sum(c_{i,act} - c_{i,pred})^2$, A is a trial number of factors and A* corresponds to the minimum PRESS. The number of optimum factors was selected as the one leading to a probability of less than 75% and F>1. Since the present study was carried out with four metabolites, A was equal to 4. Because the blank signal was eliminated by the pre-treatment procedure, an additional latent variable was not necessary to model the variability of the data by N-PLS.

The next step was to estimate the number of unexpected components in validation sets #2 and #3 via the post-calibration RBL procedure. This was done by considering the variation of the residual (s_u) in Equation 3.5 as a function of the trial number of unexpected components. The stabilization of the residual around the instrumental noise (~ 8.2 x10^3 counts per second) suggested a single unexpected component for urine samples in the absence of naproxen and two unexpected components for samples containing naproxen. Figures 3.4A and B show the emission and excitation profiles obtained by residual bi-linearization of naproxen and a urine unknown component. The good agreement that exists among the predicted and the experimental profiles of naproxen demonstrates the success of RBL in extracting the spectral contribution of an unknown component from the sample. This ability – which refers to the second-order advantage with an

accurate N-PLS algorithm - makes prediction possible with no potential interference from the sample.

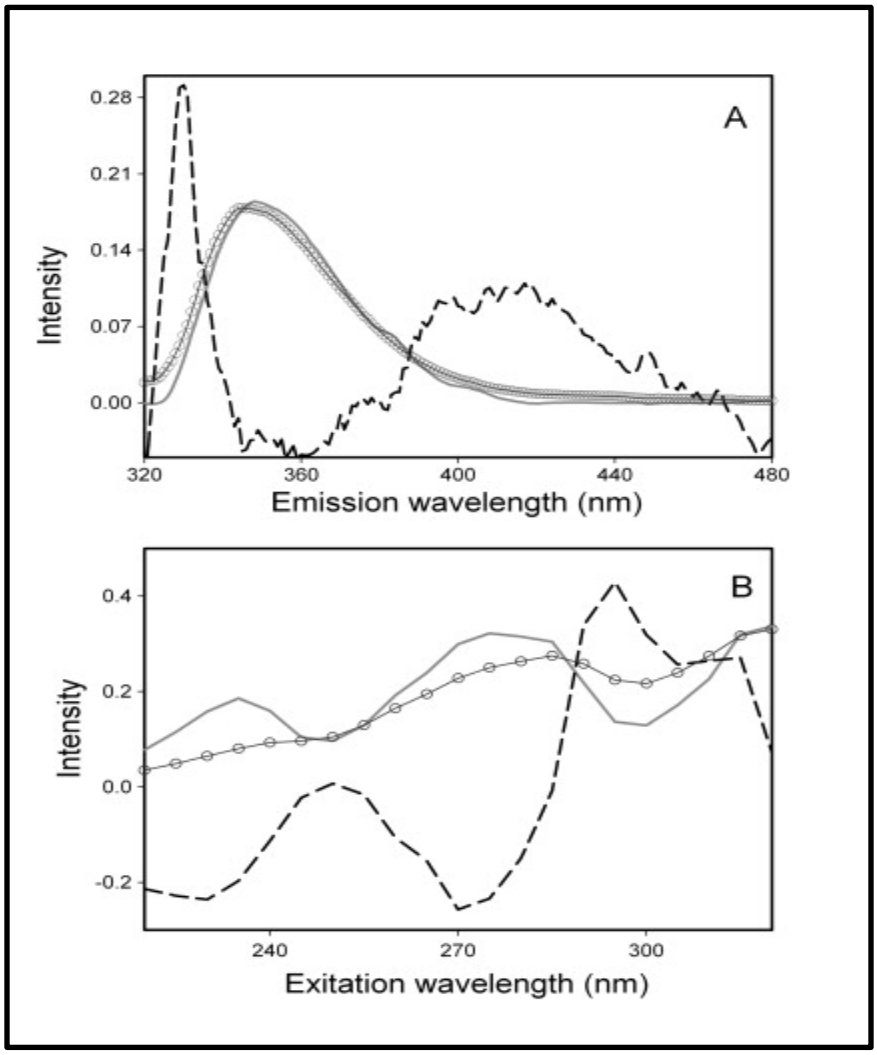

Figure 3.4 Fluorescence (A) and excitation (B) profiles obtained by residual bilinearization of naproxen (solid trace; blue = predicted; red = experimental) and a urine unknown component (broken trace). Excitation and emission bandpass = 2 nm were used to record spectra.

After correcting the N-PLS scores of validation sets #2 and #3 with the post-calibration RBL procedure, we then applied Equation 1 to predict the concentrations the four metabolites in all the studied samples. Table 3.1 compares the prediction results to the nominal concentrations of the spiked metabolites. The average recoveries for validation set #1 (S1 – S6) were as follows: 2OH-Flu = 109.7 ± 19.0, 1OH-Pyr = 95.5 ± 7.4, 3OH-B[a]P = 96.7 ± 8.7 and 9OH-Phen = 98.7 ± 11.0. Acceptable predictions were also obtained with validation set #2, i.e. urine samples in the absence of naproxen (U1 – U6): 2OH-Flu = 99.5 ± 10.0, 1OH-Pyr = 102.7 ± 4.0, 3OH-B[a]P = 91.6 ± 8.0 and 9OH-Phen = 92.9 ± 9.0. The worst results were obtained with validation set #3, i.e. urine samples containing naproxen (UN1 – UN3): 2OH-Flu = 92.0 ± 10.0, 1OH-Pyr = 81.4 ± 4.0, 3OH-B[a]P = 86.1 ± 3.0 and 9OH-Phen = 83.9 ± 7.0.

Figure 3.5A-C provides a visual comparison of RTF EEM recorded from S1 (synthetic metabolite mixture prepared in 1% methanol, no naproxen), U1 (synthetic metabolite mixture in urine, no naproxen) and UN1 (synthetic metabolite mixture in urine and 200ng.mL^{-1} of naproxen).The poorer accuracy obtained with validation set #3 can be attributed to the relatively high fluorescence signal of naproxen, which is present at a ~100-fold higher concentration than individual metabolites. Although the contribution of naproxen to the total fluorescence of the sample is overwhelming, the prediction results we obtained with set #3 are within ±20% of their nominal values. This fact makes them still acceptable for validation of trace analysis in biological samples[130]. The complete EEM set for the whole experiment are shown in Appendix C.

Table 3.1 Predictions obtained when applying N-PLS/RBL to synthetic mixtures (Si), synthetic urines (Ui) and synthetic urines spiked with naproxen 200 ng mL^{-1} (UN1), ibuprofen 100 ng mL^{-1} (UN2), diclofenac 10 ng mL^{-1} (UN3), amoxicillin 50 ng mL^{-1} (UN4), the four interferences at the previously mentioned concentrations (UN5).

Sample	2OH-Flu			1OH-Pyr			3OH-B[a]P			9OH-Phen		
	Nominal (ng mL^{-1})	Predicted (ng mL^{-1})	Recovery (%)	Nominal (ng mL^{-1})	Predicted (ng mL^{-1})	Recovery (%)	Nominal (ng mL^{-1})	Predicted (ng mL^{-1})	Recovery (%)	Nominal (ng mL^{-1})	Predicted (ng mL^{-1})	Recovery (%)
S1	1.5	2.1 (0.1)	140.0	2.5	2.2 (0.1)	88.0	2.3	2.5(0.1)	108.7	3.9	3.3(0.1)	84.6
S2	2.0	2.2	110.0	2.5	2.5	100.0	2.3	2.0	87.0	2.6	2.8	107.7
S3	2.5	3.1	124.0	2.3	2.3	100.0	1.8	1.9	105.6	3.5	3.2	91.4
S4	2.3	2.2 (0.1)	95.7	2.0	1.7 (0.2)	85.0	2.2	2.0(0.2)	90.9	3.8	3.5(0.3)	92.1
S5	2.5	2.4	96.0	2.8	2.9	103.6	2.8	2.7	96.4	3.3	3.4	103.0
S6	2.6	2.4	92.3	2.9	2.8	96.6	2.4	2.2	91.3	3.0	3.4	113.3
U1	1.5	1.3	86.7	2.5	2.6	104.0	2.3	2.4	104.3	3.9	3.8	97.4
U2	2.0	1.9	95.0	2.5	2.6	104.0	2.3	2.0	87.0	2.6	2.8	107.7
U3	2.5	2.7	108.0	2.3	2.3	100.0	1.8	1.5	83.3	3.5	3.0	85.7
U4	2.3	2.5	108.7	2.0	2.1	105.0	2.2	1.9	86.4	3.8	3.5	92.1
U5	2.5	2.6	104.0	2.8	2.7	96.4	2.8	2.6	92.9	3.3	3.0	90.9
U6	2.6	2.3	88.5	2.9	3.1	106.9	2.4	2.3	95.8	3.0	2.5	83.3
UN1	2.5	2.6	104.0	2.3	2.0	86.9	1.8	1.6	88.9	3.2	3.3	103.1
UN2	2.5	2.7	108.0	2.3	2.5	108.9	1.8	2.0	111.1	3.2	3.5	109.4
UN3	2.5	2.2	88.0	2.3	2.4	104.3	1.8	2.0	111.1	3.2	3.0	93.8
UN4	2.5	2.6	104.0	2.3	2.1	91.3	1.8	1.9	105.6	3.2	2.9	90.6
UN5	2.5	2.8	112.0	2.3	2.6	113.0	1.8	2.0	111.1	3.2	3.5	109.4

Values between parenthesis corresponds to standard deviation for n=3

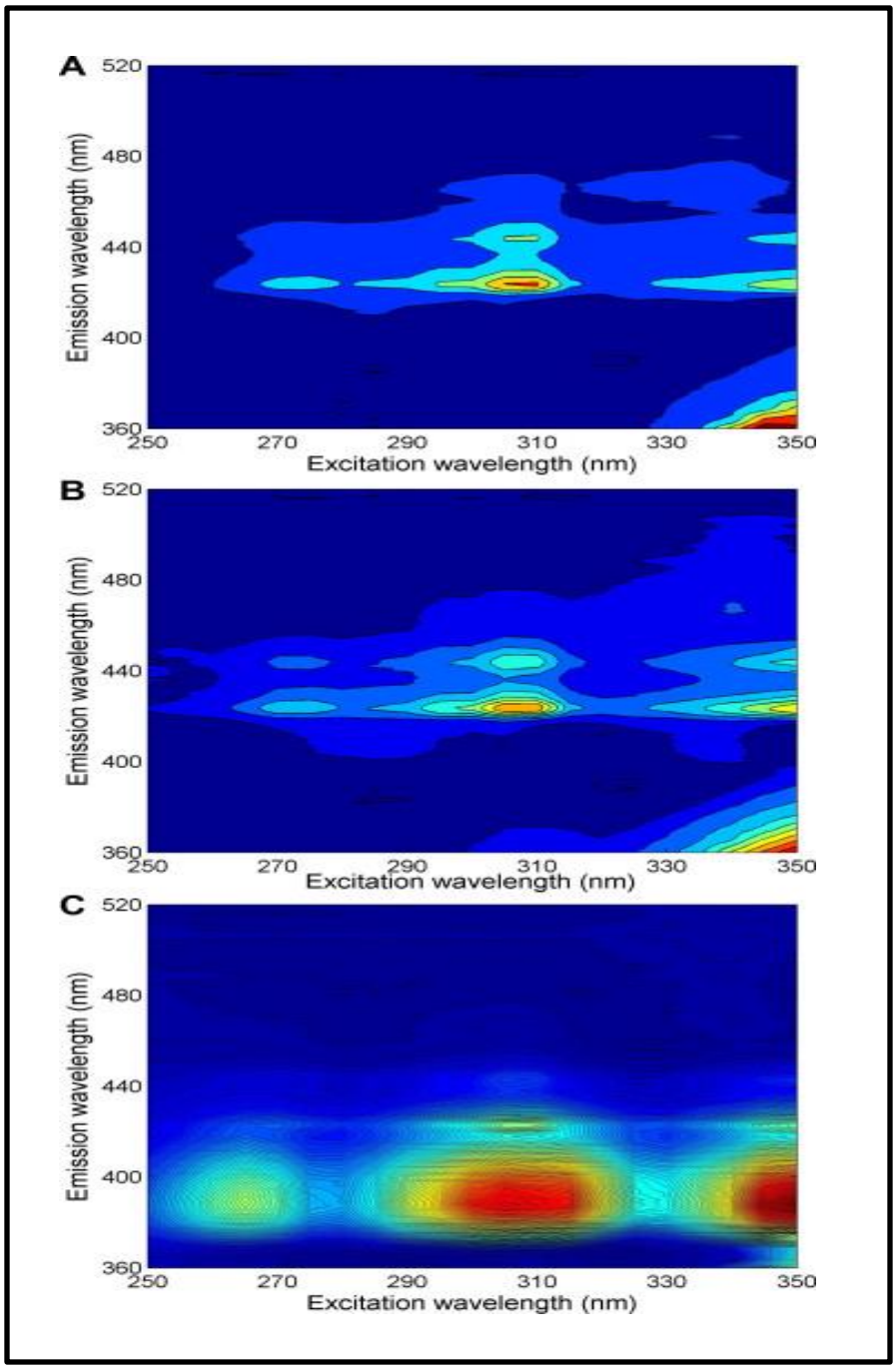

Figure 3.5 RTF EEM recorded from (A) S1 (synthetic metabolite mixture prepared in 1% methanol, no naproxen); (B) U1 (synthetic metabolite mixture in urine, no naproxen); and (C) UN1 (synthetic metabolite mixture in urine and 200 ng mL^{-1} of naproxen). Excitation and emission steps = 5 and 1nm, respectively.

3.4.2.2 MCR-ALS

The MCR-ALS algorithm was applied to samples from the three validation sets. Column-wise augmented data matrices (**D**) were generated arranging $\mathbf{D}_i$ matrices corresponding to fluorescence (emission) spectra recorded in each EEM. In all cases, non-negativity was applied to both excitation and emission profiles. The number of contributions to each **D** data matrix was determined via singular value decomposition. The computed values were 4, 5 and 6 for samples in test validation #1, #2, and #3, respectively. The $\mathbf{S}^T$-type initial estimates (see Equation 6) were built with normalized spectra from pure metabolites and – when appropriate – with random vectors for interferents. When resolution results with random estimations were unsatisfactory, the MCR spectral profiles of interferents were stored and used as initial estimations for subsequent MCR analysis until successful MCR quality parameters were reached. The effectiveness of this strategy is demonstrated in Figure 3.6, which shows the MCR-ALS spectral profiles retrieved from sample UN_1, which contained the four metabolites, an unknown urine interferent and naproxen. Their visual comparison to spectra in Figure 3.1 confirms the quality of the fitting and the ability to make reasonable predictions by gathering the second order advantage.

The results for the validation samples are summarized in Table 3.2. The average recoveries for validation set #1 (S1 – S6) were as follows: 2OH-Flu = 106.5 ± 16.9, 1OH-Pyr = 96.9 ± 7.0, 3OH-B[a]P = 97.5 ± 9.9 and 9OH-Phen = 99.7 ± 11.3. Similar predictions were obtained with urine samples (U1 – U6) from validation set #2: 2OH-Flu = 99.4 ± 10.0, 1OH-Pyr = 103.8 ± 6.0, 3OH-B[a]P = 90.6 ± 9.7 and 9OH-Phen = 94.2 ± 8.8; and with urine samples with naproxen (UN1 – UN3) from validation set #3: 2OH-Flu = 95.4 ± 11.6, 1OH-Pyr = 84.9 ± 3.0,

3OH-B[a]P = 84.3 ± 2.3 and 9OH-Phen = 85.3 ± 8.7. The similarity of these averages and their standard deviations to those obtained from Table 3.1 confirms the ability of N-PLS/RBL and MCR-ALS to provide equivalent results.

The accuracy of the two models was assessed by comparing the predicted to the nominal concentrations of the four metabolites in the three validation sets. The comparison was made applying the joint statistical test for the slope and the intercept of the linear regression between the nominal and predicted metabolites concentrations. The multivariate model is regarded as being accurate if the theoretical values of intercept and slope (zero and unity, respectively) are included within the ellipse that describes the mutual confidence region. In order to avoid oversizing of the joint confidence region due to the relatively large experimental random errors, as well as minimize the possibility to overlook the presence of bias and better estimate the variance of the linear regression, we included experimental data Values between parenthesis corresponds to standard deviation for n=3 recorded from all the studied samples[131]. Figures 7A and 7B show prediction regions of the global data sets obtained with the N-PLS/RBL and MCR-ALS algorithms. In the absence of naproxen and within a confidence level of 95%, both algorithms provide S and U ellipses that contain the theoretically expected values of the intercept (0) and the slope (1). The similar size of ellipses S and U associated to the similar positioning of the expected value (0, 1) within the predicted regions allows one to conclude a similar precision and accuracy for both algorithms. The same is not true in the presence of naproxen, i.e. UN ellipses. The theoretically expected value lies outside the predicted regions of both algorithms. This is indicative of the presence of both proportional and constant error.

Table 3.2 Predictions obtained when applying MCR-ALS to synthetic mixtures (Si), synthetic urines (Ui) and synthetic urines spiked with naproxen 200 ng mL^{-1} (UN1), ibuprofen 100 ng mL^{-1} (UN2), diclofenac 10 ng mL^{-1} (UN3), amoxicillin 50 ng mL^{-1} (UN4), the four interferences at the previously mentioned concentrations (UN5).

Sample	2OH-Flu			1OH-Pyr			3OH-B[a]P			9OH-Phen		
	Nominal (ng mL^{-1})	Predicted (ng mL^{-1})	Recovery (%)	Nominal (ngmL^{-1})	Predicted (ng mL^{-1})	Recovery (%)	Nominal (ng mL^{-1})	Predicted (ng mL^{-1})	Recovery (%)	Nominal (ng mL^{-1})	Predicted (ng mL^{-1})	Recovery (%)
S1	1.5	2.1 (0.1)	133.0	2.5	2.3 (0.1)	92.0	2.3	2.6(0.1)	113.0	3.9	3.4(0.1)	87.2
S2	2.0	2.2	110.0	2.5	2.6	104.0	2.3	2.1	91.3	2.6	2.9	111.5
S3	2.5	2.9	116.0	2.3	2.2	95.7	1.8	1.9	105.6	3.5	3.1	88.6
S4	2.3	2.1 (0.1)	91.3	2.0	1.8 (0.2)	90.0	2.2	1.9(0.2)	86.4	3.8	3.6(0.3)	94.7
S5	2.5	2.5	100.0	2.8	3.0	107.1	2.8	2.6	92.9	3.3	3.4	103.0
S6	2.6	2.3	88.5	2.9	2.7	93.1	2.4	2.3	95.8	3.0	3.4	113.3
U1	1.5	1.4	93.3	2.5	2.6	104.0	2.3	2.4	104.3	3.9	3.6	92.3
U2	2.0	1.8	90	2.5	2.7	108.0	2.3	2.1	91.3	2.6	2.9	111.5
U3	2.5	2.8	112	2.3	2.4	104.3	1.8	1.4	77.8	3.5	3.2	91.4
U4	2.3	2.4	104.3	2.0	2.2	110.0	2.2	1.8	81.8	3.8	3.5	92.1
U5	2.5	2.7	108.0	2.8	2.6	92.9	2.8	2.7	96.4	3.3	3.0	90.9
U6	2.6	2.3	88.5	2.9	3.0	103.4	2.4	2.2	91.7	3.0	2.6	86.7
UN1	2.5	2.7	108.0	2.3	1.9	82.6	1.8	1.5	83.3	3.2	3.3	103.1
UN2	2.5	2.6	104.0	2.3	2.4	104.3	1.8	2.0	111.1	3.2	3.4	106.3
UN3	2.5	2.3	92.0	2.3	2.3	100.0	1.8	1.9	105.5	3.2	3.0	93.8
UN4	2.5	2.7	108.0	2.3	2.2	95.7	1.8	2.0	111.1	3.2	3.1	96.9
UN5	2.5	2.9	116.0	2.3	2.5	108.7	1.8	2.1	116.6	3.2	3.4	106.3

Values between parenthesis corresponds to standard deviation for n=3

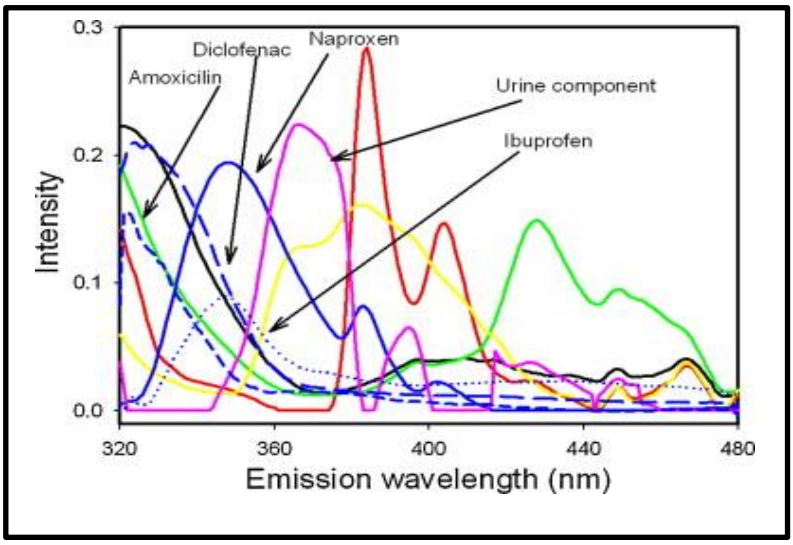

Figure 3.6 MCR-ALS spectral profiles retrieved from sample UN1, which contained the four metabolites, an unknown urine interferent and naproxen. Color code as follows: 3OH-B[a]P = green; 9OH-Phen = yellow; 2OH-Flu = black

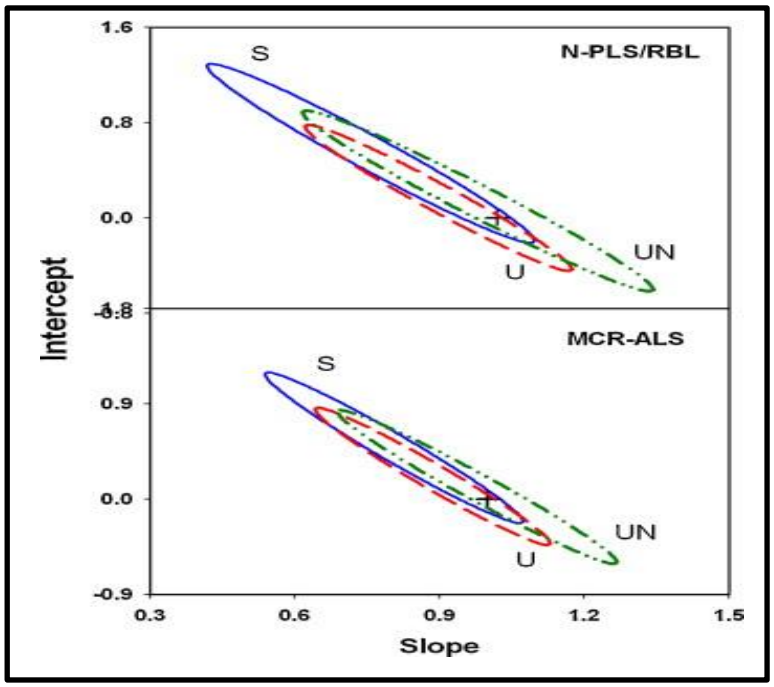

Figure 3.7 Prediction regions of the global data sets obtained with (A) N-PLS/RBL and (B) MCR-ALS B algorithms.

3.4.2.3 Analytical Figures of Merit

All experimental data was gathered from C18 membranes used to extract hydrolyzed urine samples previously spiked with OH-PAH. In all cases, the volume of extracted sample was 10 mL, which is a typical volume for urine analysis of OH-PAH. The mass of extracted metabolite did not surpass the nominal breakthrough mass (30mg) of extraction membranes. RTF-EEM were recorded at 5nm excitation steps from 220 to 360nm. Sample excitation was carried out from longer to shorter wavelengths to reduce the risk of photo-degradation due to extensive sample excitation. Fluorescence spectra were recorded at each excitation wavelength by scanning the emission monochromator at 1nm steps from 300 to 500nm. All EEM were recorded using the same excitation (2nm) and emission (2nm) band-pass.

Table 3.3 summarizes the analytical recoveries (%R) of the SPE-RTF method and compares the AFOM calculated via MCR-ALS and N-PLS/RBL. %R values were calculated with the formula $\%R = (I_{BE} - I_{AE}) \times 100$, where I_{BE} and I_{AE} refer to the fluorescence intensities before and after extraction, respectively. All measurements were made at the maximum excitation and fluorescence wavelengths of each compound. Keeping in mind that the adsorption of metabolites onto the C18 membrane occurs from an aqueous based matrix (urine) and the possibility of matrix interference on the retention of OH-PAH, we first tested their retention from standard solutions in water/water (1% v/v) and then compared their values to the extraction of spiked urine samples. No significant difference was observed in any of the studied metabolites ($\alpha = 0.05$; $N_1 = N_2 = 3$)[132].

The estimation of the MCR-ALS AFOMs was straightforward and based on the recovery

of the pure response profiles resulting from the curve resolution procedure[133]. This approach defines sensitivity (SEN_n) as the slope of the calibration curve obtained from the plot of relative fluorescence responses and standard concentrations. The analytical sensitivity (γ_n) was calculated as the ratio between the SEN_n value and the instrumental noise (s_x), which was computed from a sample of zero concentration taking into account the errors of the slope and intercept of the calibration equation[134]. The limit of detection (LOD) was calculated with the equation LOD = 3.3 s_x / SEN_n.

The N-PLS/RBL sensitivity was estimated from the following unfolded PLS/RBL equations[123].

$$SEN_n = 1 / || (\mathbf{P}_{eff}^{+})^T \mathbf{v} || \quad \textbf{(3.10)}$$

where $\mathbf{v}$ is the ($A \times 1$) latent vector of regression coefficients for the PLS model, and $\mathbf{P}_{eff}$ is a matrix given by:

$$\mathbf{P}_{eff} = (\mathbf{P}_{c,unx} \otimes \mathbf{P}_{b,unx})^T \mathbf{P} \quad \textbf{(3.11)}$$

where $\otimes$ is the Kronecker product, $\mathbf{P}$ is the ($JA \times A$) loading matrix provided by the unfolded PLS model, and $\mathbf{P}_{c,unx}$ and $\mathbf{P}_{b,unx}$ are projection matrices calculated as follows:

$$\mathbf{P}_{c,unx} = \mathbf{I} - \mathbf{C}_{unx} \mathbf{C}_{unx}^{+} \quad \textbf{(3.12)}$$

$$\mathbf{P}_{b,unx} = \mathbf{I} - \mathbf{B}_{unx} \mathbf{B}_{unx}^{+} \quad \textbf{(3.13)}$$

where the columns of $\mathbf{B}_{unx}$ and $\mathbf{C}_{unx}$ contain the profiles of the unexpected components. The γ_n and the LOD were estimated with the same equations as those previously described for the MCR-ALS method. It is important to note that, when applying the second order advantage, the SEN_n values from Equation 3.10 become sample-specific. Therefore, the results in Table 3.3

should be regarded as average values of the sets of samples we investigated and not as representative figures of the whole multivariate method. Although different schemes for achieving both the second-order data modeling and the AFOM were employed, comparable results were obtained.

Table 3.3 Analytical Figures of Merit of OH-PAH on extraction membranes calculated with N-PLS/RBL and MCR-ALS

Metabolite	Recovery (%)	N-PLS/RBL			MCR-ALS		
		SEN	γ^{-1} (ng mL^{-1})	LOD (ng mL^{-1})	SEN	γ^{-1} (ng mL^{-1})	LOD (ng mL^{-1})
2OH-FLU	99.2 ± 0.24	22	0.047	0.16	18	0.055	0.18
1OH-PYR	99.4 ± 1.32	59	0.018	0.06	40	0.025	0.083
3OH-B[a]P	99.7 ± 0.49	31	0.033	0.11	20	0.050	0.165
9OH-PHE	96.2 ± 1.35	37	0.028	0.09	25	0.040	0.132

3.5 Conclusion

The direct determination of OH-PAH on the surface of the extraction membrane makes SPE-RTF spectroscopy a well-suited approach for screening OH-PAH in urine samples. Its straightforward experimental procedure eliminates the need for subsequent elution steps and provides excellent metabolite recoveries. Comparison of LOD in Table 3.3 to those previously reported in chapter 2 (univariate data) shows multivariate values approximately one order of

magnitude higher. This was somehow predictable due to the effect of unexpected components in the multivariate figures of merit, i.e. a more realistic approach to the analysis of OH-PAH in human urine samples. It should be noted that the LOD obtained with both multivariate algorithms are still comparable to those reported via HPLC methods [[48, 115-118]. Because both N-PLS/RBL and MCR-ALS are theoretically capable to handle numerous metabolites in the presence of unknown interference, their combination to SPE-RTF appears to address the crucial issue of spectral overlapping on extraction membranes.

CHAPTER 4: ANALYSIS OF POLYCYCLIC AROMATIC HYDROCARBON METABOLITES IN URINE VIA SOLID PHASE EXTRACTION ROOM-TEMPERATURE SYNCHRONOUS FLUORESCENCE SPECTROSCOPY

4.1 Introduction

Previous research in our group demonstrated the screening potential of SPE and RTF for the analysis of OH-PAH in urine samples. Quantitative determination of metabolites was carried out either in the eluent extract[43, 100] or on the surface of the extraction membrane[3]. Spectral overlapping and matrix interference were eliminated with the aid of EEM data formats and chemometrics. In this chapter, we investigate the potential of SFS for the simultaneous analysis of OH-PAH urine samples. Originally proposed in an empirical manner for the forensic analysis of oil spills[135-138], the theory of synchronous RTF spectroscopy was introduced by Vo-Dinh[139] and further developed for the environmental analysis of poly-aromatic compounds[66, 140]. To the extent of our literature search, only a few articles exist on the SFS analysis of OH-PAH in urine samples. Lamotte and co-workers[141] determined 1OH-Pyr on the surface of solid substrates (ENVI-Disk^{TM}C18) previously immersed in urine samples. LOD at the parts-per-billion level were obtained after 30 min of substrate immersion. The simultaneous determination of other OH-PAH was not attempted. Multiple metabolite determination via SFS in urine samples was first reported for the analysis of 1OH-Pyr, 2OH-naphthol and 9OH-Phen[142]. Metabolites were liquid-liquid extracted with n-hexane and determined in the presence of β-cyclodextrin (β–CD). The sensitizing effect of β–CD provided LOD at the 10^{-8} - 10^{-9} M range. A similar approach, but

using Tween-20 as the sensitizer, was later employed for the detection of 1OH-Pyr, 2OH-Flu, 9OH-Phen, 1OH-and 2OH-naphthol at the 10^{-8} - 10^{-9} M range.[143]

In this chapter, 2OH-Flu, 1OH-Pyr, 6-hydroxychrysene (6OH-Chry), 3OH- and 4OH-B[a]P are solid-phase extracted on C18 silica cartridges with the aid of a twelve-port vacuum manifold. SFS carried out in the methanol eluent provided LOD at the sub-parts-per-billion level. To the extent of our literature search, this is the first report on the SFS determination of 6OH-Chry in urine samples. The same is true for the SFS determination of 3OH- and 4OH-B[a]P without previous chromatographic separation.

4.2 Materials and Methods

4.2.1 Reagents

All solvents were Aldrich HPLC grade. All chemicals were analytical-reagent grade and utilized without further purification. Unless otherwise noted, Nanopure water was used throughout. 2OH-Flu, 1OH-Pyr, 6OH-Chry, creatinine, amoxicillin, diclofenac, ibuprofen and naproxen were purchased from Sigma-Aldrich. 3OH-B[a]P and 4OH-B[a]P were from Midwest Research Institute. All other chemicals were purchased from Fisher Chemical. The Sep-Pak C18 cartridges were purchased from Waters (Milford, MA). The synthetic urine solution was manufactured by RICCA Chemical Company (Arlington, TX) and purchased from Fischer Scientific. Its chemical composition mimicked main components of human urine at the concentrations found in healthy urine samples. Real human urine was collected randomly from healthy individual volunteers.

Note: Use extreme caution when handling OH-PAH known to be extremely toxic.

4.2.2 RTF measurements

Excitation spectra, fluorescence spectra and signal intensities were recorded with a commercial spectrofluorimeter and the aid of an in-house sample holder previously described in chapter 2. The collection of synchronous fluorescence spectra were carried out by pouring liquids samples into standard (1x1 cm) quarts cuvette. Otherwise noticed, fluorescence was collected at 90^{o} angle from excitation using a wavelength off-set equal to 5 nm and an excitation/emission band-pass of 1 nm.

4.2.3 Preparation of stock solutions

Stock solutions of OH-PAH were prepared by dissolving pure standards in methanol. Stock solutions of amoxicillin, diclofenac, ibuprofen and naproxen stock were prepared in methanol and kept in the dark at 4^{o}C until further use. Prior to dilution, stock solutions were monitored via RTF spectroscopy for possible photo-degradation of metabolites. No changes on spectral profiles and fluorescence intensities were observed for a period of six months. Working solutions of OH-PAH and pharmaceutical drugs were prepared daily by serial dilution with methanol.

4.2.4 Hydrolysis of urine samples

Urine samples were spiked with micro-litters of stock solutions of appropriate concentrations and equilibrated for 30 min to allow for the interaction of metabolites and naproxen with urine components such as urea and various salts. Then 500 μL of 0.1 M HCl was added to the sample and the mixture was buffered with 500 μL of 0.05 M potassium biphthalate sodium hydroxide buffer (pH 5.0). The buffered sample was shaken for 30 min at 1400 rpm to allow for urine hydrolysis.

4.2.5 Solid-phase extraction of urine samples

SPE was carried out with a Visiprep 12 port vacuum manifold (Supelco). Urine samples were processed through a Sep-Pak Plus SPE cartridge pre-conditioned with 10 mL of methanol and 10 mL of buffered water (pH = 5). The cartridges were sequentially washed with 10 mL of buffered water (pH=5) and 5% methanol/water. Without letting the cartridges to dry, OH-PAHs were eluted with 3mL of pure methanol.

4.3 Results and Discussion

4.3.1 Efficiency of SPE procedure

The efficiency of SPE was investigated in two steps, which monitored the retention and the eluting efficiency of the solid sorbent and methanol, respectively. The percentage of retention (%R) was calculated according to the formula:

$$\%R = (I_1 - I_2) \times 100 \qquad (4.1)$$

Where, I_1 and I_2 refer to the fluorescence intensity of the solution before and after retention, respectively.

Keeping in mind that the adsorption of OH-PAH onto the solid sorbent occurs from an aqueous-based matrix (urine) and the possibility of matrix interference on the retention of OH-PAH, their retention was first tested from standard solutions in water (methanol/water 0.05% v/v) and then compared their values obtained from the extraction of spiked urine samples. Each OH-PAH concentration used in these studies was within the corresponding linear dynamic range of the calibration curve.

The eluting efficiency (%E) of methanol was obtained from the following equation:

$$\%E = (m_E / m_R) \times 100 \qquad (4.2)$$

where m_E and m_R refer to eluted and retained mass of OH-PAH, respectively. The mass of eluted metabolite was calculated multiplying the volume of eluted methanol (V_E) by the concentration of metabolite in the eluted solvent (C_E). The experimental values of the eluted concentrations were obtained from the calibration curves of the metabolites in methanol. The mass of retained metabolite was calculated from the product $V_S \times C_S \times (\%E)$, where V_S and C_S refer to the volume and concentration of the standard processed through the cartridge, respectively.

These calculations required the previous knowledge of the fluorescence characteristics of OH-PAH in water, methanol and urine. Preliminary studies in this direction were then undertaken by carrying out a spectral survey of the studied metabolites in the three types of liquid media. All spectra were recorded using the same excitation and emission band-pass

(2nm). No attempts were made to adjust slit widths to optimize spectra resolution, nor were the spectra corrected for instrumental response. The 2nm band-pass provided satisfactory signal-to-background ratios (> 3) for all the studied metabolites at the $ng.mL^{-1}$ concentration level. Figure 4.1 summarizes the spectral features of the studied metabolites in the three types of media. Although fluorescence intensities varied considerably with the liquid environment, the spectral profiles of the studied metabolites remained virtually the same in the three types of media. This fact provided a single set of maximum excitation (λ_{exc}) and emission (λ_{em}) wavelengths per metabolite.

Table 4.1 summarizes the RTF AFOM of the studied metabolites in methanol/water 0.05% v/v, and hydrolyzed synthetic urine, and pure methanol samples. Working solutions were prepared from intermediate stock solutions by serial dilution with the appropriate solvent - i.e., either methanol/water (0.05% v/v) or methanol – or synthetic urine. Fluorescence measurements were made at the λ_{exc}/ λ_{em} of each compound. Each calibration curve was built with a minimum of five metabolite concentrations. For each concentration plotted in the calibration graph, the RTF intensity was the average of at least three determinations taken from three sample aliquots. No efforts were made to experimentally obtain the upper concentration limit of the calibration curve. The main reason for this was that 50 and 100 ng/mL, i.e., the highest concentrations tested in these studies, are already at the highest concentration ranges of OH-PAH typically found in urine[115, 116, 144, 145]. It is important to note, however, that 50 and 100 ng/mL did not surpass the breakdown volume of the SPE device[146]. The correlation coefficients of the calibration curves were close to unity, indicating a linear relationship between OH-PAH concentration and

fluorescence intensity. Within the LDR, the (RSD at medium concentrations were lower than 2%. The LOD were calculated using the equation LOD = 3 x S_B/m, where S_B is the standard deviation of 16 blank determinations and m is the slope of the calibration curve. The LOQ were calculated according to the formula LOQ = 10 x S_B/m. The m values were calculated via the least squares method[147]. At the LOQ concentration levels, the RSD of fluorescence measurements varied between 5 and 7%, allowing us to make precise measurements at low-ppb concentration levels.

Table 4.1 RTF analytical figures of merit of OH-PAH in methanol/water, hydrolysed synthetic urine and methanol

OH-PAH	$\lambda_{ex/em}$ [a]	Methanol/water (0.05% v/v)				Hydrolysed synthetic urine				Methanol			
		LDR[b]	R^{2}[c]	LOD[d]	LOQ[e]	LDR[b]	R^{2}[c]	LOD[d]	LOQ[e]	LDR[b]	R^{2}[c]	LOD[d]	LOQ[e]
2OH-Flu	278/328	1.60 - 50	0.9999	0.48	1.58	1.47 - 50	0.9999	0.44	1.47	1.33 – 50	0.9997	0.40	1.33
6OH-Chry	270/381	0.90 - 50	0.9954	0.27	0.90	0.90 - 50	0.9954	0.26	0.87	0.60 - 50	0.9964	0.18	0.60
1OH-Pyr	348/387	0.30 - 50	0.9999	0.09	0.30	0.32 - 50	0.9972	0.10	0.32	0.23 - 50	0.9983	0.07	0.23
3OH-B[a]P	382/432	0.63 - 50	0.9947	0.19	0.63	0.81 - 50	0.9933	0.24	0.81	0.18 - 50	0.9998	0.054	0.18
4OH-B[a]P	372/421	4.85 - 50	0.9911	1.45	4.85	4.67 - 50	0.9991	1.40	4.67	0.30 - 50	0.9977	0.09	0.30

[a] *Maximum excitation and emission wavelength in nm.*
[b] *Linear dynamic range in ng/mL.*
[c] *Correlation coefficient of calibration curve.*
[d] *Limit of detection (ng/mL) is calculated from 3 x standard deviation (S_b) of 16 blank measurements divided by slope (m) of the calibration curve.*
[e] *Limit of quantification (ng/mL) is calculated from 10 S_b /m.*

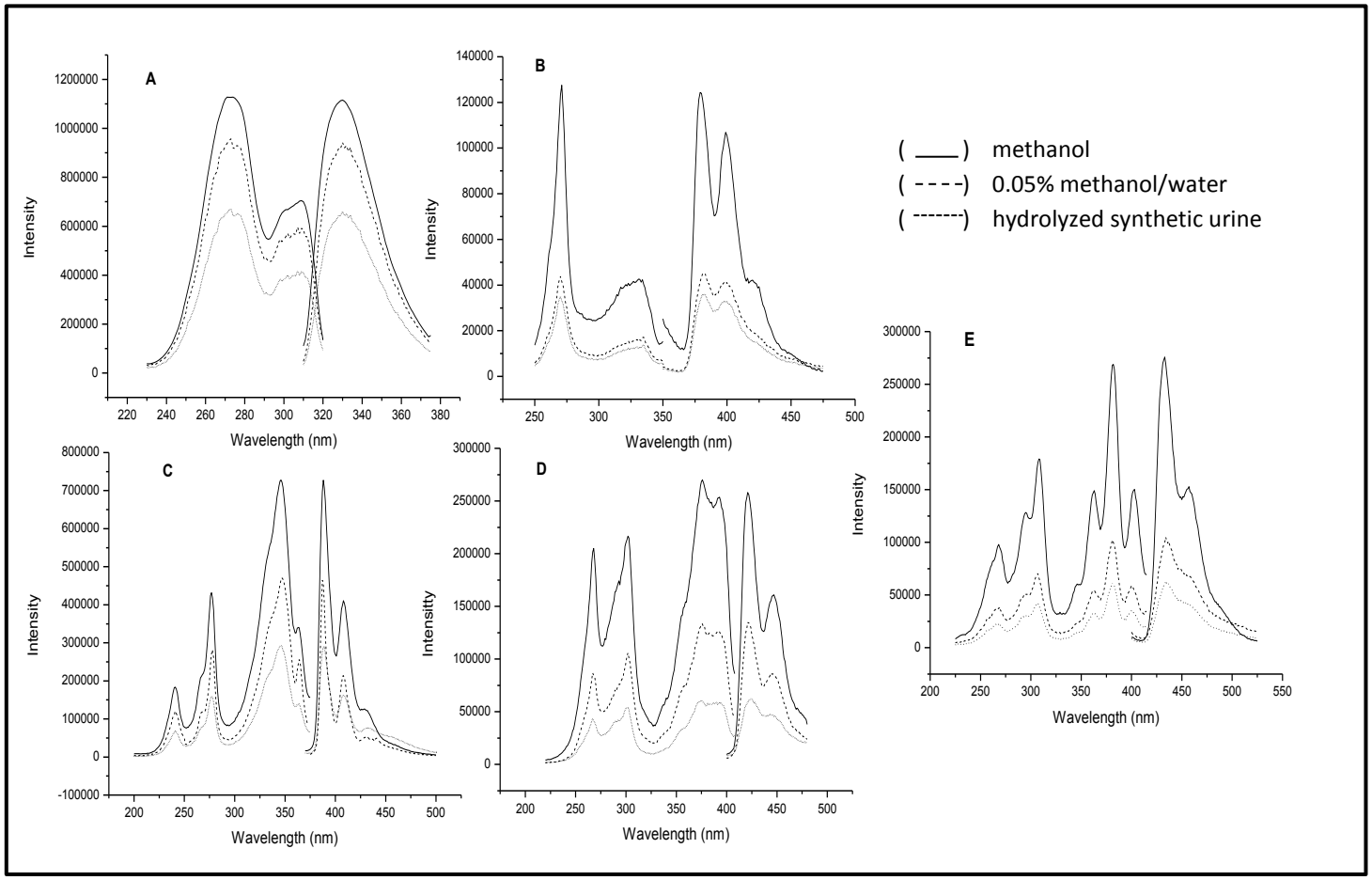

Figure 4.1 Excitation and Emission Spectra of (A) 100 ng.mL^{-1} 2OH-Flu, (B) 50 ng.mL^{-1} 6OH-Chry, (C) 20 ng.mL^{-1} 1OH-Pyr (D) 100 ng.mL^{-1} 4OH-B[a]P , and 20 ng.mL^{-1} 3OH-B[a]P in different media at excitation and emission band-pass = 2nm/2nm.

Table 4.2 summarizes the figures of merit of the SPE procedure obtained with 10mL of sample and 3 mL of eluting solvent (methanol). The choice of 10mL sample volume corresponds to the lowest end of the urine volume range (10 – 250mL) found in the literature [46, 144, 148, 149]. The volume of eluting solvent was optimized previously in our laboratory [100, 150]. Metabolites were spiked into the urine matrix 24 h prior to analysis. The spiked samples were submitted to acidic hydrolysis and then extracted via SPE. The percentages of overall recoveries (%OR) were calculated as the product of %R and %E, i.e. %OR = %R·%E.

The standard deviations of the overall recoveries (S_{OR}) were based on three independent repetitions of the entire SPE procedure and were calculated according to the formula:

$$S_{OR}/OR = [(S_R/\%R)^2 + (S_E/\%E)^2]^{1/2} \qquad (4.3)$$

where S_R and S_E are the standard deviations of %R and %E, respectively [100]. Within a confidence interval of 95% (N=3), the overall recoveries in methanol-water standards and synthetic urine samples were the same. This agreement shows no matrix interference on the extraction of metabolites from synthetic urine samples.

Table 4.2 Figures of merit for the optimized SPE procedure in aqueous and urine samples

OH-PAH	% Retention (R) $R \pm S_R$		% Elution Efficiecy(E) $E \pm S_E$		% Overall Recovery (OR) $OR \pm S_{OE}$		t_{exp}
	H_2O/CH_3OH	Urine	H_2O/CH_3OH	Urine	H_2O/CH_3OH	Urine	
2OH-Flu	99.91 ± 0.10	99.79 ± 0.28	99.26 ± 1.78	95.74 ± 2.88	99.17 ± 1.79	95.53 ± 3.02	1.838
6OH-Chry	98.70 ± 0.65	98.85 ± 0.30	99.80± 1.40	100.0 ± 1.80	98.50± 1.11	98.85 ± 1.65	0.305
1OH-Pyr	99.29 ± 0.23	99.55 ± 0.38	89.10 ±1.32	88.51 ± 0.95	88.46 ± 1.49	88.11 ± 1.13	0.331
4OH-B[a]P	96.65 ± 0.24	94.18 ± 1.90	86.15 ± 1.38	89.0 ± 1.9 0	83.26 ± 1.12	83.82 ± 3.60	0.467
3OH-B[a]P	99.03 ± 0.32	99.63 ± 0.12	99.18 ± 1.44	99.80 ± 1.04	98.22 ± 1.48	99.43 ± 1.05	1.179

[a] *The final concentrations of spiked samples are 50 ng.mL^{-1} for , 2OH-Flu, and 6OH-Chry and 20 ng/mL for 1OH-Pyr, 3OH-B[a]P, and 4OH-B[a]P*

[b] *% Standard deviation of % retention efficiency*

[c] *% Standard deviation of % elution efficiency.*

[d] *% Standard deviation of % overall efficiency.*

[e] *t_{exp} – t value calculated for experimental measurements according to 87. t_{tab} = 2.78 (α = 0.05; N1 = N2 = 3).*

4.3.2 Synchronous RTF Spectroscopy of OH-PAH

Constant energy synchronous excitation refers to varying simultaneously both the excitation (λ_0) and the emission (λ) wavelengths while keeping constant a wavelength interval ($\Delta\lambda = \lambda - \lambda_0$) between them. Along with the optimization of excitation and emission band-pass, the judicious choice of the $\Delta\lambda$ parameter usually leads to both spectral profile simplification and improvement of spectral resolution.[30, 66, 135-138, 151, 152] The most intense synchronous signal of each metabolite was observed by recording its fluorescence spectrum at $\Delta\lambda_{max} = \lambda_{em} - \lambda_{exc}$, i.e., a wavelength interval equal to the difference between its maximum emission and excitation wavelength. The resulting spectra are shown Figure 4.2. Unfortunately, the overlapping among the synchronous spectra of the five metabolites prevented the accurate determination of each metabolite at its $\Delta\lambda_{max}$. An example of the observed interference is shown in Figure 4.3 for 3OH-B[a]P. The higher intensity of the synchronous peak (433nm) of 3OH-B[a]P in the synthetic mixture results from the fluorescence contribution of 4OH- B[a]P. It should be noted that narrower excitation and emission band-pass were attempted but no success on spectral overlapping was achieved.

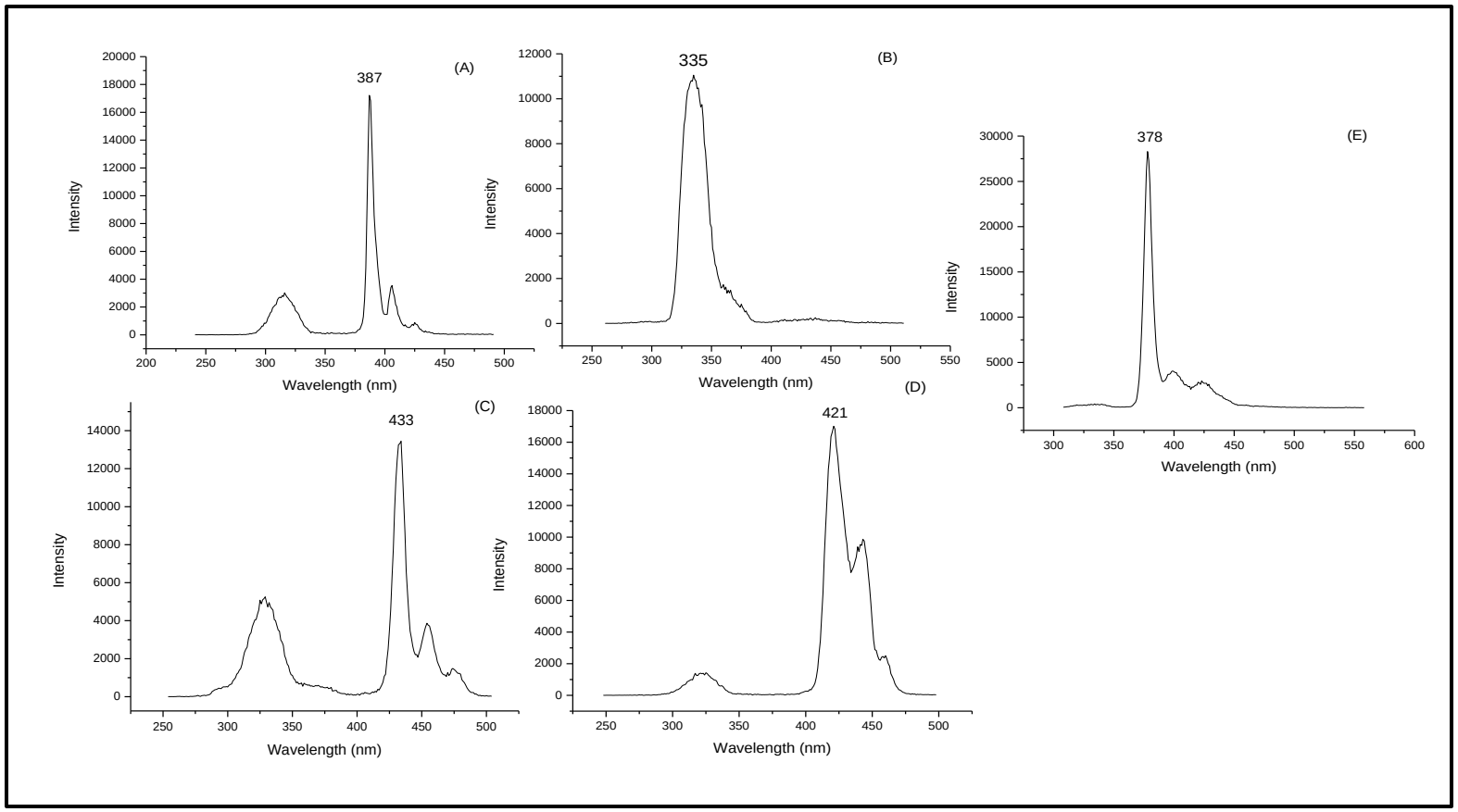

Figure 4.2 Synchronous fluorescence spectra of OH-PAH at optimum Δλ. Slit width: 1/1; step size: 1 nm. (A) 1OH-Pyr; Δλ= 41nm; 20ng.mL^{-1} (B) 2OH-Flu; Δλ= 61nm; 50ng.mL^{-1} (C) 3OH-B(a)P; Δλ= 54nm; 20ng.mL^{-1} (D) 4OH-B(a)P; Δλ= 48nm; 50ng.mL^{-1} (E) 6OH-Chr; Δλ= 108nm; 50ng.mL^{-1}.

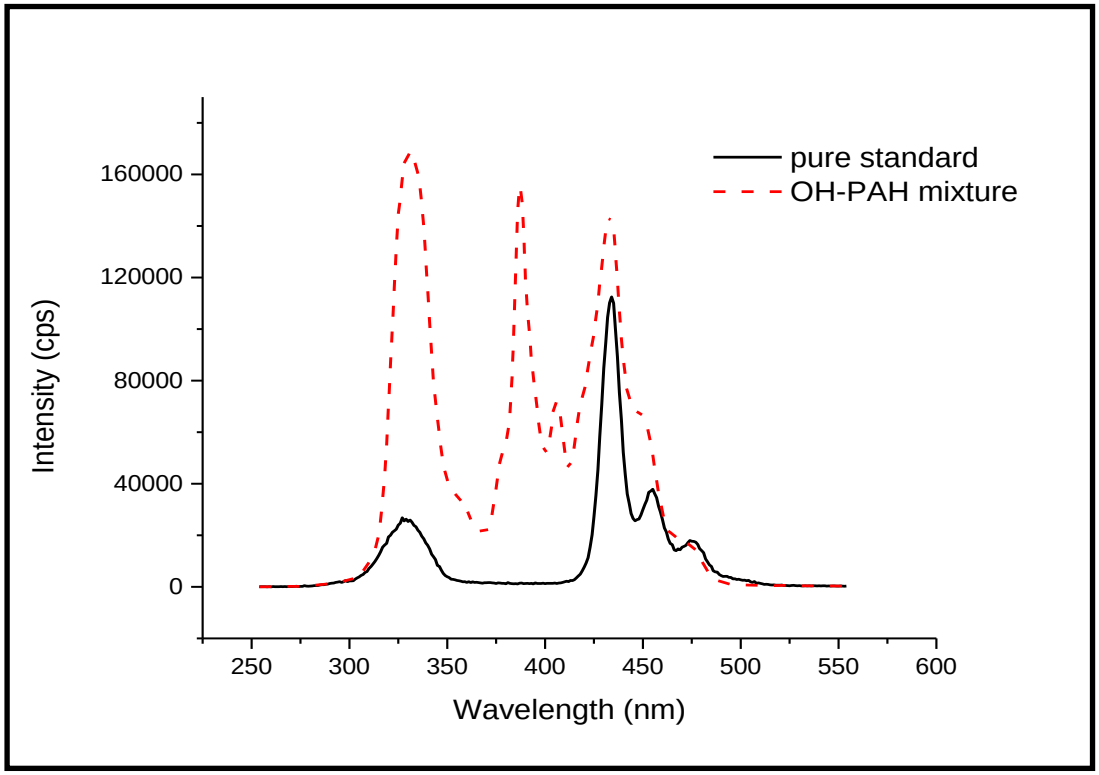

Figure 4.3 Synchronous fluorescence spectra of pure 20ng.mL^{-1} 3OH-PAH (—) and 20ng.mL^{-1} 3OH-PAH in OH-PAH mixture (----) in methanol at optimum Δλ = 54nm, $\lambda_{exc}/\lambda_{ems}$ bandpass 2nm/2nm. *(Note: mixture contains 20ng.mL^{-1} 3OH-B(a)P; 20ng.mL^{-1} 1OH-Pyr; 50ng.mL^{-1} 2OH-Flu; 50ng.mL^{-1} 4OH-B(a)P; 50ng.mL^{-1} 6OH-Chry)*

The best case scenarios were observed upon synchronous excitation with relatively small wavelength offsets. Δλ values smaller that 10nm produced single fluorescence peaks for all the studied metabolites with narrow full-width at half maxima. The best compromise between spectral resolution and fluorescence intensity was obtained with Δλ values of 7 and 5nm. The optimization of excitation /emission band-pass provided the best results with 2/2nm (Δλ = 7nm) and 1/1nm (Δλ = 5nm) and. The resulting spectra recorded from metabolite mixtures in methanol are shown in Figure 4.4.

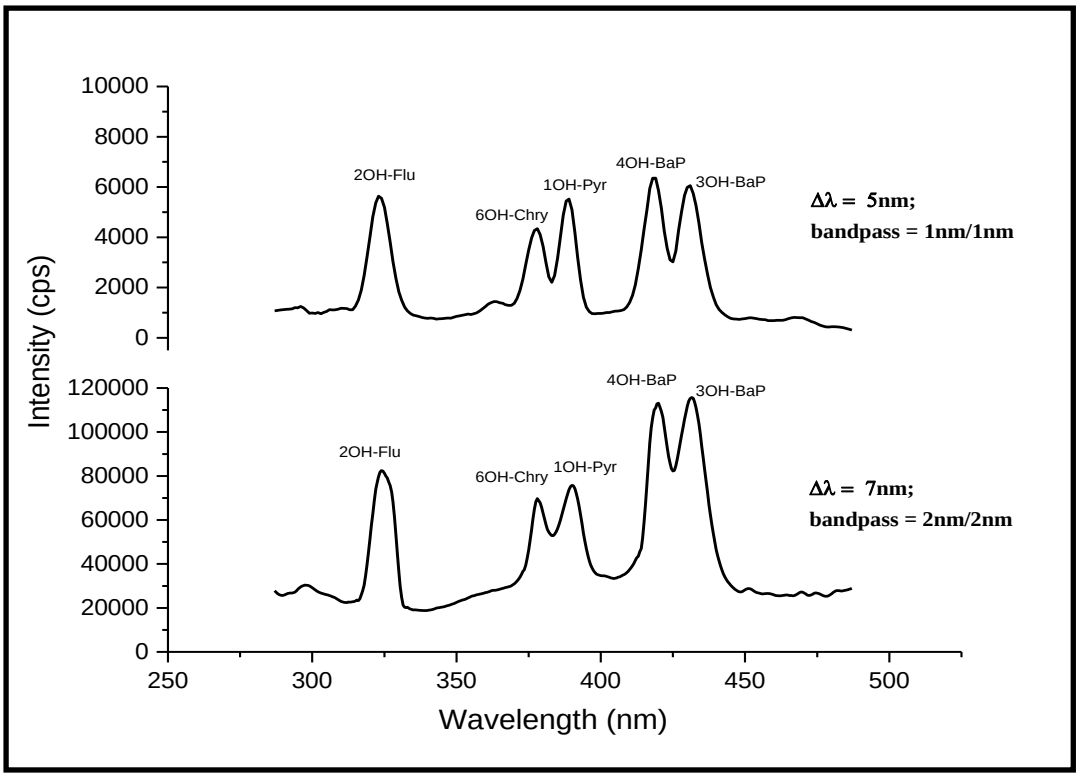

Figure 4.4 Synchronous fluorescence spectra of OH-PAH mixture in methanol at different offsets (Δλ) and Excitation/Emission bandpass. ***(Note: mixture contains 20ng.mL^{-1} 3OH-B(a)P; 20ng.mL^{-1} 1OH-Pyr; 50ng.mL^{-1} 2OH-Flu; 50ng.mL^{-1} 4OH-B(a)P; 50ng.mL^{-1} 6OH-Chry)***

Table 4.3 reports the AFOM obtained with synthetic urine samples via SPE-SFS. Calibration curves were built with spiked samples submitted to the entire experimental procedure. Signal intensities plotted in the calibration graphs corresponded to the averages of three individual determinations taken from three independently spiked samples. LDR, RSD, LOQ and LOD were calculated as those reported in Table 4.1. Comparison of LOD and LOQ values in Table 4.3 clearly show the advantage of using Δλ = 7nm and excitation/emission band-pass = 2/2nm.

Table 4.3 Analytical figures of merit of OH-PAH in methanol via SPE-SFS obtained from synthetic urine samples

OH-PAH	λ_{max} [a]	$\Delta\lambda$ = 5nm, Bandpass = 1nm/1nm				$\Delta\lambda$ = 7nm, Bandpass = 2nm/2nm			
		LDR[b]	R^{2}[c]	LOD[d]	LOQ[e]	LDR[b]	R^{2}[c]	LOD[d]	LOQ[e]
2OH-Flu	324	16.90 - 200	0.9916	5.07	16.9	1.96 - 200	0.9961	0.588	1.96
6OH-Chry	377	21.57 - 200	0.9987	6.47	21.57	2.62 - 200	0.9980	0.786	2.62
1OH-Pyr	390	1.79 - 25	0.9977	0.537	1.79	0.23 - 25	0.9968	0.070	0.23
4OH-B[a]P	418	12.80 - 100	0.9969	3.84	12.80	1.06- 100	0.9944	0.319	1.06
3OH-B[a]P	430	4.30 - 50	0.9961	1.29	4.30	0.27 - 50	0.9922	0.082	0.27

[a] *Maximum synchronous fluorescence wavelength in nm.*
[b] *Linear dynamic range in ng/mL.*
[c] *Correlation coefficient of calibration curve.*
[d] *Limit of detection (ng/mL) is calculated from 3 x standard deviation (S_b) of 16 blank measurements divided by slope (m) of the calibration curve.*
[e] *Limit of quantification (ng/mL) is calculated from 10 S_b /m.*

Figures 4.5A and 4.5B compare the SPE-SFS spectra of synthetic and real urine samples spiked with the five metabolites. Comparison to spectra in Figure 4.5 clearly shows the lack of urine interference. Figure 4.5C depicts the SPE-SFS spectrum of a real urine sample spiked with the studied metabolites and five potential concomitants. Creatinine is a metabolite usually present in human urine samples[153]. Naproxen, ibuprofen and diclofenac are non-steroidal anti-inflammatory drugs [154, 155] and amoxicillin is an antibiotic[156] of frequent use in our society. Their presence in the urine sample does not interfere with the SPE-SFS analysis of the studied metabolites.

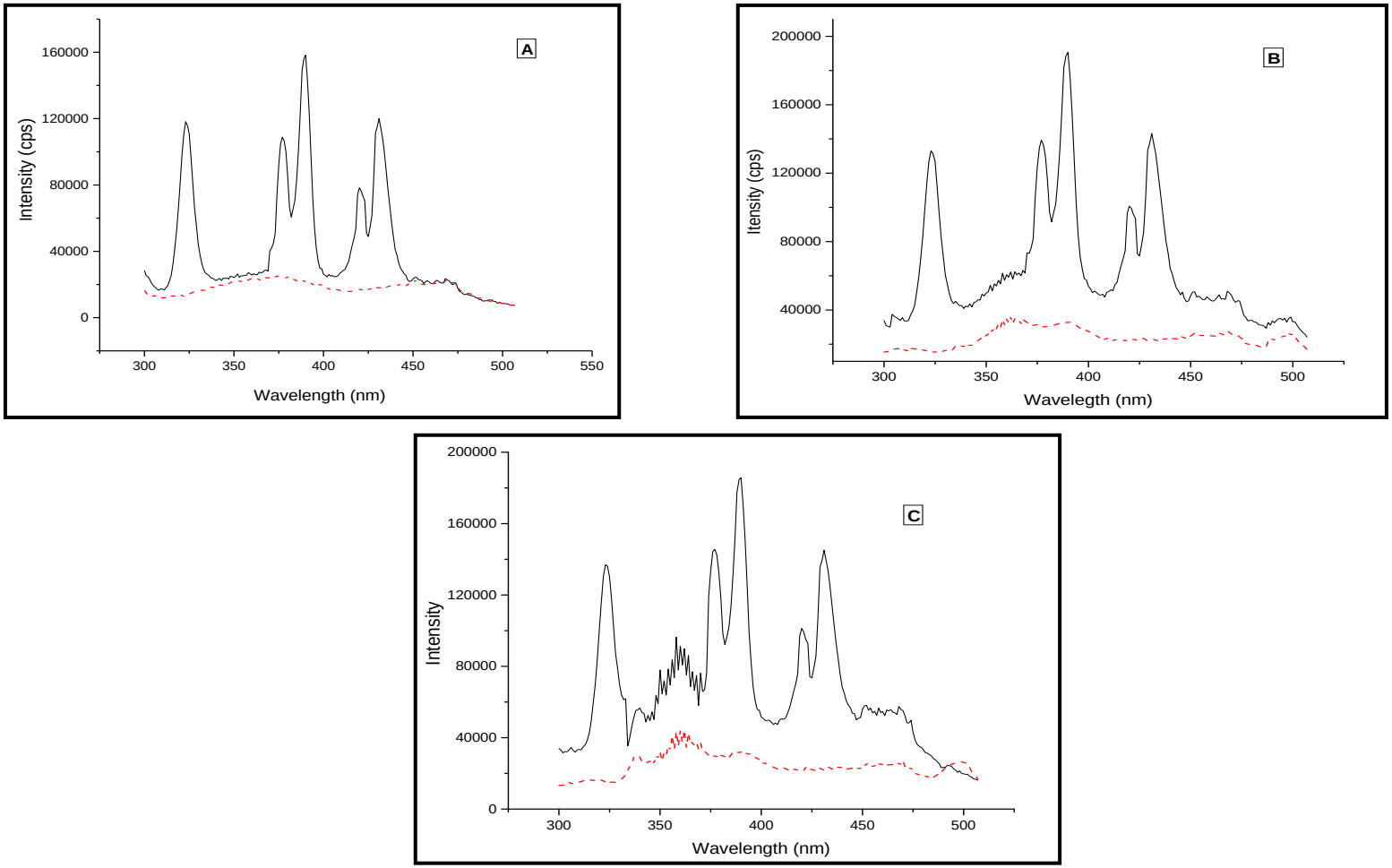

Figure 4.5 Solid phase extraction - synchronous fluorescence spectra of OH-PAH mixture in methanol obtained from spiked synthetic urine (A), real urine (B) and real urine with additional spiked with pharmaceutical concomitants (C). ***(Note: OH-PAH mixture: 10ng.mL^{-1} 3OH-B(a)P; 5ng.mL^{-1} 1OH-Pyr; 20ng.mL^{-1} 2OH-Flu; 20ng.mL^{-1} 4OH-B(a)P; 20ng.mL^{-1} 6OH-Chry; Pharmaceutical concomitants: 200ng.mL^{-1} naproxen; 10ng.mL^{-1} diclofenac; 100ng.mL^{-1} ibuprofen and 50mg.mL^{-1})***

Baseline resolution of the five metabolites was achieved via first-derivative SFS. First derivative spectra were obtained in post-acquisition mode with Origin software (version 9.0). Figure 4.6 shows a set of first-derivative SFS spectra recorded from synthetic mixtures of OH-PAH at various concentration ratios. Table 4.4 reports the AFOM obtained from synthetic urine via SPE-first derivative SFS. Calibration curves, LDR, RSD, LOQ and LOD were calculated as those reported in Table 4.3. Comparison of tabulated values shows LOQ and LOD values within the same order of magnitude.

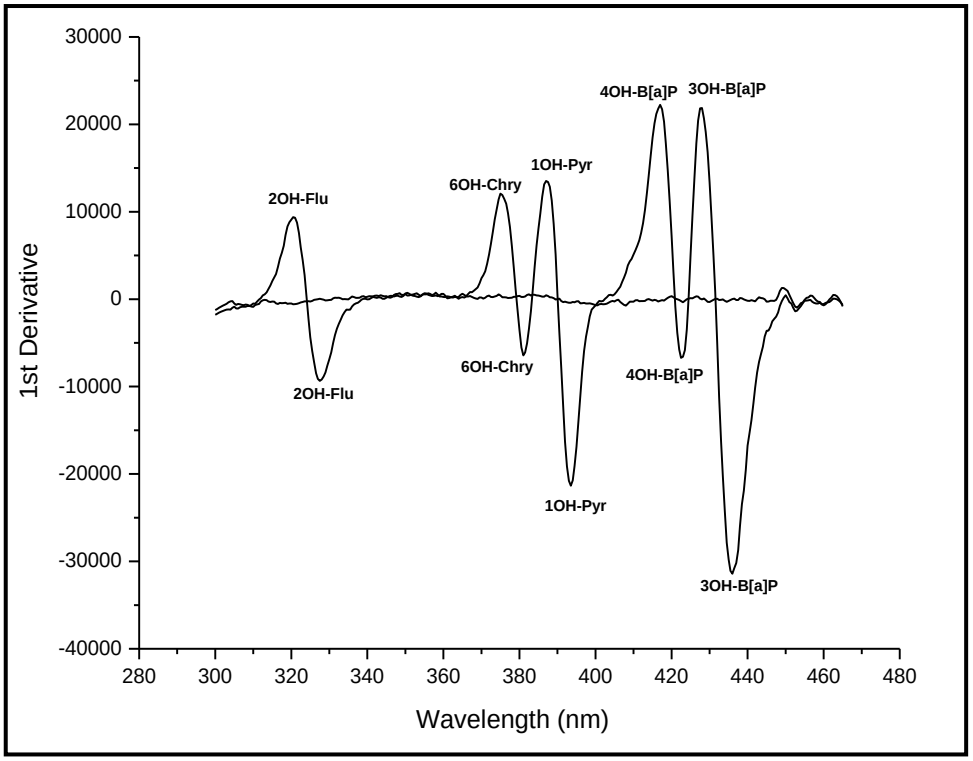

Figure 4.6 First derivative solid phase extraction - synchronous fluorescence spectra of OH-PAH mixture in methanol obtained from spiked synthetic urine. ***Note: OH-PAH mixture: 10ng.mL^{-1} 3OH-B(a)P; 5ng.mL^{-1} 1OH-Pyr; 20ng.mL^{-1} 2OH-Flu; 20ng.mL^{-1} 4OH-B(a)P; 20ng.mL^{-1} 6OH-Chry)***

Table 4.4 AFOM obtained from synthetic urine via SPE-first derivative SFS.

OH-PAH	Urine ($\Delta\lambda$ = 7nm, Bandpass = 2nm/2nm)			
	LDR[a]	R^{2}[b]	LOD[c]	LOQ[d]
2OH-Flu	1.00 – 200	0.9961	0.302	1.00
6OH-Chry	1.10 – 200	0.9980	0.329	1.10
1OH-Pyr	0.20 – 25	0.9968	0.060	0.20
4OH-B[a]P	0.51- 100	0.9944	0.153	0.51
3OH-B[a]P	0.21 – 50	0.9922	0.063	0.21

[a]*Linear dynamic range in ng/mL.*
[b]*Correlation coefficient of calibration curve.*
[c]*Limit of detection (ng/mL) is calculated from 3 x standard deviation (S_b) of 16 blank measurements divided by slope (m)of the calibration curve.*
[d] *Limit of quantification (ng/mL) is calculated from 10 S_b /m.*

4.4 Conclusion

Determination of 2OH-Flu, 1OH-Pyr, 6OH-Cry, 3OH- and 4OH-B[a]P in urine samples without the need of previous chromatographic separation was successfully accomplished via SPE-SFS. Baseline resolution of OH-PAH was made possible with the aid of first-derivative SFS. OH-PAH recoveries via SPE-SFS varied from 83% (4OH-B[a]P) to 99% (3OH-B[a]P). These values are excellent when compared to the recoveries of chromatographic methods (see Table 1.1.). Further comparison shows that the LOD obtained via SPE-SFS are within the same order as those obtained via established methodology. An additional advantage of the new method appears to be the relatively short analysis time. It should be noticed that analysis times in Table 1.1 only include instrumental times. The SPE procedure reported here takes approximately 15 min. The use of a vacuum manifold allowed its straightforward implementation to the simultaneous extraction of twelve samples. Considering the additional 3 minutes per sample that it took to perform SF measurements of the solid-phase extracts, we were able to analyze 12 samples of urine in approximately 55 min. This is equivalent to less than 5 min per sample. The non-destructive nature of the new method provides ample opportunity for OH-PAH confirmation via chromatographic techniques. Under this prospective, the determination of OH-PAH via SPE-SFS appears to be a useful approach to monitor exposure of large populations to PAH contamination.

CHAPTER 5: OVERALL CONCLUSION AND FUTURE WORK

The development of screening methods for the analysis of OH-PAH in urine samples has been accomplished with the aid of SPE and RTF spectroscopy. The analytical potential of the new methods was evaluated with six metabolites originating from parent PAH included in the EPA priority pollutants list. Quantitative determination of 1-hydroxyfluorene, 1-hydroxypyrene, 6-hydroxychrysene, 9-hydroxyphenanthrene, 3-hydroxybenzo[*a*]pyrene and 4-hydroxybenzo[a]pyrene was carried out either in the eluent extract or on the surface of extraction membranes. Their direct determination was based on the collection of EEMs and synchronous fluorescence spectra. Spectral overlapping of excitation-emission data was resolved with multivariate calibration methods. Base line resolution of the six metabolites was accomplished via first derivative synchronous fluorescence spectra. Excellent recoveries and competitive LOD were obtained for the six model biomarkers.

SPE followed by SFS in the eluent extract appears to be the simplest approach with the shortest analysis time. The use of a commercial vacuum manifold allows its straightforward implementation to the simultaneous extraction of twelve samples in approximately 15 minutes. Considering the additional 3 minutes per sample that it takes to record synchronous fluorescence spectra form the solid-phase extracts, the analysis of twelve urine samples takes approximately 55 min. This is equivalent to less than 5 min per sample. The non-destructive nature of the new method provides ample opportunity for OH-PAH confirmation via chromatographic techniques. Under this prospective, the determination of OH-PAH via SPE-SFS appears to be a useful approach to monitor exposure of large populations to PAH contamination.

Future work in our lab will focus on processing synchronous fluorescence data with multivariate calibration methods. Synchronous fluorescence spectra recorded at a single $\Delta\lambda$ value fit into the category of first-order data. The accurate determination of OH-PAH with first-order calibration methods would require the laborious preparation of extensive calibration data sets containing all sample components with potential spectral overlapping. A more attractive approach is to handle spectral overlapping with second-order calibration methods, i.e., algorithms capable to provide accurate quantitation of numerous OH-PAH in the presence of un-calibrated interference.

The application of second-order calibration methods requires second-order or tri-linear data, i.e. data describing each OH-PAH with a triad of invariant pure profiles. TSF data of OH-PAH fits into this category because their spectral profiles vary with the $\Delta\lambda$ of synchronous excitation. Analogous to the concept of an excitation-emission matrix, the complete set of synchronous fluorescence spectra as a function of $\Delta\lambda$ provides a data array with comprehensive information on the TSF of the sample. TSF spectroscopy coupled to second-order multivariate calibration methods should prove useful for the direct analysis of multiple metabolites in highly complex physiological matrixes. These include epoxides, dihydrodiols, and tetrols of difficult HPLC and/or GC-MS determination.

APPENDIX A: MOLECULAR STRUCTURES OF THE MAJOR ORGANIC COMPONENTS IN HUMAN URINE

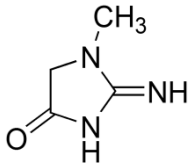

Creatinine

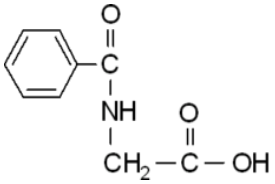

Hippuric acid

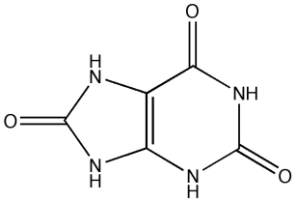

Uric acid

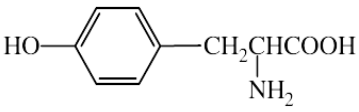

Tyrosine

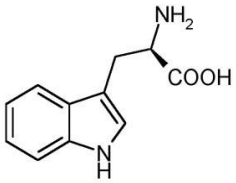

Tryptophan

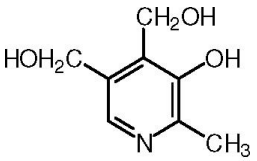

Vitamin B6

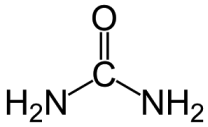

Urea

Figure A. Major components in human urine

APPENDIX B: POSSIBLE CONCOMITANTS IN OH-PAH URINE ANALYSIS

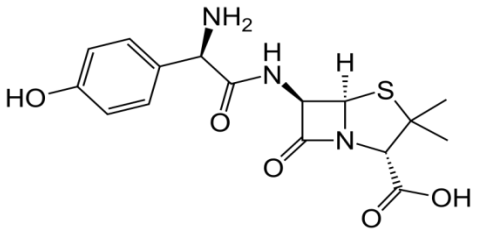

Amoxicillin

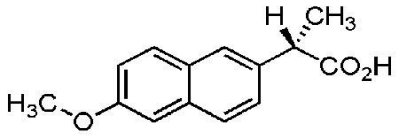

Naproxen

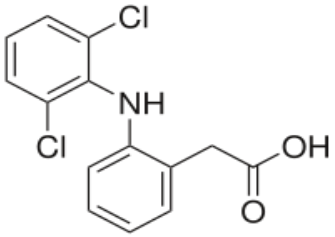

Diclofenac

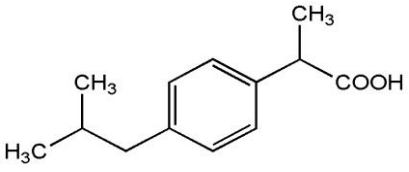

Ibuprofen

Figure B. Possible pharmaceutical concomitant in human urine for OH-PAH analysis

APPENDIX C: EEM SPECTRA OF OH-PAH

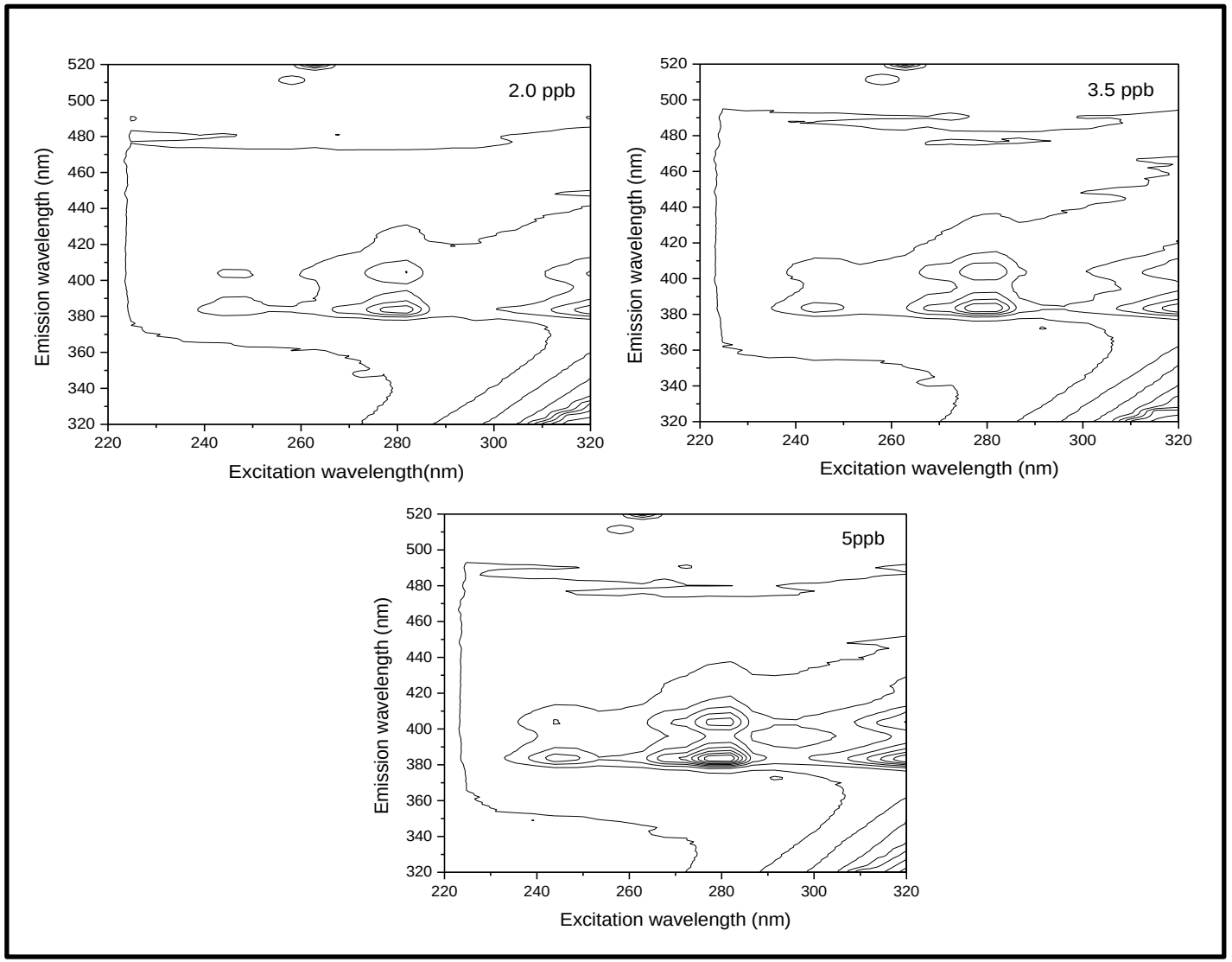

Figure C-1. EEM calibration spectra of 1OH – Pyr on C18 membrane at excitation and emission band pass 2nm/2nm.

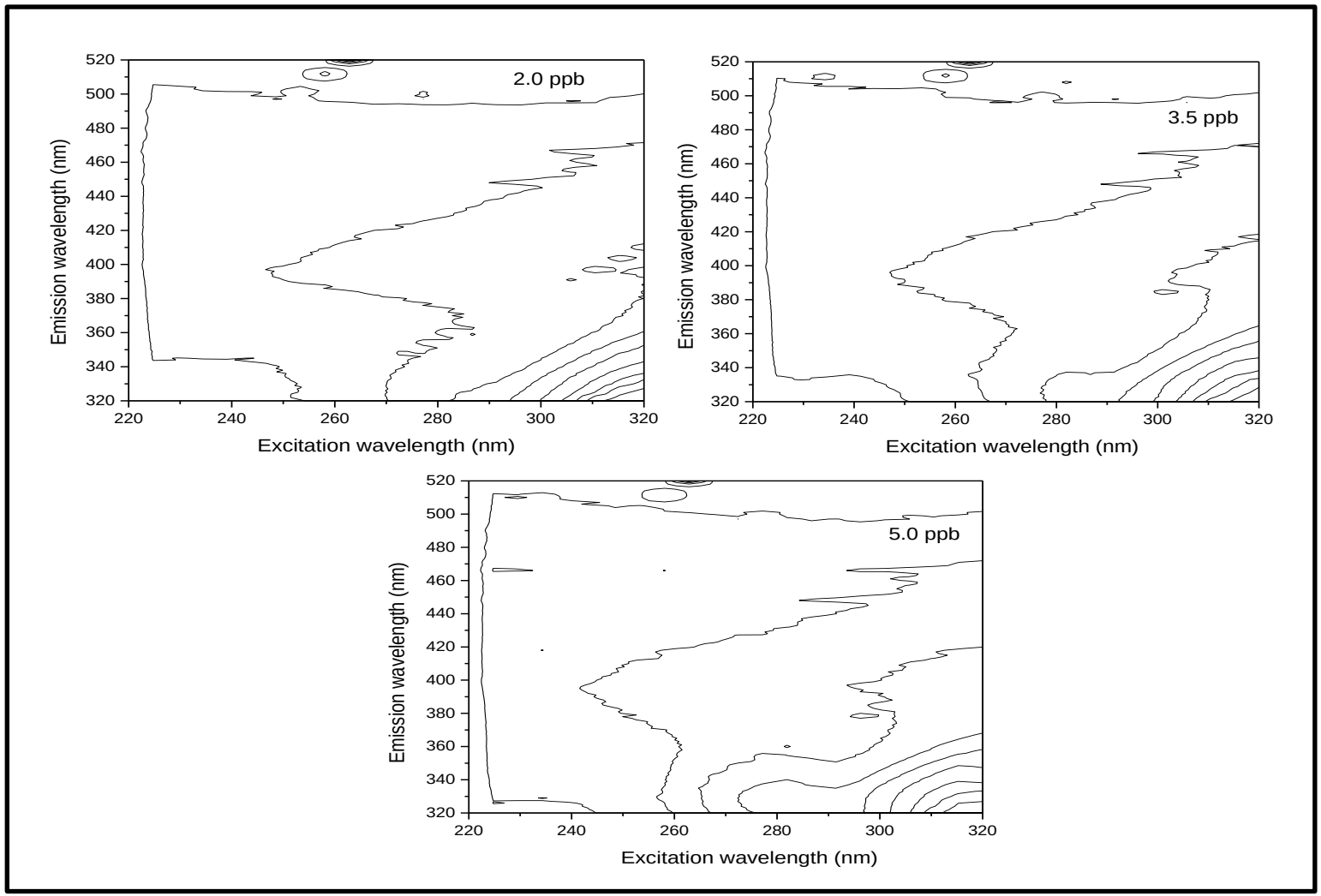

Figure C-2. EEM calibration spectra of 2OH – Flu on C18 membrane at excitation and emission band pass 2nm/2nm.

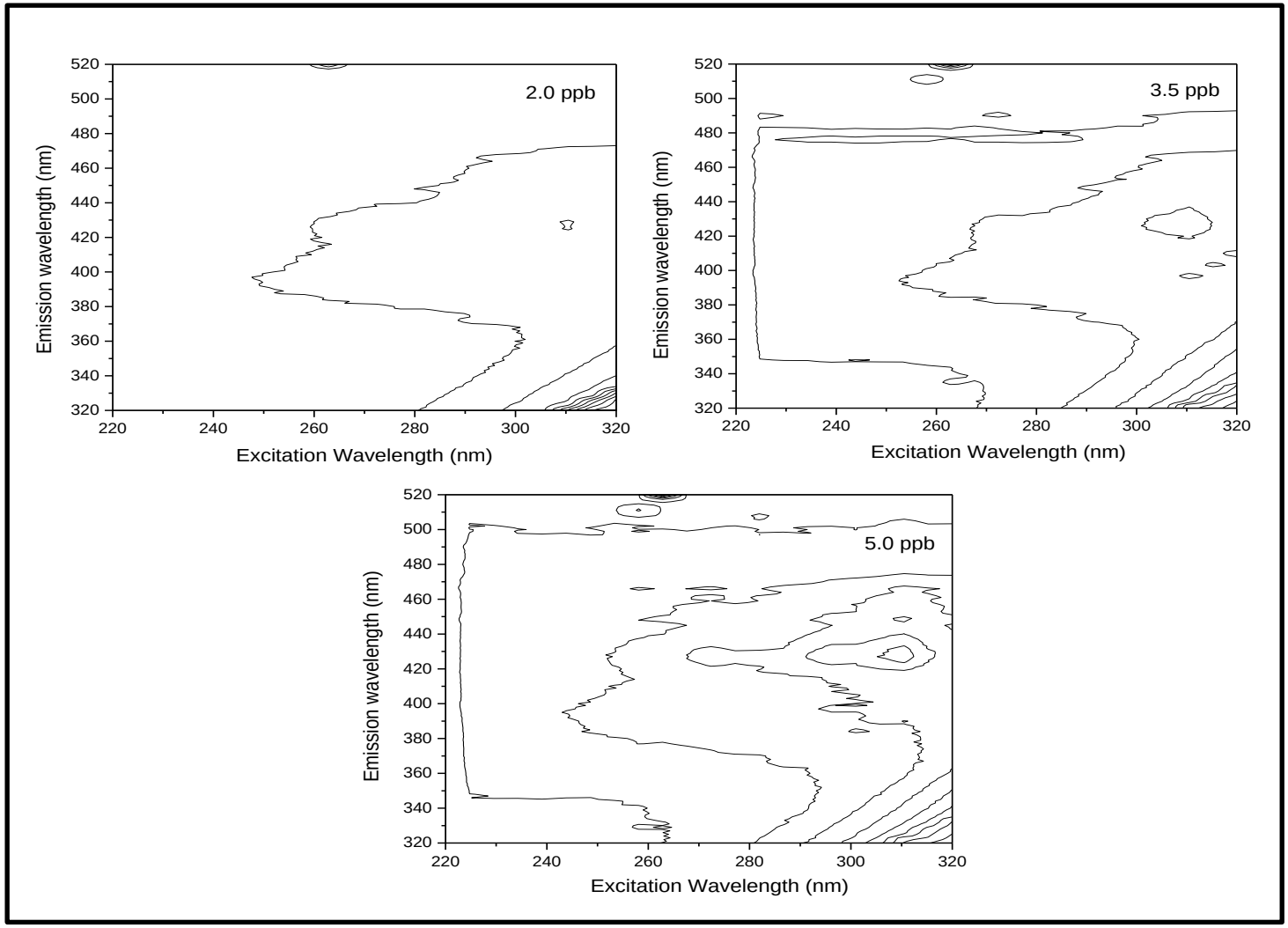

Figure C-3. EEM calibration spectra of 3OH – B[a]p on C18 membrane at excitation and emission band pass 2nm/2nm.

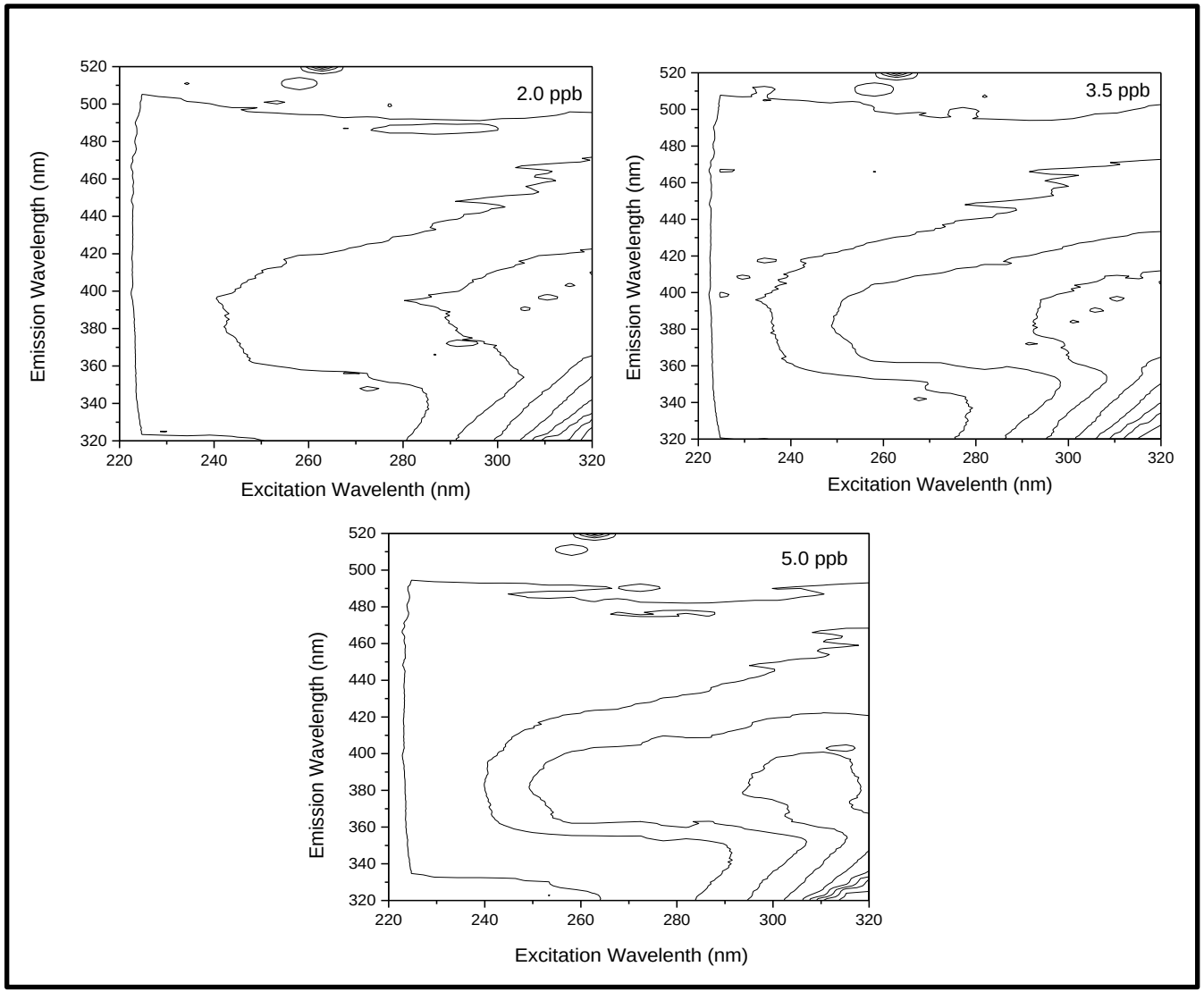

Figure C-4. EEM calibration spectra of 9OH – PHE on C18 membrane at excitation and emission band pass 2nm/2nm.

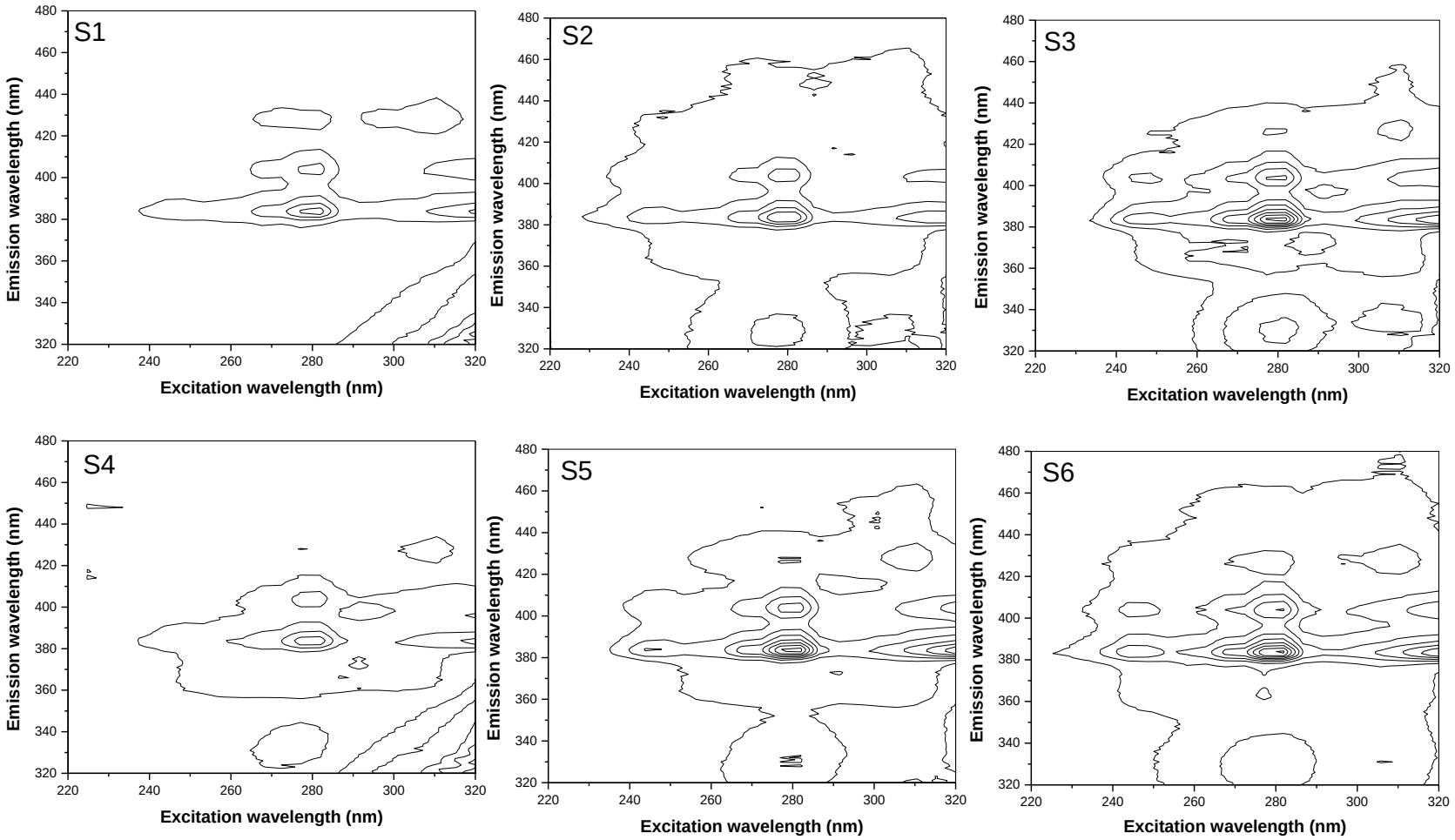

Figure C-5. Background subtracted validation EEM of all studied metabolites. Concentrations from water mixtures were at the ng/mL

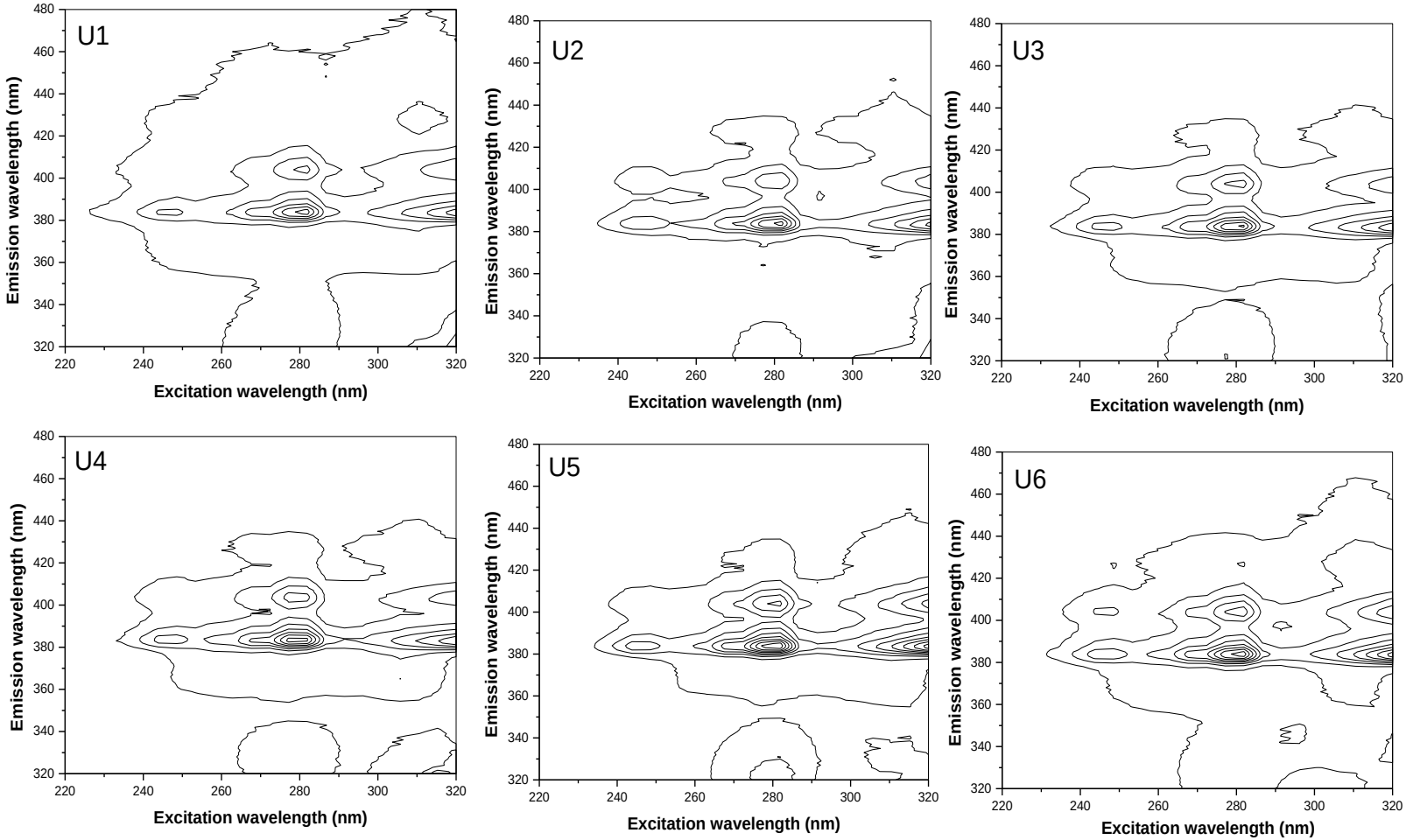

Figure C-6. Background subtracted validation EEM of all studied metabolites. Concentrations from synthetic urine mixtures were at the ng/mL.

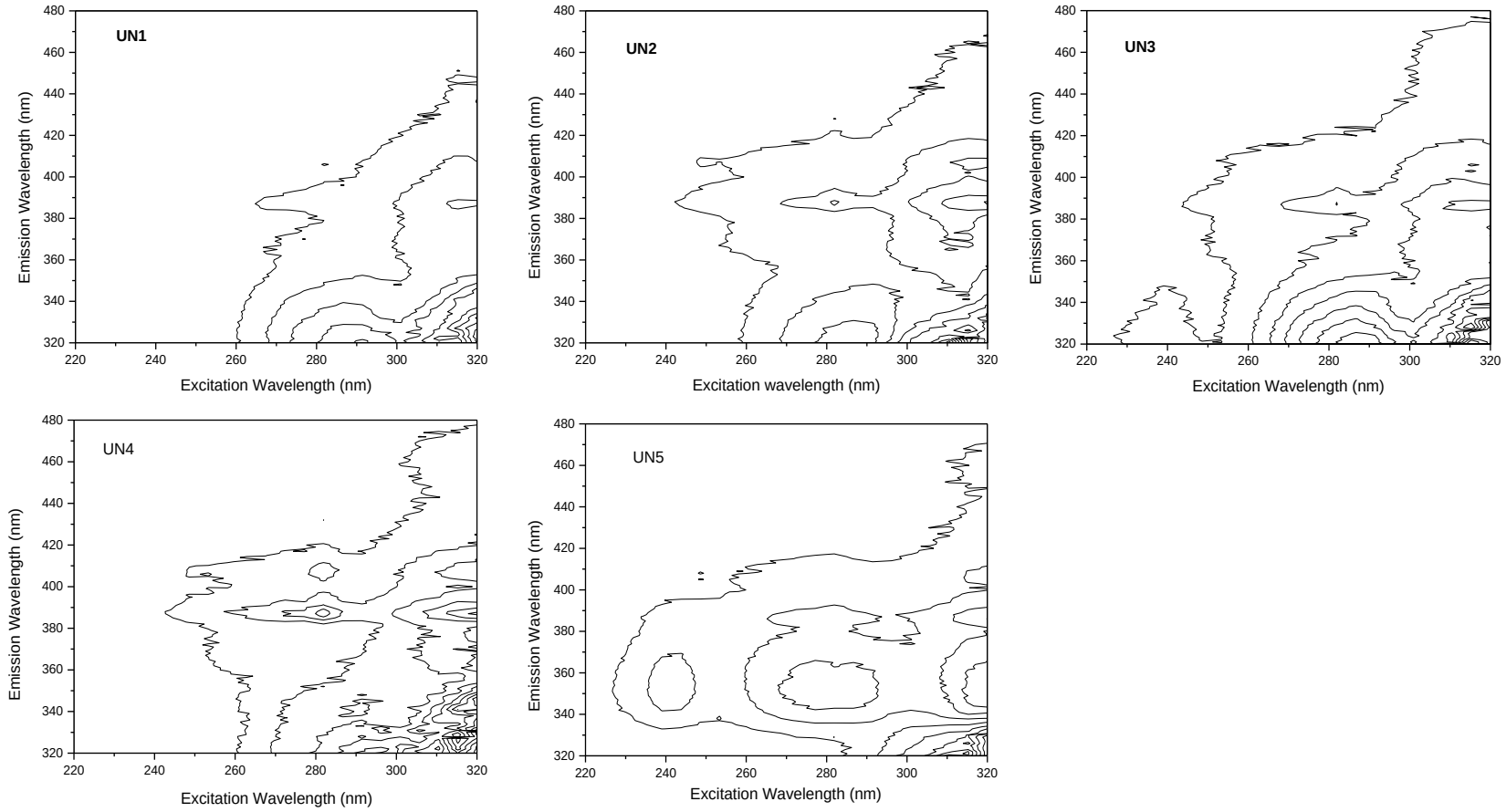

Figure C-7. Background subtracted validation EEM of all studied metabolites. Concentrations from synthetic urine mixtures with interferents were at the ng/mL.

REFERENCES

1. Vatsavai, K., H.C. Goicoechea, and A.D. Campiglia, Anal. Biochem., 2008. **376**: p. 213.

2. Calimag-Williams K.J., H.C.G.a.A.D.C., *Determination of monohydroxy-polycyclic aromatic hydrocarbons in urine samples via total synchronous fluorescence spectroscopic data modeled with multi-way partial least-squares and residual bi-linearization.* to be submitted to Analytica Chimica Acta, 2013. , to be submitted.

3. Calimag-Williams, K., H.C. Goicoechea, and A.D. Campiglia, *Room-temperature fluorescence spectroscopy of monohydroxy metabolites of polycyclic aromatic hydrocarbons on octadecyl extraction membranes.* Talanta, 2011. **85**(4): p. 1805-1811.

4. Goicoechea, H.C., K. Calimag-Williams, and A.D. Campiglia, *Multi-way partial least-squares and residual bi-linearization for the direct determination of monohydroxy-polycyclic aromatic hydrocarbons on octadecyl membranes via room-temperature fluorescence excitation emission matrices.* Analytica Chimica Acta, 2012. **717**: p. 100-109.

5. Dzepina, K., et al., Int. J. Mass Spectrom., 2007. **263**: p. 152.

6. Schelle, K.J., et al., Environ. Sci. Technol., 2007. **41**: p. 3281.

7. Zencak, Z., et al., Environ. Sci. Technol., 2007. **41**: p. 3850.

8. Cincinelli, A., et al., Chemosphere, 2007. **68**: p. 472.

9. Cai, Q.Y., et al., Chemosphere, 2007. **68**: p. 159.

10. Aichner, B., B. Glaser, and W. Zech, Org. Chem., 2007. **38**: p. 700.

11. Chung, M.K., et al., Chemosphere, 2007. **67**: p. 464.

12. Pereira, C.D., et al., Environ. Toxic. Chem., 2007. **26**: p. 462.

13. Cuo, W., et al., *68.* Chemosphere, 2007. **68**: p. 93.

14. Gobel, P., C. Dierkes, and W.C. Coldewey, J. Contam. Hydrol., 2007. **91**: p. 26.

15. Boonyatumanond, R., et al., Marine Pollut. Bulletin, 2006. **52**: p. 942.

16. Bukley, T.J., J.M. Waldman, and R. Dhara, Int. Arch. Occup. Environ. Health, 1995. **67**: p. 257.

17. Philips, D.H., Genet. Toxic. Environ. Mutagen., 1999. **443**: p. 139.

18. "U.S. Environmental Protection Agency Report on US EPA Air Monitoring of Haze Frome SE Asia Biomass Fires. Report No. EPA/600/R-98/071" 1998: p. Wahsington DC. Office of Research and Development.

19. Lee, M.L., M. Novotny, and K.D. Bartle, Anal. Chem., 1976. **48**: p. 405.

20. Hoffmann, D. and I. Hoffmann, cancer Treat. Res., 1995. **12**: p. 1.

21. Boyle, P., Lung Cancer, 1997. **17**: p. 1.

22. Lioy, P. and A. Greenberg, Toxicol. Industr. Health, 1990. **6**: p. 209.

23. Viau, C., G. hakizimana, and M. Bounchard, Int. Arch. Occup. Environ. Health, 200. **73**: p. 331.

24. Omland, O., et al., Occup. Environ. Medic., 1994. **51**: p. 513.

25. Grimmer, G., G. Dettern, and J. Jacob, Int. Arch. Occup. Environ. Health, 1993. **65**: p. 189.

26. Angerer, J., et al., Int. Arch. Occup. Environ. Health, 1992. **64**: p. 265.

27. Karahalil, B., et al., Mutat. Res. Genet. Toxic. Environ. Mutagen., 1998. **412**: p. 261.

28. Siedel, A., et al., Int. J. Hygiene Environ. Health, 2002. **204**: p. 334.

29. Overebo, S., et al., Environ. Health Perspect., 1995. **103**: p. 838.

30. Lloyd, J., J. Occup. Medic., 1971. **13**: p. 53.

31. Ramesh, A., et al., *Bioavailability and risk assessment of orally ingested polycyclic aromatic hydrocarbons.* International Journal of Toxicology, 2004. **23**(5): p. 301-333.

32. Miller, J.A., Cancer Res., 1970. **30**: p. 556.

33. Miller, E.C. and J.A. Miller, Cancer, 1981. **47**: p. 2327.

34. US-EPA, *Polycyclic aromatic hyrocarbons: 15 listing; Ninth Report on carcinogens*, 2001, U.S. Department of Health and Human Services

35. Jongeneelen, F.J., Environ. Health, 1986. **12**: p. 137.

36. Jongeneelen, F.J., Environ. Health, 1985. **57**: p. 47.

37. Grimmer, G., H. Brune, and G. Dettern, Arch. Toxicol., 1988. **62**: p. 401.

38. Smith, C.J., C.J. Walcott, and W. Huang, J. Chromatogr. B, 2002. **778**: p. 157.

39. Li, Y.H., A.C. Li, and H.S. Zhou, Rapid. Commun. Mass Spectrum., 2005. **19**: p. 3331.

40. Smith, C.J., et al., *Quantification of monohydroxy-PAH metabolites in urine by solid-phase extraction with isotope dilution-GC-MS.* Analytical and Bioanalytical Chemistry, 2002. **372**(1): p. 216-220.

41. Gundel, J. and J. Angerer, J. Chromatogr. B, 2000. **738**: p. 47.

42. Jacob, P., M. Wilson, and N.L. Benowitz, *Determination of phenolic metabolites of polycyclic aromatic hydrocarbons in human urine as their pentafluorobenzyl ether derivatives using liquid chromatography-tandem mass spectrometry.* Analytical Chemistry, 2007. **79**(2): p. 587-598.

43. Wang, Y., W. Zhang, and Y. Dong, Anal. Bioanal. Chem., 2005. **383**: p. 804.

44. Serdar, B., S. Waidyanatha, and Y. Zheng, Biomarkers, 2003. **8**: p. 93.

45. Romanoff, L.C., Z. Li, and K.J. Young, J. Chromatogr. B, 2006. **835**: p. 47.

46. Campo, L., F. Rossella, and S. Fustinoni, *Development of a gas chromatography/mass spectrometry method to quantify several urinary monohydroxy metabolites of polycyclic aromatic hydrocarbons in occupationally exposed subjects.* Journal of Chromatography B-Analytical Technologies in the Biomedical and Life Sciences, 2008. **875**(2): p. 531-540.

47. Li, Z., et al., *Measurement of urinary monohydroxy polycyclic aromatic hydrocarbons using automated liquid-liquid extraction and gas chromatography/isotope dilution high-resolution mass spectrometry.* Analytical Chemistry, 2006. **78**(16): p. 5744-5751.

48. Kuusimaki, L., et al., *Urinary hydroxy-metabolites of naphthalene, phenanthrene and pyrene as markers of exposure to diesel exhaust.* International Archives of Occupational and Environmental Health, 2004. **77**(1): p. 23-30.

49. Wang, H., W.B. Wilson, and A.D. Campiglia, J. Chromatogr. A, 2009. **385**: p. 249.

50. Pastushkova, L.K., et al., *Changes in urine protein composition in human organism during long term space flights.* Acta Astronautica, 2012. **81**(2): p. 430-434.

51. Lienert, J., K. Gudel, and B.I. Escher, *Screening method for ecotoxicological hazard assessment of 42 pharmaceuticals considering human metabolism and excretory routes.* Environmental Science & Technology, 2007. **41**(12): p. 4471-4478.

52. Winker, M., et al., *Comparison of analytical and theoretical pharmaceutical concentrations in human urine in Germany.* Water Research, 2008. **42**(14): p. 3633-3640.

53. Winker, M., *Are pharmaceutical residues in urine a constraint for using urine as a fertiliser?* Sustainable Sanitation Practice, 2010(3): p. 18-24.

54. Payan, M.R., et al., *HPLC determination of ibuprofen, diclofenac and salicylic acid using hollow fiber-based liquid phase microextraction (HF-LPME).* Analytica Chimica Acta, 2009. **653**(2): p. 184-190.

55. Kaczmarek, M., *Chemiluminescence of the Reaction System Ce(IV) - Non-Steroidal Anti-Inflammatory Drugs Containing Europium(III) Ions and its Application to the Determination of Naproxen in Pharmaceutical Preparations and Urine.* Journal of Fluorescence, 2011. **21**(6): p. 2201-2205.

56. Putnam, D.F., *Composition and concentrative properties of human urine*, 1971, National Aeronautics and Space Administration: Washington, DC.

57. Winefordner, J.D., T.C.j.a. O'Haver, and S.G.j.a. Schulman, *Luminescence spectrometry in analytical chemistry*. Chemical analysis, v. 38. 1972, New York: Wiley-Interscience.

58. *Molecular Luminescence Spectroscopy*. Methods and Applications: Part 1 and 2. New York: Wiley-Interscience.

59. Hurtubise, R.J., *Phosphorimetry: Theory, Instrumentation, and Applications*. 1990, New York: VCH Publishers Inc.

60. Vo, D.T., *Room temperature phosphorimetry for chemical analysis*. 1984: Wiley.

61. Skoog, D.A., F.J. Holler, and T.A. Nieman, Principles of instrumental analysis. 5th edition.

62. Lakowicz, J.R., Principles of fluorescence spectroscopy. New York 2nd edition.

63. Winefordner, J.D., Series Editor, Wiley, NY, 2003.

64. Ho, C.N. and I.M. Warner, *MULTICOMPONENT MIXTURE ANALYSIS BY MULTIDIMENSIONAL PHOSPHORIMETRY.* Analytical Chemistry, 1982. **54**(14): p. 2486-2491.

65. Warner, I.M., G. Patonay, and M.P. Thomas, *MULTIDIMENSIONAL LUMINESCENCE MEASUREMENTS.* Analytical Chemistry, 1985. **57**(3): p. A463-&.

66. Vo-Dinh, T., R.B. Gammage, and P.R. Martinez, *ANALYSIS OF A WORKPLACE AIR PARTICULATE SAMPLE BY SYNCHRONOUS LUMINESCENCE AND ROOM-TEMPERATURE PHOSPHORESCENCE.* Analytical Chemistry, 1981. **53**(2): p. 253-258.

67. Vo-Dinh, T. and P.R. Martinez, *DIRECT DETERMINATION OF SELECTED POLYNUCLEAR AROMATIC-HYDROCARBONS IN A COAL-LIQUEFACTION PRODUCT BY SYNCHRONOUS LUMINESCENCE TECHNIQUES.* Analytica Chimica Acta, 1981. **125**(APR): p. 13-19.

68. Vo, D.T., in *New Directions in Molecular Luminescence*. 1983, ASTM: Baltimore MD. p. 5-16.

69. da Silva, J., M. Tavares, and R. Tauler, *Multivariate curve resolution of multidimensional excitation-emission quenching matrices of a Laurentian soil fulvic acid.* Chemosphere, 2006. **64**(11): p. 1939-1948.

70. DaCosta, R.S., H. Andersson, and B.C. Wilson, *Molecular fluorescence excitation-emission matrices relevant to tissue spectroscopy.* Photochemistry and Photobiology, 2003. **78**(4): p. 384-392.

71. Warner, I.M., et al., *ANALYSIS OF MULTICOMPONENT FLUORESCENCE DATA.* Analytical Chemistry, 1977. **49**(4): p. 564-573.

72. Warner, I.M., E.R. Davidson, and G.D. Christian, *QUANTITATIVE-ANALYSES OF MULTICOMPONENT FLUORESCENCE DATA BY METHODS OF LEAST-SQUARES AND NONNEGATIVE LEAST SUM OF ERRORS.* Analytical Chemistry, 1977. **49**(14): p. 2155-2159.

73. Kasha M., *Characterization of electronic transitions in complex molecules.* Discussions of the Faraday Society, 1950. **9**: p. 14-19.

74. Patra, D. and A.K. Mishra, *Recent developments in multi-component synchronous fluorescence scan analysis.* Trac-Trends in Analytical Chemistry, 2002. **21**(12): p. 787-798.

75. Fu, X.N., J. Wang, and L. Yang, *IR Spectral-Analysis-Based Range Estimation for an Object with Small Temperature Difference from Background.* Spectroscopy and Spectral Analysis, 2013. **33**(1): p. 51-54.

76. Shao, L.M., et al., *Increasing the Quantitative Credibility of Open-Path Fourier Transform Infrared (FT-IR) Spectroscopic Data, with Focus on Several Properties of the Background Spectrum.* Applied Spectroscopy, 2013. **67**(3): p. 335-341.

77. Vogt, F., K. Rebstock, and M. Tacke, *Correction of background drifts in optical spectra by means of "pseudo principal components".* Chemometrics and Intelligent Laboratory Systems, 2000. **50**(2): p. 175-178.

78. Chen, S., et al., *Raman Spectroscopy Fluorescence Background Correction and Its Application in Clustering Analysis of Medicines.* Spectroscopy and Spectral Analysis, 2010. **30**(8): p. 2157-2160.

79. Xie, Y.L., et al., *BACKGROUND BILINEARIZATION BY THE USE OF GENERALIZED STANDARD ADDITION METHOD ON 2-DIMENSIONAL DATA.* Analytica Chimica Acta, 1993. **281**(1): p. 207-218.

80. Zhang, Z.M., et al., *An intelligent background-correction algorithm for highly fluorescent samples in Raman spectroscopy.* Journal of Raman Spectroscopy, 2010. **41**(6): p. 659-669.

81. Karstang, T.V. and O.M. Kvalheim, *MULTIVARIATE PREDICTION AND BACKGROUND CORRECTION USING LOCAL MODELING AND DERIVATIVE SPECTROSCOPY.* Analytical Chemistry, 1991. **63**(8): p. 767-772.

82. Lindberg, W., J. Ohman, and S. Wold, *MULTIVARIATE RESOLUTION OF OVERLAPPED PEAKS IN LIQUID-CHROMATOGRAPHY USING DIODE-ARRAY DETECTION.* Analytical Chemistry, 1986. **58**(2): p. 299-303.

83. Hurtubise, R., *Solid Surface Luminescence Analysis: Theory, Instrumentation, Applications*. 1981, New York: Marcel Dekker Inc.

84. Bateh, R.P., *Room Temperature phosphorescence some diagnostic studies in its application to biochemical and drug analysis*, 1982, University of Florida: Gainesville, FL.

85. Algarra, M., et al., *Detection and quantification of PAH in drinking water by front-face fluorimetry on a solid sorbent and PLS analysis.* Analytical and Bioanalytical Chemistry, 2005. **382**(4): p. 1103-1110.

86. Eastwood, D., et al., *A SOLID-PHASE EXTRACTION SOLID-STATE LUMINESCENCE APPROACH FOR MONITORING PAHS IN WATER.* Analusis, 1994. **22**(6): p. 305-310.

87. Hagestuen, E.D., A.F. Arruda, and A.D. Campiglia, *On the improvement of solid-phase extraction room-temperature phosphorimetry for the analysis of polycyclic aromatic hydrocarbons in water samples.* Talanta, 2000. **52**(4): p. 727-737.

88. Hagestuen, E.D. and A.D. Campiglia, *Phosphorimetric detection of polycyclic aromatic hydrocarbons on solid-phase extraction membranes.* Applied Spectroscopy, 1998. **52**(8): p. 1096-1102.

89. Hagestuen, E.D. and A.D. Campiglia, *Near approach for screening polycyclic aromatic hydrocarbons in*

water samples. Talanta, 1999. **49**(3): p. 547-560.

90. Ariese, F., A.N. Bader, and C. Gooijer, Trens Anal. Chem., 2008. **27**: p. 127.

91. Bystol, A.J., J.L. Whitcomb, and A.D. Campiglia, *Solid-liquid extraction laser excited time resolved Shpol'skii spectrometry: A facile method for the direct detection of 15 priority pollutants in water samples.* Environmental Science & Technology, 2001. **35**(12): p. 2566-2571.

92. Campiglia, A.D., A.J. Bystol, and S.J. Yu, *Instrumentation for multidimensional luminescence spectroscopy and its application to low-temperature analysis in Shpol'skii matrixes and optically scattering media.* Analytical Chemistry, 2006. **78**(2): p. 484-492.

93. Wang, H.Y. and A.D. Campiglia, *Direct determination of benzo a pyrene in water samples by a gold nanoparticle-based solid phase extraction method and laser-excited time-resolved Shpol'skii spectrometry.* Talanta, 2010. **83**(1): p. 233-240.

94. Poziomek, E.J., et al., *SOLID-PHASE EXTRACTION AND SOLID-STATE SPECTROSCOPY FOR MONITORING WATER-POLLUTION.* Analytical Letters, 1991. **24**(10): p. 1913-1921.

95. Ackerman, A.H. and R.J. Hurtubise, *Solid-matrix fluorescence and phosphorescence and solid-phase microextraction of polycyclic aromatic hydrocarbons with hydrophobic paper.* Applied Spectroscopy, 1999. **53**(7): p. 770-775.

96. Arruda, A.F. and A.D. Campiglia, *Screening potential of solid phase extraction room temperature phosphorimetry for the analysis of polychlorinated dibenzofurans in water samples.* Environmental Science & Technology, 2000. **34**(23): p. 4982-4988.

97. Arruda, A.F., et al., *Solid-liquid extraction room temperature phosphorimetry and pattern recognition for screening polycyclic aromatic hydrocarbons and polychlorinated biphenyls in water samples.* Environmental Science & Technology, 2003. **37**(7): p. 1385-1391.

98. Arruda, A.F. and A.D. Campiglia, *Determination of trace levels of polychlorinated biphenyls on reversed phase octadecyl bonded silica membranes.* Analytica Chimica Acta, 1999. **386**(3): p. 271-280.

99. Whitcomb, J.L. and A.D. Campiglia, *Screening potential of solid-phase extraction and solid surface room temperature fluorimetry for polycyclic aromatic hydrocarbons in water samples.* Talanta, 2001. **55**(3): p. 509-518.

100. Vatsavai, K., H.C. Goicoechea, and A.D. Campiglia, *Direct quantification of monohydroxy-polycyclic aromatic hydrocarbons in synthetic urine samples via solid-phase extraction-room-temperature fluorescence excitation-emission matrix spectroscopy.* Analytical Biochemistry, 2008. **376**(2): p. 213-220.

101. Eilers, P.H.C., *Parametric time warping.* Analytical Chemistry, 2004. **76**(2): p. 404-411.

102. Goicoechea, H.C., et al., *Chemometric strategies for enhancing the chromatographic methodologies with second-order data analysis of compounds when peaks are overlapped.* Talanta, 2011. **83**(4): p. 1098-1107.

103. Jongeneelen, F.J., et al., *1-HYDROXYPYRENE IN HUMAN-URINE AFTER EXPOSURE TO COAL-TAR AND A*

COAL-TAR DERIVED PRODUCT. International Archives of Occupational and Environmental Health, 1985. **57**(1): p. 47-55.

104. *MATLAB 7.6.0*, 2008, The Math Works: Natick,MA.

105. Currie, I.D., M. Durban, and P.H.C. Eilers, *Generalized linear array models with applications to multidimensional smoothing.* Journal of the Royal Statistical Society Series B-Statistical Methodology, 2006. **68**: p. 259-280.

106. Campiglia, A.D. and C.G. Delima, *UTILIZATION OF AN INORGANIC PHOSPHOR AS A REFERENCE SIGNAL IN SOLID-SURFACE ROOM-TEMPERATURE PHOSPHORIMETRY.* Analytical Chemistry, 1988. **60**(19): p. 2165-2167.

107. Danzer, K., L.A. Currie, and C. Commission Gen Aspects Analyt, *Guidelines for calibration in analytical chemistry - Part 1. Fundamentals and single component calibration (IUPAC recommendations 1998).* Pure and Applied Chemistry, 1998. **70**(4): p. 993-1014.

108. Wolberg, J.R., *Data Analysis using the method of least squares: extracting the most information from experiments*. 2006, New York: Springer.

109. Technologies, A.; Available from: http://www.chem.agilent.com/Library/brochures/5990-6042EN.pdf.

110. Wilcox, R., *Fundamentals of Mordern Statistical Methods: Improving power and accuracy*. 2001, New York: Springer.

111. Whitcomb, J.L., A.J. Bystol, and A.D. Campiglia, *Time-resolved laser-induced fluorimetry for screening polycylic aromatic hydrocarbons on solid-phase extraction membranes.* Analytica Chimica Acta, 2002. **464**(2): p. 261-272.

112. Aucelio, R.Q. and A.D. Campiglia, *SOLID-SURFACE ROOM-TEMPERATURE PHOSPHORIMETRY ANALYSIS OF YOHIMBINE HYDROCHLORIDE IN PHARMACEUTICAL FORMULATIONS.* Analytica Chimica Acta, 1995. **309**(1-3): p. 345-353.

113. Campiglia, A.D. and C.G. Delima, *ROOM-TEMPERATURE PHOSPHORIMETRY OF CARBARYL IN LOW-BACKGROUND PAPER.* Analytical Chemistry, 1987. **59**(23): p. 2822-2827.

114. Gioia, S.M.C. and A.D. Campiglia, *ROOM-TEMPERATURE PHOSPHORESCENCE OF BIOGENIC INDOLES IN LOW-BACKGROUND PAPER ENHANCED BY HEAVY-ATOM SALTS AND SODIUM DODECYL-SULFATE.* Analytica Chimica Acta, 1994. **287**(1-2): p. 89-94.

115. Gmeiner, G., et al., *Fast screening method for the profile analysis of polycyclic aromatic hydrocarbon metabolites in urine using derivatisation - solid-phase microextraction.* Journal of Chromatography B-Analytical Technologies in the Biomedical and Life Sciences, 1998. **705**(1): p. 132-138.

116. Gundel, J. and J. Angerer, *High-performance liquid chromatographic method with fluorescence detection for the determination of 3-hydroxybenzo a pyrene and 3-hydroxybenz a anthracene in the urine of polycyclic aromatic hydrocarbon-exposed workers.* Journal of Chromatography B, 2000. **738**(1): p. 47-55.

117. Ramsauer, B., et al., *A liquid chromatography/tandem mass spectrometry (LC-MS/MS) method for the determination of phenolic polycyclic aromatic hydrocarbons (OH-PAH) in urine of non-smokers and smokers.* Analytical and Bioanalytical Chemistry, 2011. **399**(2): p. 877-889.

118. Xu, X., et al., *Selective detection of monohydroxy metabolites of polycyclic aromatic hydrocarbons in urine using liquid chromatography/triple quadrupole tandem mass spectrometry.* Rapid Communications in Mass Spectrometry, 2004. **18**(19): p. 2299-2308.

119. Galera, M.M., et al., *Determination of pharmaceuticals in river water by column switching of large sample volumes and liquid chromatography-diode array detection, assisted by chemometrics: An integrated approach to green analytical methodologies.* Journal of Chromatography A, 2010. **1217**(13): p. 2042-2049.

120. Bro, R., *PARAFAC. Tutorial and applications.* Chemometrics and Intelligent Laboratory Systems, 1997. **38**(2): p. 149-171.

121. de Juan, A. and R. Tauler, *Comparison of three-way resolution methods for non-trilinear chemical data sets.* Journal of Chemometrics, 2001. **15**(10): p. 749-772.

122. Wold, S., K. Esbensen, and P. Geladi, *PRINCIPAL COMPONENT ANALYSIS.* Chemometrics and Intelligent Laboratory Systems, 1987. **2**(1-3): p. 37-52.

123. Olivieri, A.C. and N.M. Faber, *A closed-form expression for computing the sensitivity in second-order bilinear calibration.* Journal of Chemometrics, 2005. **19**(11-12): p. 583-592.

124. Lozano, V.A., G.A. Ibanez, and A.C. Olivieri, *Three-way partial least-squares/residual bilinearization study of second-order lanthanide-sensitized luminescence excitation-time decay data - Analysis of benzoic acid in beverage samples.* Analytica Chimica Acta, 2008. **610**(2): p. 186-195.

125. Lozano, V.A., G.A. Ibanez, and A.C. Olivieri, *A novel second-order standard addition analytical method based on data processing with multidimensional partial least-squares and residual bilinearization.* Analytica Chimica Acta, 2009. **651**(2): p. 165-172.

126. Kaczmarek, K., et al., *Baseline reduction in two dimensional gel electrophoresis images.* Acta Chromatographica, 2005. **15**: p. 82-96.

127. Jaumot, J., et al., *A graphical user-friendly interface for MCR-ALS: a new tool for multivariate curve resolution in MATLAB.* Chemometrics and Intelligent Laboratory Systems, 2005. **76**(1): p. 101-110.

128. Olivieri, A.C., H.L. Wu, and R.Q. Yu, *MVC2: A MATLAB graphical interface toolbox for second-order multivariate calibration.* Chemometrics and Intelligent Laboratory Systems, 2009. **96**(2): p. 246-251.

129. ; Available from: http://www.chemometry.com.

130. Fajgelj, A. and Á. Ambrus, *Guidelines for single-laboratory validation of analytical methods for trace-level concentrations of organic chemicals.* 2007.

131. Martinez, A., et al., *Validation of bias in multianalyte determination methods. Application to RP-HPLC derivatizing methodologies.* Analytica Chimica Acta, 2000. **406**(2): p. 257-278.

132. Miller, M.J. and J.C. Miller, Statistics and Chemometrics for Analytical Chemistry, 4th ed., 2000: p. Prentice-Hall, Inc., New York.

133. Saurina, J., et al., *Estimation of figures of merit using univariate statistics for quantitative second-order multivariate curve resolution.* Analytica Chimica Acta, 2001. **432**(2): p. 241-251.

134. Currie, L.A., *Detection and quantification limits: origins and historical overview.* Analytica Chimica Acta, 1999. **391**(2): p. 127-134.

135. Lloyd, J.B.F., *NATURE AND EVIDENTIAL VALUE OF LUMINESCENCE OF AUTOMOBILE ENGINE OILS AND RELATED MATERIALS .1. SYNCHRONOUS EXCITATION OF FLUORESCENCE EMISSION.* Journal of the Forensic Science Society, 1971. **11**(2): p. 83-&.

136. Lloyd, J.B.F., *NATURE AND EVIDENTIAL VALUE OF LUMINESCENCE OF AUTOMOBILE ENGINE OILS AND RELATED MATERIALS .2. AGGREGATE LUMINESCENCE.* Journal of the Forensic Science Society, 1971. **11**(3): p. 153-&.

137. Lloyd, J.B.F., *SYNCHRONIZED EXCITATION OF FLUORESCENCE EMISSION SPECTRA.* Nature-Physical Science, 1971. **231**(20): p. 64-&.

138. John, P. and I. Soutar, *IDENTIFICATION OF CRUDE OILS BY SYNCHRONOUS EXCITATION SPECTROFLUORIMETRY.* Analytical Chemistry, 1976. **48**(3): p. 520-524.

139. Vo-Dinh, T., *MULTICOMPONENT ANALYSIS BY SYNCHRONOUS LUMINESCENCE SPECTROMETRY.* Analytical Chemistry, 1978. **50**(3): p. 396-401.

140. Vo-Dinh, T., J. Fetzer, and A.D. Campiglia, *Monitoring and characterization of polyaromatic compounds in the environment.* Talanta, 1998. **47**(4): p. 943-969.

141. Lamotte, M., et al., *Detection of 1-hydroxypyrene in urine by direct fluorometric analysis on a solid sorbing phase. Validation and application of the method to biological monitoring of PAH-exposed persons.* Analytical and Bioanalytical Chemistry, 2003. **376**(6): p. 816-821.

142. Yang, H.M., et al., *Synchronous fluorescence determination of urinary 1-hydroxypyrene, beta-naphthol and 9-hydroxyphenanthrene based on the sensitizing effect of beta-cyclodextrin.* Analytica Chimica Acta, 2009. **636**(1): p. 51-57.

143. Kang, R.H., et al., *Rapid simultaneous analysis of 1-hydroxypyrene, 2-hydroxyfluorene, 9-hydroxyphenanthrene, 1-and 2-naphthol in urine by first derivative synchronous fluorescence spectrometry using Tween-20 as a sensitizer.* Analytica Chimica Acta, 2010. **658**(2): p. 180-186.

144. Romanoff, L.C., et al., *Automated solid-phase extraction method for measuring urinary polycyclic aromatic hydrocarbon metabolites in human biomonitoring using isotope-dilution gas chromatography high-resolution mass spectrometry.* Journal of Chromatography B-Analytical Technologies in the Biomedical and Life Sciences, 2006. **835**(1-2): p. 47-54.

145. Kuusimaki, L., Y. Peltonen, and P. Mutanen, Int. Arch. Occup. Environ. Health, 2000. **77**: p. 23.

146. Waters, *Sep-Pak Cartridges and Plates Care and Use Manual.*

147. Miller, J.C. and J.N. Miller, *Statistics for analytical chemistry*. 2nd ed. ed. Ellis Horwood series in analytical chemistry. 1988, Chichester: Ellis Horwood.

148. Rodriguez-Gonzalo, E., et al., *In-capillary preconcentration of pirimicarb and carbendazim with a monolithic polymeric sorbent prior to separation by CZE.* Electrophoresis, 2008. **29**(19): p. 4066-4077.

149. Santos, D.P., M.F. Bergamini, and M.V.B. Zanoni, *Voltammetric sensor for amoxicillin determination in human urine using polyglutamic acid/glutaraldehyde film.* Sensors and Actuators B-Chemical, 2008. **133**(2): p. 398-403.

150. Knobel, G., K. Calimag-Williams, and A.D. Campiglia, *Solid-phase extraction, sample stacking and capillary zone electrophoresis for the analysis of urinary polycyclic aromatic hydrocarbon metabolites.* Analyst, 2012. **137**(23): p. 5639-5647.

151. Lloyd, J.B.F., *NATURE AND EVIDENTIAL VALUE OF LUMINESCENCE OF AUTOMOBILE ENGINE OILS AND RELATED MATERIALS .3. SEPARATED LUMINESCENCE.* Journal of the Forensic Science Society, 1971. **11**(4): p. 235-&.

152. Shpol'skii, E.V., A.A. Il'ina, and L.A. Klimova, Dokl. Akad. Nauk SSSR, 1952. **87**: p. 935.

153. Xu, X. and R.J. Hurtubise, *Influence of organic solvents in the capillary zone electrophoresis of polycyclic aromatic hydrocarbon metabolites.* Journal of Chromatography A, 1998. **829**(1-2): p. 289-299.

154. Xu, X. and R.J. Hurtubise, *Determination of the pK(a) values of polycyclic aromatic hydrocarbon metabolites by capillary zone electrophoresis.* Journal of Liquid Chromatography & Related Technologies, 1999. **22**(5): p. 669-679.

155. Xu, X. and R.J. Hurtubise, *Separation of polycyclic aromatic hydrocarbon metabolites by gamma-cyclodextrin-modified micellar electrokinetic chromatography.* Journal of Liquid Chromatography & Related Technologies, 2000. **23**(11): p. 1657-1670.

156. Yang, L., et al., *Gold nanoparticle-modified etched capillaries for open-tubular capillary electrochromatography.* Analytical Chemistry, 2005. **77**(6): p. 1840-1846.